

Potential Impacts of Nanoparticles on Bacterial Systems

by

Xiaohui Sun

A thesis submitted in partial fulfillment of the requirements for the degree of

Doctor of Philosophy

in

Environmental Engineering

Department of Civil and Environmental Engineering

University of Alberta

© Xiaohui Sun, 2015

Abstract

With the widespread use of nanoparticles (NPs) in commercial products, it is inevitable that NPs will be released into and accumulated in domestic and industrial waste streams (such as wastewater treatment systems), which might have unknown effects. To determine the effects of Ag NPs on the complex microbial communities present in activated sludge, experiments were performed to determine the effects of 1 mg/L Ag NPs on microbial communities in activated sludge. Activated sludge samples with and without gravity settling were compared to evaluate the impact of activated sludge flocs structure on the response of microbial communities to Ag NPs. The effects of Ag NPs on the entire microbial community in activated sludge were analyzed using 16S rRNA gene based polymerase chain reaction-denaturing gradient gel electrophoresis (PCR-DGGE). The results suggest that certain microbial species in the intact activated sludge were highly sensitive to Ag NPs treatment, although no reduction in cell culturability was detected through heterotrophic plate counts (HPCs) during the 24 hours Ag NPs treatment. Conversely, one log unit reduction in the HPCs with no microbial community structure changes was observed for unsettled activated sludge flocs (intact activated sludge treated by 3 hours gravity-settling) after 24 hours Ag NPs treatment. These results strongly suggest that Ag NPs can impact the activated sludge microbial community and cell culturability depending on the physical structure of the activated sludge flocs, the spatial distribution of microorganisms in activated sludge flocs, and the community structures in the activated sludge.

In comparison to metal NPs, cellulose nanocrystals (CNC) is a type of rod-shaped

biodegradable NPs. Depletion induced flocculation and phase separation of *Pseudomonas aeruginosa* PAO1 bacteria due to the presence of CNC particles were observed by using confocal laser scanning microscopy and turbidity measurements. CNC with length of 90 nm, diameter of 8 nm and zeta potential of -51.5 mV (in H₂O at neutral pH) was used to investigate the depletion effect of CNC in bacterial systems. Bacterial flocculation was observed at the CNC concentration of less than 0.1% due to the depletion effect. These results indicate that rod-shaped nanosized CNC are effective for the depletion flocculation of colloidal size bacteria and that phase separation of bacteria can occur at very low concentrations of CNC particles. In order to verify the impact of extracellular polymeric substance (EPS) on bacterial aggregation and adhesion in the presence of CNC, deposition on silica surfaces of two *Pseudomonas fluorescens* strains (CHA0 and CHA19-WS) having different EPS producing capacities, was studied in the absence and presence of CNC. The results demonstrate that bacterial initial adhesion to solid surfaces can be significantly hindered by CNC and this hinderance is related to the amount of EPS. In the presence of CNC, bacteria with more EPS aggregated more significantly compared to bacteria with less EPS, and that bacterial deposition in this condition decreased to a greater extent. The effects of pH and IS on the aggregation and deposition of *E. coli* K12 on silica surfaces were investigated in the absence and presence of CNC. The results indicate that at pH ranging from 5.2 to 7.2 and IS ranging from 10 mM to 50 mM conditions, depletion attraction is the dominant mechanism for CNC induced bacterial aggregation.

Preface

Research for this thesis was conducted under the supervision of Dr. Yang Liu at the University of Alberta. Part of Chapter 3 was published as Sun X, Sheng Z and Liu Y, “Effects of silver nanoparticles on microbial community structure in activated sludge”. *Science of the Total Environment* 2013, 443: 828–835. Portions of Chapter 4 were published as Sun X, Danumah C, Liu Y and Boluk Y, “Flocculation of bacteria by depletion interactions due to rod-shaped cellulose nanocrystals.” *Chemical Engineering Journal* 2012, 198: 476–481. Part of Chapter 5 was published as Sun X, Lu Q, Boluk Y and Liu Y, “The impact of cellulose nanocrystals on the aggregation and initial adhesion of *Pseudomonas fluorescens* bacteria.” *Soft Matter* 2014, 10: 8923–8931. I, Xiaohui Sun, was in charge of performing experiments and analysis, and manuscripts composition, while my supervisor provided guidance and comments on the manuscripts.

Acknowledgment

It has been a great honor to spend five years in the Department of Civil and Environmental Engineering at University of Alberta. I would like to acknowledge all the persons who have supported me to complete my PhD program.

My first sincere gratitude is to my supervisor, Dr. Yang Liu, who gave me the opportunity to University of Alberta to start my PhD program. It is her continuous support, motivation, and helpful guidance over the past five years that made it possible for me to finish my degree. I would not have been able to proceed through the PhD program and complete my dissertation without her hands-on instructions and encouragement on both my professional and personal life.

I would also like to thank Dr. Yaman Boluk for serving as my committee member, and for his help on my projects, including providing samples, insightful comments and suggestions for my publications. Sincere appreciation is due to Dr. Chuanwu Xi of University of Michigan for serving as the external examiner for this dissertation. Constructive and professional comments from all committee members are highly appreciated.

All my fellow labmates in Dr. Liu's Group and other groups deserve my gratitude: Dr. Hamed Mahdavi, Dr. Shahinoor Islam, Dr. Yijing Shi, Jiaming Liang, and Huixin Zhang, for their help with experiments, for the stimulating discussions, for the time we were working together, and for all the fun we have had during my PhD program. In particular, I am grateful to Zhiya Sheng, Elena Dlusskaya, and Chen Liang for teaching me molecular biology techniques and for helpful suggestions throughout my experiments.

My thanks to the financial supports from Natural Sciences and Engineering Research Council (NSERC) of Canada.

Last but not least, a special thanks to my family. The love, unconditional support, and encouragement from my parents, my husband, and my daughter, and all of the sacrifices you have made provided my inspiration and allowed me to get through those rough roads.

Table of Contents

Chapter 1 Introduction.....	1
1.1. Background.....	1
1.1.1. Nanoparticles and their antimicrobial effects	1
1.1.2. The application of cellulose nanocrystals (CNC) in bacterial systems	3
1.2. Objectives	6
1.2.1. Impact of Ag NPs on activated sludge microbial community structures	7
1.2.2. Impact of CNC on bacterial aggregation and adhesion.....	8
1.3. Significance of the Research.....	9
1.4. Thesis Outline	10
References	12
Chapter 2 Literature Review	17
2.1. Antimicrobial Mechanisms and Efficiency of Ag NPs	17
2.2. Activated Sludge Wastewater Treatment Process	18
2.3. Research Progress on Ag NPs Antimicrobial Effects and Gaps	19
2.4. Bacterial Aggregation and Depletion Mechanism	21
2.5. Bacterial Adhesion	25

2.6. Factors Impacting Bacterial Aggregation and Adhesion	26
2.6.1. Bacterial surface structure	26
2.6.2. Solution chemistry: pH and IS.....	27
2.7. Approaches/Models for Understanding Mechanisms of Bacterial	
Aggregation and Adhesion	27
2.7.1. Thermodynamic approach	28
2.7.2. Classic Derjaguin-Landau-Verwey-Overbeek (DLVO) theory	30
2.7.3. Extended DLVO (XDLVO) theory	33
2.7.4. Steric (polymer-mediated) interactions	34
References	36
Chapter 3 Effects of Silver NPs on Microbial Community Structure in Activated	
Sludge.....	51
3.1. Introduction	51
3.2. Material and Methods.....	53
3.2.1. Activated sludge samples	53
3.2.2. Preparation and characterization of Ag NPs suspensions	54
3.2.3. Ag NPs toxicity experiments.....	54
3.2.4. Bacterial enumeration using HPC	55
3.2.5. Activated sludge microbial community analysis using PCR-DGGE	55
3.3. Results	55
3.3.1. Activated sludge characterization.....	55

3.3.2. Ag NPs characterization	57
3.3.3. Effects of Ag NPs on heterotrophic cell culturability in activated sludge samples	59
3.3.4. Microbial communities in activated sludge samples	61
3.4. Discussion	65
3.4.1. Mechanisms involved in activated sludge susceptibility to Ag NPs	65
3.4.2. Environmental implications	69
Supplementary Material.....	71
References	74
Chapter 4 Flocculation of Bacteria by Depletion Interactions	82
Due to Rod-shaped CNC	82
4.1. Introduction	82
4.2. Experimental.....	84
4.2.1. CNC suspension preparation	84
4.2.2. Bacterial system.....	86
4.2.3. Aggregation measurements with CLSM	87
4.2.4. Jar test for coagulation.....	88
4.3. Results and Discussion	88
4.4. Conclusion.....	94
References	95

Chapter 5 Impact of CNC on the Aggregation and Initial Adhesion of	
Pseudomonas fluorescens Bacteria.....	99
5.1. Introduction	99
5.2. Material and Methods.....	101
5.2.1. Culture and characterization of bacteria	101
5.2.2. CNC suspension: preparation and characterization.....	102
5.2.3. Bacterial aggregation experiments	102
5.2.4. Bacterial initial adhesion experiments: batch method.....	103
5.2.5. Bacterial initial adhesion experiments: continuous flow method.....	104
5.2.6. DLVO interaction energy calculations	106
5.3. Results	107
5.3.1. Characterization of bacterial cells and CNC particles.....	107
5.3.2. Bacterial aggregation.....	108
5.3.3. Batch bacterial initial adhesion.....	110
5.3.4. Bacterial initial adhesion under continuous flow conditions.....	111
5.3.5. Classic DLVO interactions.....	115
5.4. Discussion.....	118
5.4.1. Impact of CNC on bacterial aggregation.....	118
5.4.2. Impact of CNC on bacterial initial adhesion	120
5.5. Conclusion.....	123
Supplementary Material.....	124

References	130
Chapter 6 Impact of CNC on the Aggregation and Initial Adhesion to a Solid	
Surface of Escherichia coli K12: Role of Solution Chemistry	137
6.1. Introduction	137
6.2. Material and Methods.....	138
6.2.1. Culture and characterization of bacterial cells	138
6.2.2. CNC suspension preparation and characterization	139
6.2.3. Bacterial aggregation experiment.....	140
6.2.4. Bacterial initial adhesion to a silica surface	140
6.2.5. Theoretical interaction energy calculations for bacterial aggregation.....	141
6.3. Results and Discussion	143
6.3.1. Characterization of bacterial cells and CNC particles.....	143
6.3.2. Impact of IS on bacterial aggregation and initial bacterial adhesion (pH =	
7.2).....	145
6.3.3. Impact of pH on bacterial aggregation and initial bacterial adhesion (IS =	
10 mM)	150
6.4. Conclusion.....	153
Supplementary Material.....	154
References	158

Chapter 7 Impact of CNC on the Aggregation of Pseudomonas aeruginosa: Role of EPS	162
7.1. Background	162
7.2. Experimental	163
7.2.1. Cellulose nanocrystals (CNC)	163
7.2.2. Bacterial system.....	163
7.2.3. EPS isolation.....	164
7.2.4. Preparation of glucose and humic acid suspension	164
7.2.5. Experimental protocols.....	164
7.3. Results and Discussion	165
References	169
Chapter 8 Conclusions	171
8.1. Impact of Ag NPs on Wastewater Activated Sludge	171
8.2. Impact of CNC on Bacterial Aggregation/Adhesion and Their Environmental Implications	172
References	175

List of Figures

- Figure 1.1. Structure formula of CNC 4
- Figure 2.1. Schematic of the depletion interaction 22
- Figure 3.1. Activated sludge floc size distribution and light microscopy images of activated sludge samples: (A) Floc size distribution in intact sludge samples and unsettled sludge samples; (B) Light microscopy image of an intact sludge sample; (C) Light microscopy image of an unsettled sludge sample 56
- Figure 3.2. Effects of 1 mg/L Ag NPs on the surface structure of activated sludge samples with and without 3 hours gravity-settling: (A) SEM of an intact sludge sample (no Ag NPs treatment); (B) SEM of an intact sludge sample treated with 1 mg/L Ag NPs for 24 hours; (C) SEM of an unsettled sludge sample (no Ag NPs treatment); (D) SEM of an unsettled sludge sample treated with 1 mg/L Ag NPs for 24 hours. (2000 × magnification, bar size = 15 μm) 58
- Figure 3.3. Effects of 1 mg/L Ag NPs on heterotrophic cell culturability in activated sludge samples (error bars represent one standard deviation): (A) number of fast-growing heterotrophic bacteria (24 hours after plating) in intact sludge samples with and without 1 mg/L Ag NPs treatment; (B) number of total heterotrophic bacteria (3 days after plating) in intact sludge samples with and without 1 mg/L Ag NPs treatment; (C) number of fast-growing heterotrophic bacteria (24 hours after plating) in unsettled sludge samples with and without 1 mg/L Ag NPs treatment; (D) number of total heterotrophic bacteria (3 days after plating) in unsettled sludge samples with and without 1 mg/L Ag NPs treatment 60

Figure 3.4. Microbial community profile of activated sludge: (A) phylogenetic tree based on DGGE bands; (B) Linkage analysis dendrogram of DGGE profiles of the intact sludge (lane 1), intact sludge treated with 1 mg/L Ag NPs (lane 2), the unsettled sludge (lane 3), and the unsettled sludge treated with 1 mg/L Ag NPs (lane 4)	63
Figure 3.5. Schematic of the physical structure of activated sludge flocs in the intact sludge (left) and the unsettled sludge (right). Dashed lines with arrowheads show the diffusion gradients of Ag NPs in an good settleability activated sludge floc (not to scale)	67
Figure 4.1. An AFM image of CNC particles	85
Figure 4.2. An SEM image of <i>P. aeruginosa</i> PAO1 (bar = 1µm)	86
Figure 4.3. Confocal fluorescence slices from the substrate surface and the sidebars illustrate sectional view of the structure along the z-axis. (A) Bacteria without CNC; (B) Bacteria with CNC presence (bacteria to CNC ratio was 1:100,000)	88
Figure 4.4. Aggregation percentage change over 24 hours of bacterial suspensions with and without CNC (Error bars represent one standard deviation)	89
Figure 4.5. Schematic depiction of depletion and phase separation of bacteria due to the presence of rod shaped nanoparticles	90
Figure 5.1. Representative SEM micrographs of (A) <i>P. flu</i> CHA0 and (B) <i>P. flu</i> CHA19-WS	106
Figure 5.2. A TEM image of CNC particles (Bar size = 200 nm)	106

Figure 5.3. Enumeration of batch bacterial adhesion studies. Each data point represents the average of three measurements for one sample. Error bars represent the standard deviation

109

Figure 5.4. Representative QCM-D adhesion results (The frequency change ΔF and dissipation change ΔD responses for the adsorption of CNC, bacteria with CNC and bacteria respectively obtained from QCM-D measurements. Solutions were sequentially pumped through the SiO₂ sensor surface in the following order: 10 mM of NaCl (0–10 minutes, flat line in the figure), samples (CNC, mixture of bacteria and CNC, bacteria) in 10 mM NaCl (starting from the arrowed position), and 10 mM of NaCl (starting from the arrowed position) at 0.15 mL/min.) (A) Adsorption profile of *P. flu* CHA0 with and without CNC; (B) Adsorption profile of *P. flu* CHA19-WS with and without CNC; (C) Cell density (cells/cm²) on silica surface after QCM-D adhesion experiments. Each data point represents the average of three measurements for one sample. Error bars represent the standard deviation

110

Figure 6.1. An SEM micrograph of *E. coli* K12

140

Figure 6.2. Zeta potential of CNC and *E. coli* K12 as a function of pH (in 10 mM of NaCl) (A) and IS (at pH = 7.2) (B). Each data point represents the average of three measurements for one sample. Error bars represent the standard deviation

141

Figure 6.3. Impact of IS on *E. coli* K12 aggregation and adhesion with and without CNC.

(A) Average aggregates size (the equivalent spherical radius of one bacterial

cluster); (B) DLVO interaction energy profiles; (C) Depletion interaction energy profiles; (D) Average adhesion cell density (error bars represent one standard deviation) (pH = 7.2) 143

Figure 6.4. Impact of pH on bacterial aggregation and adhesion with and without CNC.

(A) Average aggregates size (the equivalent spherical radius of one bacterial cluster); (B) DLVO interaction energy profiles; (C) Depletion interaction energy profiles; (D) Average adhesion cell density (error bars represent one standard deviation) (IS = 10 mM) 148

Figure 7.1. Representative images of bacterial aggregation with and without CNC. (Bar size = 20 μm) 163

List of Tables

Table 5.1. Key parameters used in DLVO calculations and interaction energies as calculated by DLVO theory	107
Table 7.1. Samples and average size of bacterial flocs in each sample	162

List of Abbreviations

NPs	Nanoparticles
CNC	Cellulose Nanocrystals
EPS	Extracellular Polymeric Substances
LPS	Lipopolysaccharide
ROS	Reactive Oxygen Species
DNA	Deoxyribonucleic Acid
rRNA	Ribosomal Ribonucleic Acid
PCR	Polymerase Chain Reaction
DGGE	Denaturing Gradient Gel Electrophoresis
HPC	Heterotrophic Plate Count
SEM	Scanning Electron Microscopy
TEM	Transmission Electron Microscopy
CLSM	Confocal Laser Scanning Microscopy
QCM-D	Quartz Crystal Microbalance with Dissipation
DLS	Dynamic Light Scattering
OD₆₀₀	Optical Density at 600 nm
IS	Ionic Strength
EDL	Electrical Double Layer
DLVO	Derjaguin-Landau-Verwey-Overbeek Theory
XDLVO	Extended DLVO Theory

Chapter 1 Introduction

1.1. Background

1.1.1. Nanoparticles and their antimicrobial effects

Engineered nanoparticles (NPs) are intentionally manufactured chemical substances or materials roughly 1–100 nm in size (Abraham et al., 2013; Dale et al., 2015; Lowry et al., 2012). Due to their extremely small size, NPs have large surface areas, and possess unique physical and chemical properties that are not seen in their macroscopic counterparts. The enhanced strength, durability, flexibility, and performance associated with nanomaterials have been exploited in various applications including consumer products, alternative energy, and medicinal uses (Louie et al., 2013). Despite a bright outlook for the future of nanotechnology, the increasing manufacture and application of NPs have raised concerns over their potential risks to human health and the environment. For instance, with the widespread use of NPs in commercial products (e.g., home appliances, medical equipment), it is inevitable that NPs will be released into and accumulated in domestic and industrial waste streams (such as wastewater treatment systems), which might have unknown effects. A recent study on the fate of NPs in wastewater treatment systems showed that most NPs are retained in biological wastewater treatment systems (Kiser et al., 2009). Because many NPs are designed to inhibit or prevent biological activities (known as the antimicrobial property) through different antimicrobial mechanisms, those NPs retained in biological wastewater treatment systems could decrease the effectiveness of contaminant removal and cause noncompliance with effluent discharge limits.

NPs of interest include metal or metal oxide NPs, fullerenes (C_{60}), and carbon nanotubes (CNTs). The antimicrobial properties of metal or metal oxide NPs (such as silver, TiO_2) have been investigated in recent studies (Cho et al., 2005; Choi et al., 2008; Choi and Hu, 2008; Lok et al., 2006; Morones et al., 2005) because of their widespread application in commercial products. Among different engineered metal NPs, the antimicrobial activities of silver NPs (Ag NPs) have been studied the most because they are the NPs most commonly used to disinfect appliances in the home, medical institutions, food industries, and in water treatment and distribution systems (Konopka et al., 2009; Kumar and Raza, 2009; Silvestry-Rodriguez et al., 2008). For example, Ag NPs are extensively used as antimicrobial agents in washing machines and as disinfectants in medical equipment. Although extensive studies have been performed on the antimicrobial effect of Ag NPs on certain lab-cultured microorganisms (such as *Escherichia coli*, *Pseudomonas*) under lab scale conditions, the impact of retained Ag NPs on environmental biological systems (e.g., biological wastewater treatment systems) is not clear; and the environmental implications are largely unknown. Moreover, there are conflicting results reported by previous studies on the antimicrobial effects of Ag NPs on environmental samples. For example, Bradford et al. (2009) found that Ag NPs presented little or no impact on estuarine sediment bacterial diversity, but Fabrega et al. (2011) indicated that Ag NPs could affect the relative abundance of major bacterial groups in the natural marine biofilm community with potential longer-term effects on biofilm development. In order to maximize the potential benefits of nanotechnology while minimizing the unintended negative effects on the environment, it is therefore necessary

to investigate the impact of retained Ag NPs on biological wastewater treatment systems, and the environmental implications. A very recent study reported that Ag NPs have pronounced side effects on activated sludge community structure and floc structure (Yang et al., 2014). However, the impact of the physical structure of activated sludge flocs on the response of microbial community structure to the toxicity of Ag NPs is unknown. The physical structures of activated sludge flocs are essential for their biological treatment efficiency; these structures can be evaluated using flocs settleability. Activated sludge flocs with good settleability are usually large in size, while flocs with poor settleability are usually small (“pinpoint flocs”) (Andreadakis, 1993; Grijspeerdt and Verstraete, 1997; Jin et al., 2003). Since mass transfer into the microbial flocs is driven by diffusion, physical structures of activated sludge flocs may be a critical factor for the diffusion and transportation of Ag NPs inside the flocs. Furthermore, the spatial distribution of the microbes on activated sludge flocs is important to bacterial activities. It is possible that bacteria on the surface of activated sludge flocs are more exposed to a relatively higher threat of Ag NPs. In addition, the toxicity of Ag NPs is strain-dependent (Gao et al., 2011; Sheng and Liu, 2011). Community structures of microorganisms in activated sludge may impact the response of bacteria to Ag NPs. To the best of the author’s knowledge, no study has previously been performed to evaluate the impact of activated sludge floc structure (such as the floc size) and the spatial distribution of microorganisms in the flocs on the microbial community’s response to the toxicity of NPs.

1.1.2. The application of cellulose nanocrystals (CNC) in bacterial systems

In comparison to metal and metal oxide NPs, cellulose nanocrystals (CNC) are a type of biodegradable NP, which have aroused public attention recently. Due to their uniform size distribution, low density (1.5 g/cm^3), and high aspect ratio (L/D typically 25) (Hemraz et al., 2014), CNC can increase the strength and stiffness of materials to which they are added, and are therefore widely used in coatings, films, textiles, and reinforcing fillers. CNC are prepared by sulfuric acid hydrolysis of pure cellulose, which is the most important component of cell walls of plants. The hydrolysis of cellulose by concentrated sulfuric acid in a controlled mode removes the amorphous regions (areas of low crystallinity) of cellulose molecules and isolates homogeneous regions (areas of high crystallinity), which are the nanocrystals. CNC particles in aqueous solutions are negatively charged due to sulfate ester groups on the surface (Figure 1.1) introduced by the esterification reaction. Therefore, sulfuric acid processed CNC surfaces yield stable suspensions in water (Boluk et al., 2012). CNC are typically 6–10 nm in width and 80–200 nm in length (Boluk et al., 2011).

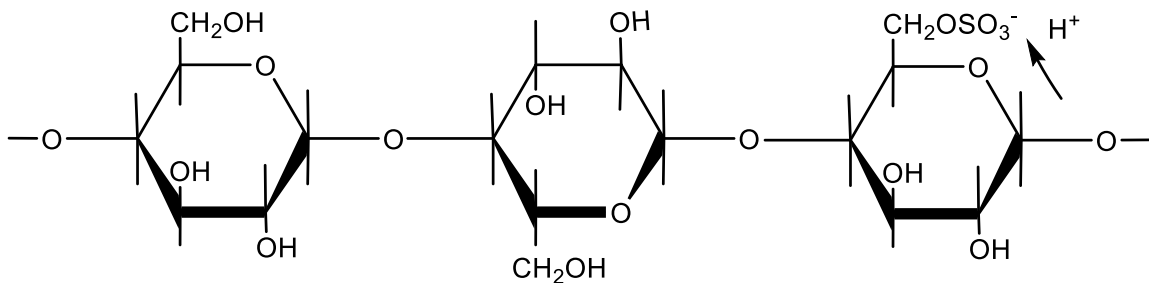


Figure 1.1. Structure formula of CNC

Bacterial aggregation and adhesion, resulting in the formation of bioflocs and biofilm, is one of such key colloidal activities that water treatment aims to control. For instance, the formation of activated sludge flocs in clarifiers, aerated lagoons, or anaerobic sludge

blanket bioreactors is critical for bioreactors to achieve a wide range of remediation results, including nutrient consumption, xenobiotic compound degradation, and metal immobilization (Gavrilescu and Macoveanu, 1999; Moharikar et al., 2005; Okunuki et al., 2004). In contrast, biofouling and biocorrosion (Kumar and Anand, 1998; Mattilasandholm and Wirtanen, 1992) in food industry, water treatment, and distribution systems are typical adverse effects of biofilm formation. Bacteria can be considered to be dispersions of negatively charged colloidal particles surrounded by non-adsorbing polyelectrolytes—extracellular polymeric substances (EPS). Controlling the stability of bacterial systems is critical in water treatment as well as in a range of other industrial applications, such as in the manufacture of paints, coatings, papers, pharmaceuticals, and ceramics (Farinato and Dubin, 1999).

Destabilization of bacterial systems (bacterial aggregation and adhesion), like other inert colloidal systems, depends on van der Waals forces, electrostatic forces, hydrophobic, and steric forces between bacteria (Liang et al., 2007). Steric forces become important if polymers exist in colloidal suspensions. Steric interactions are due to either adsorption or non-adsorption of polymers onto colloidal particle surfaces. Most of the previous work to control microbial aggregation and to understand the susceptibility of microbial aggregations investigates the role of adsorbing polymers, which involves the chemical or physical adsorption of macromolecular chains to the bacteria interface. The presence of adsorbed macromolecular chains on bacterial surfaces can destabilize the colloidal system by bridging the particles and promoting the formation of flocs. Alternatively, non-adsorbing polymers can also cause flocculation through a depletion

mechanism (Jenkins and Snowden, 1996). If macromolecular chains are not adsorbing on particle surfaces, they can cause attraction between particles by a mechanism called depletion (Asakura and Oosawa, 1958). Some experimental observations have been made on various colloidal particles–non-adsorbing polymer mixtures, such as mixtures of filamentous virus and the neutral polymer dextran (Dogic et al., 2004), silica particles and non-adsorbing polymers (Snowden et al., 1991), CNC and dextran (Edgar and Gray, 2002), and CNC and hydroxyethyl cellulose (Boluk et al., 2012). Nevertheless, the depletion of non-adsorbing polymers for the aggregation of bacterial suspensions is not well exploited despite the fact that bacteria can be considered as dispersions of negatively charged colloidal particles.

Likewise, the addition of repelling NPs (negatively charged), such as CNC, into the dispersion of bigger colloidal bacterial particles (negatively charged) might also be able to destabilize and flocculate the system by a depletion mechanism. If so, CNC might be an excellent candidate for the creation and manipulation of bacterial flocs. Artificial formation of bioflocs and control of the development of biofilms are relevant to many applications involving biodegradation or bioremediation. Thus, it would be beneficial to better understand the susceptibility of bacterial aggregation and adhesion to CNC.

1.2. Objectives

There are two general objectives of this thesis research. The first one is to understand the potential antibacterial effect of Ag NPs on biological wastewater treatment processes (activated sludge system). The second is to understand the impact of CNC on bacterial aggregation and adhesion. Details related to these objectives are listed below:

1.2.1. Impact of Ag NPs on activated sludge microbial community structures

It is hypothesized that the impact of Ag NPs on activated sludge microbial community structures depends on the physical structure of the activated sludge flocs (such as floc size). The goal is to assess the impact of activated sludge floc size on the response of microorganisms to Ag NPs.

Self-dispersing silver nanopowder was purchased from SkySpring Nanomaterials, Inc. (Houston, USA). According to the specification of the Ag NPs product, the particle size is less than 15 nm, and the particle composition is 10% silver (99.99% purity) and 90% polyvinylpyrrolidone (PVP) coating, which is similar to the Ag NPs that are commonly used in commercial products (Brar et al., 2010).

Activated sludge samples were collected (February, 2011) from Gold Bar Wastewater Treatment Plant located in Edmonton, Alberta, Canada right before each experiment. Samples were allowed to settle by gravity to separate good and poor settleability flocs; samples at time 0 hour (unsettled samples) and supernatants at time 3 hours were removed and used for Ag NPs toxicity experiments. Light microscopy was applied to characterize activated sludge samples. Floc size distribution was determined based on light microscopy images. Experiments were performed to determine the effects of 1 mg/L Ag NPs on microbial communities in activated sludge. Activated sludge samples with and without gravity settling were compared to evaluate the impact of activated sludge floc size on the response of microbial communities to Ag NPs. The effects of 10 mg/L, and 200 mg/L Ag NPs on microbial communities in activated sludge were also investigated and compared with 1 mg/L Ag NPs. The effects of Ag NPs on the entire

microbial community in activated sludge were analyzed using 16S rRNA gene based polymerase chain reaction-denaturing gradient gel electrophoresis (PCR-DGGE). Bacterial enumeration was achieved by the heterotrophic plate count (HPC) assay. Scanning electron microscopy (SEM) and light microscopy were applied to characterize the activated sludge flocs. For each batch of experiments, one control was analyzed together with the treated samples. Different samples were analyzed in triplicate, then averaged.

1.2.2. Impact of CNC on bacterial aggregation and adhesion

It is hypothesized that CNC can cause bacterial aggregation and also affect bacterial adhesion, and these effects are concentration dependent. The goal is to evaluate the factors (CNC concentration, solution pH, ionic strength (IS), EPS) that impact bacterial aggregation and initial adhesion in the presence of CNC, and to understand the mechanisms involved in bacterial aggregation and initial adhesion in the presence of CNC.

Gram-negative *Pseudomonas aeruginosa* PAO1 was selected to perform CNC-induced bacterial aggregation experiments in the presence of CNC with different concentrations. Confocal laser scanning microscopy (CLSM) was used to photograph the morphology of the bacterial aggregates. Optical density of the samples at 600 nm (OD₆₀₀) was measured to determine the aggregation percentage over time.

Gram-negative strains of *Pseudomonas fluorescence* wild type with GFP (*P. fluorescence* CHA0, normal EPS production) and the mutant with GFP that can overproduce some sugars of the EPS (*P. fluorescence* CHA19-WS, increased EPS

production) were selected to perform the impact of EPS on CNC-induced bacterial aggregation and their impact on bacterial initial adhesion experiments. SEM and transmission electron microscopy (TEM) were used to photograph the surface structure of bacterial cells and CNC particles respectively. Fluorescent microscopy was applied to illustrate the size of aggregates. HPC was used to complete bacterial enumeration for adhesion experiments.

Escherichia coli K12 was selected to perform the impact of pH and IS on CNC-induced bacterial aggregation and their impact on bacterial initial adhesion experiments. Fluorescent microscopy was applied to illustrate the size of *E. coli* K12 aggregates. HPC was used to complete bacterial enumeration for adhesion experiments.

Impact of EPS, glucose, and humic acid (HA) on bacterial aggregation in the presence of CNC was investigated.

Qualitative and quantitative analysis on bacterial aggregation and bacterial adhesion were performed by using microscopic techniques and the quartz crystal microbalance with dissipation (QCM-D, Q-sense E4, Biolin Scientific, Sweden) technique, both of which are very useful for understanding the mechanisms of bacterial aggregation and initial adhesion in the presence of CNC.

1.3. Significance of the Research

This study investigates the effect of engineered NPs on environmental biological systems. The knowledge obtained will enable the future development of strategies for maximizing the benefits and minimizing the potential risks of nanotechnology in environmental biological systems. This is the first detailed investigation of the

antimicrobial effects of Ag NPs on bacterial community structure in an activated sludge system and the impact of sludge floc structure on the response of bacteria to the toxicity effects of Ag NPs. The information obtained from this thesis research is critical to wastewater treatment facilities, as biological treatment is the backbone of their operations and any unanticipated loss of efficiency would significantly reduce the contaminant loads they are able to process. This is also the first detailed study on the impact of CNC on bacterial aggregation and adhesion. The information obtained through this line of inquiry will provide better understanding of the susceptibility of bacterial aggregation and adhesion to CNC. The results will also benefit wastewater treatment facilities, because CNC might be an excellent candidate for the creation and manipulation of bacterial flocs, and artificial formation of bioflocs and control of the development of biofilms are of interest in many applications involving biodegradation or bioremediation.

1.4. Thesis Outline

The structure of this dissertation is presented below.

Chapter 1 introduces the background, research objectives, and significance of this study.

Chapter 2 reviews previous research in seven sections: (1) antimicrobial mechanisms and efficiency of Ag NPs; (2) activated sludge wastewater treatment process; (3) the antimicrobial effects of Ag NPs; (4) depletion interaction in bacterial aggregation; (5) bacterial adhesion; (6) factors impact bacterial aggregation and adhesion; (7) approaches/models for understanding mechanisms of bacterial aggregation and adhesion.

Chapter 3 presents a study of the effects of silver NPs on microbial community structure in activated sludge. The physical structure of activated sludge flocs on the response of microbial community structure to the toxicity of Ag NPs was evaluated.

Chapter 4 investigates the impact of rod-shaped CNC on flocculation of bacteria by depletion interaction; these effects are concentration dependent.

Chapter 5 presents a study which evaluates the impact of CNC on the aggregation and initial adhesion of bacterial cells with different EPS-producing capabilities.

Chapter 6 evaluates the impact of solution chemistry (pH and IS) on bacterial aggregation and initial adhesion in the presence of CNC.

Chapter 7 evaluates the impact of EPS on bacterial aggregation in the presence of CNC. The role of glucose and humic acid is also investigated.

Chapter 8 provides the conclusions of this dissertation.

References

- Abraham PM, Barnikol S, Baumann T, Kuehn M, Ivleva NP, Schaumann GE. Sorption of silver nanoparticles to environmental and model surfaces. *Environmental Science & Technology* 2013; 47: 5083-5091.
- Andreadakis AD. Physical and chemical-properties of activated-sludge floc. *Water Research* 1993; 27: 1707-1714.
- Asakura S, Oosawa F. Interaction between particles suspended in solutions of macromolecules. *Journal of Polymer Science* 1958; 33: 183-192.
- Boluk Y, Lahiji R, Zhao L, McDermott MT. Suspension viscosities and shape parameter of cellulose nanocrystals (CNC). *Colloids and Surfaces a-Physicochemical and Engineering Aspects* 2011; 377: 297-303.
- Boluk Y, Zhao LY, Incani V. Dispersions of nanocrystalline cellulose in aqueous polymer solutions: Structure Formation of Colloidal Rods. *Langmuir* 2012; 28: 6114-6123.
- Bradford A, Handy RD, Readman JW, Atfield A, Muehling M. Impact of silver nanoparticle contamination on the genetic diversity of natural bacterial assemblages in estuarine sediments. *Environmental Science & Technology* 2009; 43: 4530-4536.
- Brar SK, Verma M, Tyagi RD, Surampalli RY. Engineered nanoparticles in wastewater and wastewater sludge - Evidence and impacts. *Waste Management* 2010; 30: 504-520.

- Cho M, Chung HM, Choi WY, Yoon JY. Different inactivation behaviors of MS-2 phage and *Escherichia coli* in TiO₂ photocatalytic disinfection. *Applied and Environmental Microbiology* 2005; 71: 270-275.
- Choi O, Deng KK, Kim NJ, Ross L, Surampalli RY, Hu ZQ. The inhibitory effects of silver nanoparticles, silver ions, and silver chloride colloids on microbial growth. *Water Research* 2008; 42: 3066-3074.
- Choi O, Hu ZQ. Size dependent and reactive oxygen species related nanosilver toxicity to nitrifying bacteria. *Environmental Science & Technology* 2008; 42: 4583-4588.
- Dale AL, Casman EA, Lowry GV, Lead JR, Viparelli E, Baalousha M. Modeling Nanomaterial environmental fate in aquatic systems. *Environmental Science & Technology* 2015; 49: 2587-2593.
- Dogic Z, Purdy KR, Grelet E, Adams M, Fraden S. Isotropic-nematic phase transition in suspensions of filamentous virus and the neutral polymer Dextran. *Physical Review E* 2004; 69.
- Edgar CD, Gray DG. Influence of dextran on the phase behavior of suspensions of cellulose nanocrystals. *Macromolecules* 2002; 35: 7400-7406.
- Fabrega J, Zhang R, Renshaw JC, Liu WT, Lead JR. Impact of silver nanoparticles on natural marine biofilm bacteria. *Chemosphere* 2011; 85: 961-966.
- Farinato RS, Dubin PL. *Colloid-polymer interactions: from fundamentals to practice*. New York: John Wiley, 1999.

- Gao J, Wang Y, Hovsepian A, Bonzongo JCJ. Effects of engineered nanomaterials on microbial catalyzed biogeochemical processes in sediments. *J Hazard Mater* 2011;186:940-5.
- Gavrilescu M, Macoveanu M. Process engineering in biological aerobic wastewater treatment. *Acta Biotechnologica* 1999; 19: 111-145.
- Grijspeerdt K, Verstraete W. Image analysis to estimate the settleability and concentration of activated sludge. *Water Research* 1997; 31: 1126-1134.
- Hemraz UD, Lu A, Sunasee R, Boluk Y. Structure of poly(N-isopropylacrylamide) brushes and steric stability of their grafted cellulose nanocrystal dispersions. *Journal of Colloid and Interface Science* 2014; 430: 157-165.
- Jenkins P, Snowden M. Depletion flocculation in colloidal dispersions. *Advances in Colloid and Interface Science* 1996; 68: 57-96.
- Jin B, Wilen BM, Lant P. A comprehensive insight into floc characteristics and their impact on compressibility and settleability of activated sludge. *Chemical Engineering Journal* 2003; 95: 221-234.
- Kiser MA, Westerhoff P, Benn T, Wang Y, Perez-Rivera J, Hristovski K. Titanium nanomaterial removal and release from wastewater treatment plants. *Environmental Science & Technology* 2009; 43: 6757-6763.
- Konopka M, Kowalski Z, Wzorek Z. Disinfection of meat industry equipment and production rooms with the use of liquids containing silver nanoparticles. *Archives of Environmental Protection* 2009; 35: 107-115.

- Kumar CG, Anand SK. Significance of microbial biofilms in food industry: a review. *International Journal of Food Microbiology* 1998; 42: 9-27.
- Kumar RV, Raza G. Photocatalytic disinfection of water with Ag-TiO₂ nanocrystalline composite. *Ionics* 2009; 15: 579-587.
- Liang Y, Hilal N, Langston P, Starov V. Interaction forces between colloidal particles in liquid: theory and experiment. *Advances in Colloid and Interface Science* 2007; 134-35: 151-166.
- Lok CN, Ho CM, Chen R, He QY, Yu WY, Sun HZ, et al. Proteomic analysis of the mode of antibacterial action of silver nanoparticles. *Journal of Proteome Research* 2006; 5: 916-924.
- Louie SM, Tilton RD, Lowry GV. Effects of molecular weight distribution and chemical properties of natural organic matter on gold nanoparticle aggregation. *Environmental Science & Technology* 2013; 47: 4245-4254.
- Lowry GV, Gregory KB, Apte SC, Lead JR. Transformations of nanomaterials in the environment. *Environmental Science & Technology* 2012; 46: 6893-6899.
- Mattilasandholm T, Wirtanen G. Biofilm formation in the industry - a review. *Food Reviews International* 1992; 8: 573-603.
- Moharikar A, Purohit HJ, Kumar R. Microbial population dynamics at effluent treatment plants. *Journal of Environmental Monitoring* 2005; 7: 552-558.
- Morones JR, Elechiguerra JL, Camacho A, Holt K, Kouri JB, Ramirez JT, et al. The bactericidal effect of silver nanoparticles. *Nanotechnology* 2005; 16: 2346-2353.

- Okunuki S, Kawaharasaki M, Tanaka H, Kanagawa T. Changes in phosphorus removing performance and bacterial community structure in an enhanced biological phosphorus removal reactor. *Water Research* 2004; 38: 2433-2439.
- Sheng ZY, Liu Y. Effects of silver nanoparticles on wastewater biofilms. *Water Research* 2011; 45: 6039-6050.
- Silvestry-Rodriguez N, Bright KR, Slack DC, Uhlmann DR, Gerba CP. Silver as a residual disinfectant to prevent biofilm formation in water distribution systems. *Applied and Environmental Microbiology* 2008; 74: 1639-1641.
- Snowden MJ, Clegg SM, Williams PA, Robb ID. Flocculation of silica particles by adsorbing and nonadsorbing polymers. *Journal of the Chemical Society-Faraday Transactions* 1991; 87: 2201-2207.
- Yang Y, Quensen J, Mathieu J, Wang Q, Wang J, Li M, et al. Pyrosequencing reveals higher impact of silver nanoparticles than Ag^+ on the microbial community structure of activated sludge. *Water Research* 2014; 48: 317-325.

Chapter 2 Literature Review

2.1. Antimicrobial Mechanisms and Efficiency of Ag NPs

Previous studies reported various antimicrobial mechanisms of Ag NPs. For instance, some studies proposed that the toxicity of Ag NPs to microorganisms is associated with the oxidative stress generated by the formation of reactive oxygen species (ROS, include $^1\text{O}_2$, O_2^- , H_2O_2 , $\text{OH}\cdot$) on the surface of Ag NPs (Akdin et al., 2008; Choi and Hu, 2008; Hwang et al., 2008; Kim et al., 2014). Furthermore, Choi et al. (2008) indicated that Ag NPs can pass through cell membranes and accumulate in the cell causing cell malfunction. Other studies revealed that Ag NPs attached to the cell membrane can change membrane permeability and cause final cell death (Lok et al., 2006; Morones et al., 2005; Sondi and Salopek-Sondi, 2004). Some researchers have also suggested that Ag NPs might weaken cell membranes by damaging enzymes (Morones et al., 2005). Gou et al. (2010) and Dimkpa et al. (2011) discovered that Ag NPs do not damage the cell membrane, but affect the electron transport. Ag NPs might damage DNA and thus prevent cell replication (Berger, 2007). Release of Ag^+ from Ag NPs can enhance antimicrobial effect of Ag NPs (Bottero et al., 2011; Ratte, 1999), but it remains unclear if Ag NPs are the primary cause of the enhanced toxicity. Sotiriou and Pratsinis (2010) reported that when the average size of Ag NPs is smaller than 10 nm, Ag NPs will release many Ag^+ , which is the dominant reason of toxicity. However, when the size of Ag NPs exceed 10 nm, less Ag^+ is released and the primary reason of toxicity is Ag NPs. Yang et al. (2014) reported that compared to Ag^+ , Ag NPs result in a more pronounced effect on activated sludge community structure, possibly because Ag^+ can more easily be

scavenged by inorganic ligands and organic matter than Ag NPs can be. It has also been reported that the overall negative charge of bacterial EPS repels Ag NPs (Luongo and Zhang, 2010; Sheng and Liu, 2011), which are also negatively charged and thus protect bacteria from Ag NPs' toxicity. EPS can also quench ROS generated by Ag treatments or EPS may bind Ag⁺ released from Ag NPs and reduce the extent of their cellular contact. However, EPS protection can be circumvented at high concentrations of Ag NPs (Dimkpa et al., 2011).

Several studies have been performed to evaluate the efficiency with which Ag NPs inhibit microorganisms. Choi and Hu (2008) showed that Ag NPs at a concentration of 1 mg/L can inhibit more than 80% of the growth of autotrophic nitrifying organisms. They also demonstrated that Ag NPs have the highest potential among all the Ag species tested (including Ag NPs, Ag⁺ ions and AgCl colloids) to inhibit the growth of nitrifying bacteria, and the effect of Ag NPs on bacteria growth was size-dependent. Ag NPs less than 5 nm in size were more toxic to bacteria than larger Ag NPs. Similar results were obtained by Elechiguerra et al. (2005) who found that the average size of Ag NPs penetrating an *E. coli* membrane was about 5 nm.

2.2. Activated Sludge Wastewater Treatment Process

Activated sludge system is one widely used biological wastewater treatment process, which is the most common suspended growth process used for both municipal and industrial wastewater treatment. In the aeration tank, extensive organic compounds and nutrients (nitrogen and phosphorus) will be consumed by microorganisms through the metabolic reactions under aerobic conditions. The settled biomass (described as activated

sludge) will be partially returned to the aeration tank to provide sufficient solids for solid flocculation and clarification, and partially removed from secondary clarifier, leaving a relatively clear liquid as the treated effluent. An important feature of the activated sludge process is the formation of biological flocs, ranging in size from approximately 10–600 μm , and comprised of microorganisms, extracellular biopolymers, and organic and inorganic compounds (De Clercq et al., 2004; Metcalf and Eddy, 2003). The microorganisms are the backbone of the activated sludge flocs used to degrade and remove pollutants, so any unanticipated effects on the microorganisms (such as the microbial viability and diversity) would significantly reduce the contaminant removal efficiency that they are able to achieve.

2.3. Research Progress and Gaps on Ag NPs Antimicrobial Effects

Previous research has focused on the toxic effect of Ag NPs on pure cultured microorganisms, such as *E. coli* (Dror-Ehre et al., 2009; Elechiguerra et al., 2005; Sondi and Salopek-Sondi, 2004) and *Pseudomonas putida* (Fabrega et al., 2009), cultivated under laboratory conditions. However, microorganisms in natural environments often exist as complex communities; for instance, multi-species assemblages may share an ecological niche and interact among themselves and with their environment. Microbial communities play a critical role in various engineering applications including wastewater treatment and food processing (Mohanty et al., 2014). The Web of Science database contains a very limited number of studies that have investigated the impact of Ag NPs on complex microorganism communities in natural and engineered ecosystems (Bradford et al., 2009; Fabrega et al., 2011; Priester et al., 2014; Sheng and Liu, 2011). For instance,

Sheng and Liu (2011) reported that original wastewater biofilms are resistant to Ag NP treatment but become more sensitive after soluble EPS is removed from the biofilms. Bradford et al. (2009) reported that the microbial community diversity in estuarine sediments is only slightly impacted by Ag NPs treatment. Similarly, the bacterial communities in activated sludge are not altered by Ag NPs (Priester et al., 2014). Conversely, Fabrega et al. (2011) found that Ag NPs have significant adverse effects on microbial communities in natural marine biofilms. These conflicting results might be due to different environmental factors or different microbial community structures.

Ag NPs adsorbed to activated sludge biomass are, in general, toxic to microbial communities present in the biomass. For example, Priester et al. (2014) demonstrated that Ag NPs can potentially inhibit biological phosphorus removal through the toxic effects of dissolved Ag⁺ on polyhydroxybutyrate (PHB) producers (lower PHB biosynthesis). Jeong et al. (2014) reported that microbial susceptibility of activated sludge bacteria to Ag NPs is different and that the microbial diversity decreases dramatically after continuous exposure to Ag NPs, resulting in a decrease of wastewater treatment efficiency. To assess the toxicity of Ag NPs on engineered ecosystems, microbial communities in waste or wastewater treatment processes (such as the activated sludge process) are often used as model systems and most studies focus on the microbial growth activity, microbial community structure, and community function in terms of treatment efficiency of the processes (Mohanty et al., 2014). The effects of CuO NPs on the physicochemical properties of the activated sludge flocs and the production and composition of the EPS have just been reported recently (Hou et al., 2015). Nevertheless, the impact of activated

sludge flocs' physical structures (such as floc size) and the spatial distribution of microorganisms in the flocs on the response of microbial community to the toxicity of Ag NPs remain unclear.

2.4. Bacterial Aggregation and Depletion Mechanism

Similar to any other inert colloidal particles, aggregation of bacteria is facilitated by van der Waals forces, electrostatic forces and steric forces between bacteria (Liang et al., 2007). The electrostatic repulsive interaction is associated with the fact that bacterial cells are, in general, negatively charged and plays a crucial role in the stability of bacterial systems. Steric forces become important if polymers exist in colloidal suspensions. Steric interactions are due to either adsorption or non-adsorption of polymers onto colloidal particle surfaces. The presence of adsorbed macromolecular chains on bacterial surfaces can destabilize the colloidal system by bridging bacteria and promoting the formation of bioflocs. In bacterial systems, the secretion of EPS, consisting polysaccharides, proteins, nucleic acids, lipids, and humic substances are believed to play role in the microbial dispersion stability and floc formation (Flemming and Wingender, 2001a; Flemming and Wingender, 2001b; Kreft and Wimpenny, 2001). In addition, synthetic cationic or non-ionic polymers are also added into microbial systems to facilitate microbial aggregation, where charge neutralization and inter-particle bridging are the mechanisms at work (Larsen et al., 2009; Strand et al., 2001).

Alternatively, non-adsorbing polymers can also destabilize a colloidal system through a depletion mechanism (Jenkins and Snowden, 1996). The depletion force between colloidal particles due to the presence of non-adsorbing polymers was first described

theoretically by Asakura and Oosawa (1958). Later, through theoretical and experimental study, Vrij (1976) further developed the theory that colloidal dispersions are destabilized by non-adsorbing polymers. The depletion interaction is schematically demonstrated in Figure 2.1, where colloidal particles are hard spheres each with a radius R in a polymer solution where polymer chains are represented with smaller spheres each of a diameter σ . Each colloidal particle is surrounded by a layer (the depletion layer) into which polymer chains cannot penetrate. The concentration of polymer molecules outside of the depletion layer is equal to the polymer's bulk concentration.

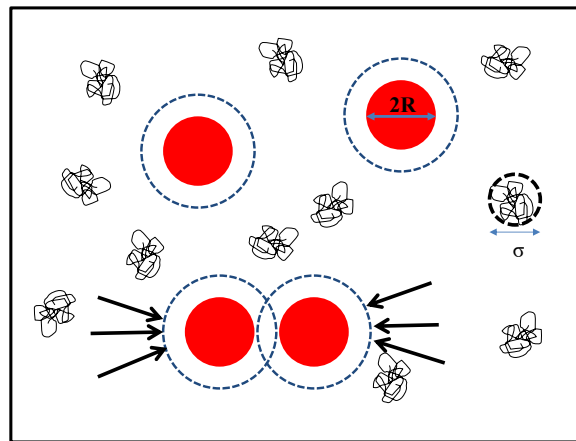


Figure 2.1. Schematic of the depletion interaction

The existing osmotic pressure gradient is isotropic for a single sphere. However, for particles separated by less than σ , the depletion layers of the particles overlap. Hence, the depletion is caused by an imbalance in osmotic pressure when two particles approach each other and their polymer nonaccessible layer volumes overlap. Exclusion of polymers in depletion zones next to particle surfaces maximizes the entropy of the system and drives the coagulation of particles (Lekkerkerker and Tuinier, 2011; Tuinier et al., 2003).

Depletion forces have been applied widely to destabilize colloids. By introducing small particles into a bigger colloidal dispersion, depletion attraction can be induced between dispersed colloidal particles. These attractive interactions bring the dispersed particles together resulting in flocculation; consequently, flocs can be easily removed through filtration processes. Therefore, in wastewater treatment process, coagulants and flocculants are usually introduced to create depletion forces between the dispersed particles and initiate flocculation of contaminants.

Theoretical studies on the depletion of colloids have been advanced by applying theories of the behavior of polymer solutions developed by Flory (1953), Gennes (1979) and Fleer and Scheutjens (1983). Depletion interactions between two flat plates, two spheres, and a sphere and a flat plate are calculated while the depleting polymer is modeled as penetrable hard spheres or ideal chains as reviewed by Lekkerkerker and Tuinier (2011). The models work very well to show the interaction potential and explain the phase separation of depleted particles if the colloidal particles are larger than the characteristic size of the polymers ($2R \gg \sigma$). The range covered with this assumption is called the “colloidal limit” (Fuchs and Schweizer, 2002). Experimental observations of many colloidal particles–non-adsorbing polymer mixtures and direct and indirect measurements of interaction potentials agree with model predictions (Dogic et al., 2004; Edgar and Gray, 2002; Snowden et al., 1991). Nevertheless, the depletion of non-adsorbing polymers in bacterial suspensions has not been well studied despite the fact that bacteria can be considered as a dispersion of negatively charged colloidal particles surrounded by non-adsorbing polyelectrolytes—EPS. Aggregation and phase separation

of *E. coli* bacteria due to the presence of sodium polystyrene sulfonate has only been reported recently (Eboigbodin et al., 2005). According to the theory, rod-shaped particles are more efficient depletion agents than spherical particles, and can flocculate and phase separate colloids at concentrations lower than spherical depletants can. However, to phase separate colloidal particles of 1 μm radii, depletant particles must each have a length, L , much smaller than the radius, R , of each of the large colloidal particles, and must also have a high aspect ratio (L/D). As an example, phase separation of colloidal particles of 1 μm radii in the presence of thin, rod-shaped particles needs NPs of a length in the order of 100 nm and diameter less than 10 nm with appropriate surface chemistry. Such prediction has been experimentally verified only once with the depletion of silica particles in the presence of silica coated, rod-shaped nano-boehmite particles (Koenderink et al., 1999). Nevertheless, due to the limited number of commercially available NPs, this effect has never been experimentally shown in an industrially applicable scheme. Experimental observations on aggregation and phase separation of big colloidal particles due to the presence of very small (nanosize) depletant colloidal particles are also scarce. Until now, only the phase separation of micrometer-sized silica particles due to the presence of silica-coated, nanosized boehmite rods have been reported (Lyon et al., 2008; Silvestry-Rodriguez et al., 2008). Likewise, the introduction of NPs into the dispersion of bigger colloidal bacterial cells should also be capable of destabilizing the bacterial system by way of a depletion mechanism. Thus, rod-shaped NPs, namely CNC, must be good candidates for depleting bacterial systems. It is important to note that enhancement of depletion forces by electrostatic depletant

repulsion was previously reported by Buzzaccaro et al. (2010). Thus, due to the negative surface charge of both bacteria and CNC particles, the electrostatic repulsion between bacteria and CNC should enhance the depletion attraction resulting in more effective depletion.

2.5. Bacterial Adhesion

Bacterial adhesion to a substratum is a two-stage process consisting of the initial reversible adhesion of cells followed by a time-dependent firmer and irreversible attachment (An and Friedman, 1998; Dan, 2003; Marshall, 1985; Marshall et al., 1971). Initial adhesion is dominated by physical forces between the cells and the substrate, such as Brownian motion, van der Waals forces, gravitational forces, electrostatic forces, and hydrophobic interactions (An and Friedman, 1998; Busscher et al., 1992). In the second-stage adhesion, polymer bridging or binding by means of surface adhesins and substrates become dominant because bacteria consolidate the adhesion via surface polymers, such as EPS, lipopolysaccharide (LPS) (Czaczyk and Myszka, 2007), proteins (Dufrene et al., 1996), pili or fimbriae (Krogfelt, 1991), and flagella. Their compositions and amount may vary with the environment conditions (Vandevivere and Kirchman, 1993).

The net sum of attractive and repulsive forces generated between the bacterium and the substrate dominates the strength of bacterial adhesion (Dunne, 2002). Because most bacterial and inert surfaces are negatively charged (Jucker et al., 1996), repulsions are electrostatically favored. Attractive or repulsive hydrophobic interactions are important due to their polar origin and can be up to two orders of magnitude higher than Van der Waals or electrostatic forces (Carpentier and Cerf, 1993; Olofsson et al., 1998; Ubbink

and Schar-Zammaretti, 2007). Bacterial adhesion is significantly affected by various environmental factors such as pH, and IS. The properties of the bacterial surface also play important roles in bacterial adhesion. The physico-chemical properties of bacterial surface structures vary according to bacteria species and strains, and result in different bacterial adhesion behaviors (An and Friedman, 2000; Høgt et al., 1985).

Bacterial adhesion can be detrimental to both human life and industrial processes, causing pathogen contamination, biocorrosion, and biofouling (Kumar and Anand, 1998; Mattilasandholm and Wirtanen, 1992). Conversely, microbial adhesion can be beneficial when it is employed in bioreactors to remove contaminants, degrade xenobiotic compounds, and immobilize metals (Habash and Reid, 1999; Salerno et al., 2007).

2.6. Factors Impacting Bacterial Aggregation and Adhesion

2.6.1. Bacterial surface structure

Unlike other inert collidal particles, the complex and heterogeneous surface structures of bacteria, such as the surface appendages, complicate the interactions between bacteria and bacteria, and bacteria and substratum surfaces. Thus, bacterial aggregation and adhesion are also associated with the physico-chemical properties of the bacterial surface. Bacterial surface appendages, such as EPS, are believed to contribute to bacterial aggregation and adhesion, although their presence cannot be expressed by microbial contact angles and zeta potentials measurements (Bos et al., 1999). Because of its composition and properties, EPS can provide an attractive force with which to induce microbial aggregation into flocs and biological sludge, and to attach biofilms to solid surfaces (Flemming and Wingender, 2001b; Kreft and Wimpenny, 2001). It is essential to

understand the susceptibility of these biopolymers to these behaviours. Eboigbodin et al. (2005) showed that EPS were involved in the depletion attraction-induced bacterial aggregation and phase separation of *E. coli* cells.

2.6.2. Solution chemistry: pH and IS

It is well known that the properties of the dispersant, such as the pH and/or IS, will significantly affect the surface properties of the colloidal particles, such as zeta potential. Due to the net negative charge of most bacterial surfaces and solid surfaces, electrostatic interactions are involved between bacteria and bacteria, and bacteria and the support (McEldowney and Fletcher, 1986). The electrostatic repulsion between cells, as well as between cells and the support surface, can be controlled by pH. Cell surfaces are less negatively charged at lower pH due to the deprotonation of various chemical groups, such as carboxyl (Rijnaarts et al., 1995b), which results in a decreased electrostatic repulsion and enhanced adhesion between the bacteria and the support (Jiang et al., 2011).

The IS of the medium is another important factor affecting electrostatic interaction. Based on the electrical double layer (EDL) theory, an increase of IS will suppress the EDL, resulting in a decrease of the zeta potential of a colloidal particle (Berg, 2010). The reduced repulsive electrostatic forces may facilitate bacterial aggregation or adhesion through the attractive Lifshitz-van der Waals and Lewis acid-base forces (Jiang et al., 2011). However, some studies showed contradictory results, steric forces may play the role (McEldowney and Fletcher, 1986; Otto et al., 1999; Yee et al., 2000).

2.7. Approaches/Models for Understanding Mechanisms of Bacterial Aggregation and Adhesion

2.7.1. Thermodynamic approach

In the thermodynamic approach towards bacterial adhesion, the interfacial free energies γ between the interacting surfaces are compared. Accordingly, the free energy of adhesion ΔG_{adh} is measured using equation 1.1 (Absolom et al., 1983; Busscher et al., 1984) and applied to express this comparison:

$$\Delta G_{adh} = \gamma_{sb} - \gamma_{sl} - \gamma_{bl} \quad 1.1$$

where γ_{sb} , γ_{sl} , and γ_{bl} are solid-bacterium, solid-liquid, and bacterium-liquid interfacial free energies, respectively. Bacterial adhesion is favored when ΔG_{adh} is negative, while it is energetically unfavorable when ΔG_{adh} is positive. Equation 1.1 can also be constructed to cover bacterial coaggregation and coadhesive interactions by replacing the solid with an identical bacterium or partner organisms.

The interfacial free energy is related to contact angle θ in the contact angle equilibrium according to Young's equation:

$$\gamma_{lv} \cos\theta = \gamma_{sv} - \gamma_{sl} \quad 1.2$$

in which the subscripts l , v , and s denote liquid, vapor, and solid, respectively. Contact angles with liquids can be measured both on solid substrata and on bacterial lawns (Vanoss and Gillman, 1972) simply by putting microliter-sized liquid droplets on the surface. When contact angles on bacterial lawns are measured, the subscript s should be replaced by b .

The surface free energy consists of an apolar of Lifshitz-van der Waals (LW) component γ^{LW} and a polar of Lewis acid-base (AB) component γ^{AB} . The most

commonly used combination of these components is the geometric mean shown in equation 1.3:

$$\gamma_{sl} = \left(\sqrt{\gamma_{sv}^{LW}} - \sqrt{\gamma_{lv}^{LW}} \right)^2 + \left(\sqrt{\gamma_{sv}^{AB}} - \sqrt{\gamma_{lv}^{AB}} \right)^2 \quad 1.3$$

γ^{AB} can be further separated into an electron pair-donating component γ^- and an electron pair-accepting component γ^+ (van Oss et al., 1987), yielding equation 1.4:

$$\gamma_{sl} = \left(\sqrt{\gamma_{sv}^{LW}} - \sqrt{\gamma_{lv}^{LW}} \right)^2 + 2 \left(\sqrt{\gamma_{sv}^+ \gamma_{sv}^-} + \sqrt{\gamma_{lv}^+ \gamma_{lv}^-} - \sqrt{\gamma_{sv}^- \gamma_{lv}^+} - \sqrt{\gamma_{sv}^+ \gamma_{lv}^-} \right) \quad 1.4$$

combining equations 1.2 and 1.4 yields:

$$(1 + \cos\theta)\gamma_l = 2 \left(\sqrt{\gamma_s^{LW} \gamma_l^{LW}} + \sqrt{\gamma_s^+ \gamma_l^-} + \sqrt{\gamma_s^- \gamma_l^+} \right) \quad 1.5$$

It should be noted that the surface free energy components (γ^{LW} , γ^+ , and γ^-) are associated with contact angle θ measurements with at least three different liquids, such as water, formamide (or glycerol), and methylene iodide (or α -bromonaphthalene) (Bos et al., 1999).

In the LW-AB approach, the total Gibbs free energy for the adhesion of bacterial cells to a solid substrate in water ΔG_{slb}^{TOT} is the sum of a LW component ΔG_{slb}^{LW} and an AB component ΔG_{slb}^{AB} , as evaluated in equations 1.6, 1.7 and 1.8 (Bayouhd et al., 2009; Bhattacharjee and Elimelech, 1997).

$$\Delta G_{slb}^{TOT} = \Delta G_{slb}^{LW} + \Delta G_{slb}^{AB} \quad 1.6$$

$$\Delta G_{slb}^{LW} = -2 \left(\sqrt{\gamma_{sv}^{LW}} - \sqrt{\gamma_{lv}^{LW}} \right) \left(\sqrt{\gamma_{bv}^{LW}} - \sqrt{\gamma_{lv}^{LW}} \right) \quad 1.7$$

$$\Delta G_{slb}^{AB} = +2\left[\left(\sqrt{\gamma_{sv}^+} - \sqrt{\gamma_{bv}^+}\right)\left(\sqrt{\gamma_{sv}^-} - \sqrt{\gamma_{bv}^-}\right) - \left(\sqrt{\gamma_{sv}^+} - \sqrt{\gamma_{lv}^+}\right)\left(\sqrt{\gamma_{sv}^-} - \sqrt{\gamma_{lv}^-}\right) - \left(\sqrt{\gamma_{bv}^+} - \sqrt{\gamma_{lv}^+}\right)\left(\sqrt{\gamma_{bv}^-} - \sqrt{\gamma_{lv}^-}\right)\right] \quad 1.8$$

Once the surface tension components for the solid are determined from equation 1.5, ΔG_{slb}^{LW} and ΔG_{slb}^{AB} can be calculated from equations 1.7 and 1.8. Since LW forces are predominantly attractive, the ΔG_{adh}^{LW} values in bacterial interactions are nearly always negative. Accordingly, more or less favorable conditions for interactions must be inferred from the acid-base interactions ΔG_{adh}^{AB} , which can be positive or negative.

In the thermodynamic model, it is assumed that the interacting surfaces are physically in contact each other under conditions of thermodynamic equilibrium (reversible adhesion). The model only provides a straightforward examination of the cell surface free energy change without considering the electrostatic interactions. The physical and chemical heterogeneity of bacterial and solid surfaces, and the complex bacteria-surface interactions, are not fully accounted for in the thermodynamic model (Bos et al., 1999; Chen and Strevett, 2003; Hori and Matsumoto, 2010; Ong et al., 1999; Tufenkji, 2007; Tufenkji and Elimelech, 2005; Vadhillo-Rodriguez et al., 2005).

2.7.2. Classic Derjaguin-Landau-Verwey-Overbeek (DLVO) theory

Classic DLVO theory describes total energies between interacting surfaces in solution as a balance between attractive LW and repulsive or attractive electrostatic interactions as a function of separation distance, d (equation 1.9) (Berkeley, 1980):

$$\Delta G^{TOT}(d)_{classic} = \Delta G^{LW}(d) + \Delta G^{EL}(d) \quad 1.9$$

in which ΔG^{TOT} , ΔG^{LW} , and ΔG^{EL} denote the total, the LW and the electrostatic interaction energy, respectively. Classic DLVO theory has been applied to explain bacterial adhesion to surfaces (Hermansson, 1999; Palmer et al., 2007). In addition to contact angle θ measurements, zeta potentials of the interacting surfaces are required to apply this theory. Bacterial adhesion to a substratum surface can be assumed to take the form of a sphere (with a radius of a) approaching a semi-infinite plate, and $\Delta G^{LW}(d)$ and $\Delta G^{EL}(d)$ are expressed as:

$$\Delta G^{LW}(d) = -\frac{A}{6} \left[\frac{a}{d} + \frac{a}{d+2a} + \ln \left(\frac{d}{d+2a} \right) \right]$$

$$\Delta G^{EL}(d) = \pi \epsilon a (\zeta_1^2 + \zeta_2^2) \left[\frac{2\zeta_1 \zeta_2}{\zeta_1^2 + \zeta_2^2} \ln \frac{1 + \exp(-\kappa d)}{1 - \exp(-\kappa d)} + \ln \{1 - \exp(-2\kappa d)\} \right] \quad 1.10$$

$$A = -12\pi d_0^2 \Delta G_{adh}^{LW}$$

where A , ϵ , ζ , and κ^{-1} are Hamaker constant, the permittivity of the medium, the zeta potential, the Debye length, respectively; d_0 is the closest approach distance between two surfaces; ϵ represents the product of the permittivity of a vacuum ϵ_0 (8.854×10^{-12} C²/J·m) and the relative permittivity (formerly called the dielectric constant) of the medium ϵ_r (80 for water at 20°C). κ^{-1} is expressed as:

$$1/\kappa = \left[(\epsilon k T) / (e^2 \sum v_i^2 n_i) \right]^{1/2} \quad 1.11$$

where k and e are the Boltzmann constant ($k = 1.38 \times 10^{-23}$ J/K) and the charge of an electron ($e = 1.602 \times 10^{-19}$ C), respectively; T is the absolute temperature in degrees K; and v_i and n_i are the valency and the number density (per mL of bulk liquid) of each

ionic species, respectively. For two interacting spherical particles with the respective radii a_1 and a_2 (bacterial coaggregation), $\Delta G^{LW}(d)$ and $\Delta G^{EL}(d)$, are expressed as:

$$\begin{aligned}\Delta G^{LW}(d) &= -\frac{A(a_1 a_2)}{6d(a_1 + a_2)} \\ \Delta G^{EL}(d) &= \frac{\pi \epsilon a_1 a_2 (\zeta_1^2 + \zeta_2^2)}{(a_1 + a_2)} \left[\frac{2\zeta_1 \zeta_2}{\zeta_1^2 + \zeta_2^2} \ln \frac{1 + \exp(-\kappa d)}{1 - \exp(-\kappa d)} + \ln\{1 - \exp(-2\kappa d)\} \right] \\ A &= -12\pi d_0^2 \Delta G_{adh}^{LW}\end{aligned}\tag{1.12}$$

$\Delta G^{LW}(d)$ in solution is normally attractive, while $\Delta G^{EL}(d)$ may be attractive or repulsive depending on surface charges and solution IS. IS does not affect the LW attraction, but affects both the range and the magnitude of the electrostatic interactions. At low IS, long-range electrostatic repulsion or attraction dominates bacterial adhesion, but at high IS, electrostatic interactions lose their influence. Depending on the IS, a so-called secondary minimum of a few kT exists, in which microorganisms are believed to become reversibly captured prior to the primary minimum adhesion that requires a closer approach (Zeng, 2013).

Based on the assumption that bacteria can be seen as model colloidal particles, the classic DLVO theory can successfully explain bacterial adhesion behavior when LW and electrostatic interactions have a dominant role during adhesion (Rijnaarts et al., 1999). However, the bacterial surface is highly complex and dynamic, leading to inconsistencies in the classic DLVO prediction of bacterial adhesion results (Abu-Lail and Camesano, 2003a; Abu-Lail and Camesano, 2003b; Jucker et al., 1998; Lu et al., 2011; Velegol and Logan, 2002; Walker et al., 2004). Considering that the bacterial surface is uneven and lacks evenly distributed surface charges, some previous studies modify the classic DLVO

theory (called soft-particle DLVO) by assuming that a bacterium is a rigid core surrounded by an ion-penetrable, charged polyelectrolyte layer (Abu-Lail and Camesano, 2003b; Hayashi et al., 2001). However, phenomena such as hydrophobic attractive (Ducker et al., 1994; Wood and Sharma, 1995) and hydrophilic repulsive (Elimelech, 1990) interactions between surfaces, as measured by force balance instruments, are inadequately explained by the classic DLVO theory.

2.7.3. Extended DLVO (XDLVO) theory

To consider hydrophobic attraction and hydrophilic repulsion, van Oss et al. (1986) introduced a so-called “extended” DLVO (XDLVO) theory by incorporating the short-range Lewis AB interaction energy $\Delta G^{AB}(d)$ in equation 1.9, yielding:

$$\Delta G^{TOT}(d)_{extended} = \Delta G^{LW}(d) + \Delta G^{EL}(d) + \Delta G^{AB}(d) \quad 1.13$$

The AB interaction energies $\Delta G^{AB}(d)$ as a function of separation distance, d , for the sphere-plate (equation 1.14) and sphere-sphere (equation 1.15) configurations are evaluated as:

$$\Delta G^{AB}(d) = 2\pi\alpha\lambda\Delta G_{adh}^{AB} \exp[(d_0 - d)/\lambda] \quad 1.14$$

$$\Delta G^{AB}(d) = \pi\alpha\lambda\Delta G_{adh}^{AB} \exp[(d_0 - d)/\lambda] \quad 1.15$$

Considering Lewis AB interaction energy $\Delta G^{AB}(d)$, the total interaction energies may be significantly changed. The XDLVO theory accounts for bacterial surface hydrophobicity, but the model is still not consistent with the bacterial adhesion results when considering a wide range of bacteria and surfaces (Li and Logan, 2004);

furthermore, the complexity of surface polymers is still not involved in the XDLVO theory.

2.7.4. Steric (polymer-mediated) interactions

The structural and chemical heterogeneity of the bacterial surface implies that bacterial adhesion will frequently deviate from theoretical adhesion models derived from simple colloidal particles. Surface polymers (such as EPS, LPS, and proteins) are associated with steric interactions with substrate surfaces. Strong steric repulsions have been detected between LPS layers and polystyrene surfaces (Lu et al., 2011; Strauss et al., 2009), as LPS O-antigens can mediate polymer-bridging (i.e., hydrogen-bonding) to mineral oxides (Jucker et al., 1997). Such polymer-mediated interactions can be repulsive or attractive depending on polymer and solid surface properties (Jucker et al., 1997; Jucker et al., 1998; Kim et al., 2010; Rijnaarts et al., 1999; Vanloosdrecht et al., 1990).

2.7.4.1 Steric repulsion

Bacterial surface biopolymers can be considered to constitute a polyelectrolyte brush layer; the increased local density of polymer segments leads to an increase in osmotic pressure and repulsive interaction energy. In aqueous media, steric repulsion occurs when the bacterial surface macromolecules are hydrophilic and have no affinity for the substratum. There is no simple and comprehensive theory available to cover the magnitude of the force between surfaces coated with polymers, whether the adsorption process is reversible or irreversible, and the solvent quality factor (de Gennes, 1987; Hesselink, 1971; Milner et al., 1988; Vrij, 1976).

2.7.4.2 Polymer bridging

Unlike steric repulsion, attractive polymer-mediated interactions (i.e., polymer bridging) take place if bacterial surface macromolecules, or parts of them, have an affinity for the substratum exceeding a certain critical value (Dobiás, 1993). Attractive polymer-mediated forces can be weak van der Waals bonding, strong van der Waals bonding (in liquid), hydrogen bonding, or strong ionic or biospecific ligand-receptor bonding (Israelachvili, 1992). Biopolymers on bacterial surfaces and biofilms may present different bridging mechanisms to NPs that depend on NPs surface properties and solution conditions (Jucker et al., 1997; Rijnaarts et al., 1999). Polymer bridging is generally observed for solids and microorganisms that are both hydrophobic (Absolom et al., 1983; Busscher et al., 1984; Rijnaarts et al., 1993; van Loosdrecht et al., 1987; van Loosdrecht et al., 1990).

References

- Absolom DR, Lamberti FV, Policova Z, Zingg W, van Oss CJ, Neumann AW. Surface thermodynamics of bacterial adhesion. *Applied and Environmental Microbiology* 1983; 46: 90-97.
- Abu-Lail NI, Camesano TA. Role of ionic strength on the relationship of biopolymer conformation, DLVO contributions, and steric interactions to bioadhesion of *Pseudomonas putida* KT2442. *Biomacromolecules* 2003a; 4: 1000-1012.
- Abu-Lail NI, Camesano TA. Role of lipopolysaccharides in the adhesion, retention, and transport of *Escherichia coli* JM109. *Environmental Science & Technology* 2003b; 37: 2173-2183.
- Akdim B, Hussain S, Pachter R. A density functional theory study of oxygen adsorption at silver surfaces: implications for nanotoxicity. *Computational Science - Iccs* 2008, Pt 2 2008; 5102: 353-359.
- An YH, Friedman RJ. Concise Review of mechanisms of bacterial adhesion to biomaterial surfaces. *Journal of Biomedical Materials Research* 1998; 43: 338-348.
- An YH, Friedman RJ. *Handbook of bacterial adhesion*. Totowa, NJ: Humana Press, 2000.
- Bayouhdh S, Othmane A, Mora L, Ben Ouada H. Assessing bacterial adhesion using DLVO and XDLVO theories and the jet impingement technique. *Colloids and Surfaces B-Biointerfaces* 2009; 73: 1-9.
- Berg JC. *An introduction to interfaces & colloids The bridge to Nanoscience*. New Jersey: World Scientific, 2010.

- Berger M. Stabilizing antimicrobial nanosilver on a natural porous plant material. 2010. Nanowerk Spotlight, 2007.
- Berkeley RCW. Microbial adhesion to surfaces. Chichester: Ellis Horwood, 1980.
- Bhattacharjee S, Elimelech M. Surface element integration: a novel technique for evaluation of DLVO interaction between a particle and a flat plate. *Journal of Colloid and Interface Science* 1997; 193: 273-285.
- Bos R, van der Mei HC, Busscher HJ. Physico-chemistry of initial microbial adhesive interactions - its mechanisms and methods for study. *Fems Microbiology Reviews* 1999; 23: 179-230.
- Bottero J-Y, Auffan M, Rose J, Mouneyrac C, Botta C, Labille J, et al. Manufactured metal and metal-oxide nanoparticles: properties and perturbing mechanisms of their biological activity in ecosystems. *Comptes Rendus Geoscience* 2011; 343: 168-176.
- Bradford A, Handy RD, Readman JW, Atfield A, Muehling M. Impact of silver nanoparticle contamination on the genetic diversity of natural bacterial assemblages in estuarine sediments. *Environmental Science & Technology* 2009; 43: 4530-4536.
- Busscher HJ, Cowan MM, Vandermei HC. On the relative importance of specific and nonspecific approaches to oral microbial adhesion. *Fems Microbiology Reviews* 1992; 88: 199-209.

- Busscher HJ, Weerkamp AH, van der Mei HC, van Pelt AW, de Jong HP, Arends J. Measurement of the surface free energy of bacterial cell surfaces and its relevance for adhesion. *Applied and Environmental Microbiology* 1984; 48: 980-983.
- Buzzaccaro S, Piazza R, Colombo J, Parola A. Enhancement of depletion forces by electrostatic depletant repulsion. *Journal of Chemical Physics* 2010; 132.
- Camesano TA, Liu YT, Datta M. Measuring bacterial adhesion at environmental interfaces with single-cell and single-molecule techniques. *Advances in Water Resources* 2007; 30: 1470-1491.
- Carpentier B, Cerf O. Biofilms and their consequences, with particular reference to hygiene in the food-industry. *Journal of Applied Bacteriology* 1993; 75: 499-511.
- Chen G, Strevett KA. Microbial surface thermodynamics and interactions in aqueous media. *Journal of Colloid and Interface Science* 2003; 261: 283-290.
- Choi O, Deng KK, Kim NJ, Ross L, Surampalli RY, Hu ZQ. The inhibitory effects of silver nanoparticles, silver ions, and silver chloride colloids on microbial growth. *Water Research* 2008; 42: 3066-3074.
- Choi O, Hu ZQ. Size dependent and reactive oxygen species related nanosilver toxicity to nitrifying bacteria. *Environmental Science & Technology* 2008; 42: 4583-4588.
- Czaczyk K, Myszka K. Biosynthesis of extracellular polymeric substances (EPS) and its role in microbial biofilm formation. *Polish Journal of Environmental Studies* 2007; 16: 799-806.
- Dan N. The Effect of charge regulation on cell adhesion to substrates: salt-induced repulsion. *Colloids and Surfaces B-Biointerfaces* 2003; 27: 41-47.

- De Clercq B, Lant PA, Vanrolleghem PA. Focused beam reflectance technique for in situ particle sizing in wastewater treatment settling tanks. *Journal of Chemical Technology and Biotechnology* 2004; 79: 610-618.
- de Gennes PG. Polymers at an interface; a simplified view. *Advances in Colloid and Interface Science* 1987; 27: 189-209.
- Dimkpa CO, Calder A, Gajjar P, Merugu S, Huang WJ, Britt DW, et al. Interaction of silver nanoparticles with an environmentally beneficial bacterium, *Pseudomonas chlororaphis*. *Journal of Hazardous Materials* 2011; 188: 428-435.
- Dobiás B. Coagulation and flocculation: theory and applications. New York: M. Dekker, 1993.
- Dogic Z, Purdy KR, Grelet E, Adams M, Fraden S. Isotropic-nematic phase transition in suspensions of filamentous virus and the neutral polymer Dextran. *Physical Review E* 2004; 69.
- Dror-Ehre A, Mamane H, Belenkova T, Markovich G, Adin A. Silver nanoparticle-*E. coli* colloidal interaction in water and effect on *E. coli* survival. *Journal of Colloid and Interface Science* 2009; 339: 521-526.
- Ducker WA, Xu Z, Israelachvili JN. Measurements of hydrophobic and DLVO forces in bubble-surface interactions in aqueous solutions. *Langmuir* 1994; 10: 3279-3289.
- Dufrene YF, Boonaert CJP, Rouxhet PG. Adhesion of *Azospirillum brasilense*: role of proteins at the cell-support interface. *Colloids and Surfaces B-Biointerfaces* 1996; 7: 113-128.

- Dunne WM. Bacterial adhesion: seen any good biofilms lately? *Clinical Microbiology Reviews* 2002; 15: 155-+.
- Eboigbodin KE, Newton JRA, Routh AF, Biggs CA. Role of nonadsorbing polymers in bacterial aggregation. *Langmuir* 2005; 21: 12315-12319.
- Edgar CD, Gray DG. Influence of dextran on the phase Behavior of suspensions of cellulose nanocrystals. *Macromolecules* 2002; 35: 7400-7406.
- Elechiguerra JL, Burt JL, Morones JR, Camacho-Bragado A, Gao X, Lara HH, et al. Interaction of silver nanoparticles with HIV-1. *J Nanobiotechnology* 2005; 3: 6.
- Elimelech M. Indirect evidence for hydration forces in the deposition of polystyrene latex colloids on glass surfaces. *Journal of the Chemical Society, Faraday Transactions* 1990; 86: 1623-1624.
- Fabrega J, Renshaw JC, Lead JR. Interactions of silver nanoparticles with *Pseudomonas putida* biofilms. *Environmental Science & Technology* 2009; 43: 9004-9009.
- Fabrega J, Zhang R, Renshaw JC, Liu WT, Lead JR. Impact of silver nanoparticles on natural marine biofilm bacteria. *Chemosphere* 2011; 85: 961-966.
- Fleer GJ, Scheutjens J. Depletion flocculation and stabilization. *Abstracts of Papers of the American Chemical Society* 1983; 186: 65-COLL.
- Flemming HC, Wingender J. Relevance of microbial extracellular polymeric substances (EPSs) - Part I: Structural and ecological aspects. *Water Science and Technology* 2001a; 43: 1-8.

- Flemming HC, Wingender J. Relevance of microbial extracellular polymeric substances (EPSs) - Part II: Technical aspects. *Water Science and Technology* 2001b; 43: 9-16.
- Flory PJ. Principles of polymer chemistry. Ithaca: Cornell University Press, 1953.
- Fuchs M, Schweizer KS. Structure of colloid-polymer suspensions. *Journal of Physics-Condensed Matter* 2002; 14: R239-R269.
- Genes P-Gd. Scaling concepts in polymer physics. Ithaca: Cornell University Press, 1979.
- Gou N, Onnis-Hayden A, Gu AZ. Mechanistic toxicity assessment of nanomaterials by whole-cell-array stress genes expression analysis. *Environmental Science & Technology* 2010; 44: 5964-5970.
- Habash M, Reid G. Microbial Biofilms: Their development and significance for medical device-related infections. *Journal of Clinical Pharmacology* 1999; 39: 887-898.
- Hayashi H, Tsuneda S, Hirata A, Sasaki H. Soft particle analysis of bacterial cells and its interpretation of cell adhesion behaviors in terms of DLVO theory. *Colloids and Surfaces B-Biointerfaces* 2001; 22: 149-157.
- Hermansson M. The DLVO theory in microbial adhesion. *Colloids and Surfaces B-Biointerfaces* 1999; 14: 105-119.
- Hesselink FT. Theory of the stabilization of dispersions by adsorbed macromolecules. I. Statistics of the change of some configurational properties of adsorbed macromolecules on the approach of an impenetrable interface. *The Journal of Physical Chemistry* 1971; 75: 65-71.

- Hogt AH, Dankert J, Feijen J. Adhesion of staphylococcus-epidermidis and staphylococcus-saprophyticus to a hydrophobic biomaterial. *Journal of General Microbiology* 1985; 131: 2485-2491.
- Hori K, Matsumoto S. Bacterial adhesion: From mechanism to control. *Biochemical Engineering Journal* 2010; 48: 424-434.
- Hou J, Miao L, Wang C, Wang P, Ao Y, Lv B. Effect of CuO nanoparticles on the production and composition of extracellular polymeric substances and physicochemical stability of activated sludge flocs. *Bioresource Technology* 2015; 176: 65-70.
- Hwang ET, Lee JH, Chae YJ, Kim YS, Kim BC, Sang B-I, et al. Analysis of the toxic mode of action of silver nanoparticles using stress-specific bioluminescent bacteria. *Small* 2008; 4: 746-750.
- Israelachvili JN. *Intermolecular and surface forces*. London, England: Academic Press Ltd., 1992.
- Jenkins P, Snowden M. Depletion flocculation in colloidal dispersions. *Advances in Colloid and Interface Science* 1996; 68: 57-96.
- Jeong E, Im W-T, Kim D-H, Kim M-S, Kang S, Shin H-S, et al. Different susceptibilities of bacterial community to silver nanoparticles in wastewater treatment systems. *Journal of Environmental Science and Health Part a-Toxic/Hazardous Substances & Environmental Engineering* 2014; 49: 685-693.

- Jiang L, Wang JF, Liang SZ, Cai J, Xu ZN. Control and optimization of *Clostridium tyrobutyricum* ATCC 25755 adhesion into fibrous matrix in a fibrous bed bioreactor. *Applied Biochemistry and Biotechnology* 2011; 165: 98-108.
- Jucker BA, Harms H, Hug SJ, Zehnder AJB. Adsorption of bacterial surface polysaccharides on mineral oxides is mediated by hydrogen bonds. *Colloids and Surfaces B-Biointerfaces* 1997; 9: 331-343.
- Jucker BA, Harms H, Zehnder AJB. Adhesion of the positively charged bacterium *Stenotrophomonas (Xanthomonas) maltophilia* 70401 to glass and teflon. *Journal of Bacteriology* 1996; 178: 5472-5479.
- Jucker BA, Zehnder AJB, Harms H. Quantification of polymer interactions in bacterial adhesion. *Environmental Science & Technology* 1998; 32: 2909-2915.
- Kim HN, Walker SL, Bradford SA. Macromolecule mediated transport and retention of *Escherichia coli* O157:H7 in saturated porous media. *Water Research* 2010; 44: 1082-1093.
- Kim JS, Kuk E, Yu KN, Kim J-H, Park SJ, Lee HJ, et al. Antimicrobial effects of silver nanoparticles (vol 1, pg 95, 2007). *Nanomedicine-Nanotechnology Biology and Medicine* 2014; 10: 1119-1119.
- Koenderink GH, Vliegthart GA, Kluijtmans S, van Blaaderen A, Philipse AP, Lekkerkerker HNW. Depletion-induced crystallization in colloidal rod-sphere mixtures. *Langmuir* 1999; 15: 4693-4696.

- Kreft JU, Wimpenny JWT. Effect of EPS on biofilm structure and function as revealed by an individual-based model of biofilm growth. *Water Science and Technology* 2001; 43: 135-141.
- Krogfelt KA. Bacterial adhesion - genetics, biogenesis, and role in pathogenesis of fimbrial adhesins of *Escherichia-Coli*. *Reviews of Infectious Diseases* 1991; 13: 721-735.
- Kumar CG, Anand SK. Significance of microbial biofilms in food industry: a review. *International Journal of Food Microbiology* 1998; 42: 9-27.
- Larsen MU, Seward M, Tripathi A, Shapley NC. Biocompatible nanoparticles trigger rapid bacteria clustering. *Biotechnology Progress* 2009; 25: 1094-1102.
- Lekkerkerker HNW, Tuinier R. *Colloids and Depletion*. Springer 2011; 100.
- Li BK, Logan BE. Bacterial adhesion to glass and metal-oxide surfaces. *Colloids and Surfaces B-Biointerfaces* 2004; 36: 81-90.
- Liang Y, Hilal N, Langston P, Starov V. Interaction forces between colloidal particles in liquid: theory and experiment. *Advances in Colloid and Interface Science* 2007; 134-35: 151-166.
- Lok CN, Ho CM, Chen R, He QY, Yu WY, Sun HZ, et al. Proteomic analysis of the mode of antibacterial action of silver nanoparticles. *Journal of Proteome Research* 2006; 5: 916-924.
- Lu QY, Wang J, Faghihnejad A, Zeng HB, Liu Y. Understanding the molecular interactions of lipopolysaccharides during *E. coli* initial adhesion with a surface forces apparatus. *Soft Matter* 2011; 7: 9366-9379.

- Luongo LA, Zhang XQ. Toxicity of carbon nanotubes to the activated sludge process. *Journal of Hazardous Materials* 2010; 178: 356-362.
- Lyon DY, Brown DA, Alvarez PJJ. Implications and potential applications of bactericidal fullerene water suspensions: effect of nC(60) concentration, exposure conditions and shelf life. *Water Science and Technology* 2008; 57: 1533-1538.
- Marshall KC. Bacterial adhesion in oligotrophic habitats. *Microbiological Sciences* 1985; 2: 321-&.
- Marshall KC, Stout R, Mitchell R. Mechanism of initial events in sorption of marine bacteria to surfaces. *Journal of General Microbiology* 1971; 68: 337-&.
- Mattilasandholm T, Wirtanen G. Biofilm formation in the industry - a review. *Food Reviews International* 1992; 8: 573-603.
- Metcalf and Eddy. *Wastewater Engineering: Treatment and Reuse (4th Edition)*. McGraw-Hill, New York, 2003.
- McEldowney S, Fletcher M. Variability of the influence of physicochemical factors affecting bacterial adhesion to polystyrene substrata. *Applied and Environmental Microbiology* 1986; 52: 460-465.
- Milner ST, Witten TA, Cates ME. Theory of the grafted polymer brush. *Macromolecules* 1988; 21: 2610-2619.
- Mohanty A, Wu Y, Cao B. Impacts of engineered nanomaterials on microbial community structure and function in natural and engineered ecosystems. *Applied Microbiology and Biotechnology* 2014; 98: 8457-8468.

- Morones JR, Elechiguerra JL, Camacho A, Holt K, Kouri JB, Ramirez JT, et al. The bactericidal effect of silver nanoparticles. *Nanotechnology* 2005; 16: 2346-2353.
- Olofsson AC, Zita A, Hermansson M. Floc stability and adhesion of green-fluorescent-protein-marked bacteria to flocs in activated sludge. *Microbiology-Sgm* 1998; 144: 519-528.
- Olsson ALJ, van der Mei HC, Busscher HJ, Sharma PK. Novel analysis of bacterium-substratum bond maturation measured using a quartz crystal microbalance. *Langmuir* 2010; 26: 11113-11117.
- Olsson ALJ, van der Mei HC, Busscher HJ, Sharma PK. Acoustic sensing of the bacterium-substratum interface using QCM-D and the influence of extracellular polymeric substances. *Journal of Colloid and Interface Science* 2011; 357: 135-138.
- Ong YL, Razatos A, Georgiou G, Sharma MM. Adhesion forces between *E. coli* bacteria and biomaterial surfaces. *Langmuir* 1999; 15: 2719-2725.
- Otto K, Elwing H, Hermansson M. Effect of ionic strength on initial interactions of *Escherichia coli* with surfaces, studied on-line by a novel quartz crystal microbalance technique. *Journal of Bacteriology* 1999; 181: 5210-5218.
- Palmer J, Flint S, Brooks J. Bacterial cell attachment, the beginning of a biofilm. *Journal of Industrial Microbiology & Biotechnology* 2007; 34: 577-588.
- Priester JH, Van De Werfhorst LC, Ge Y, Adeleye AS, Tomar S, Tom LM, et al. Effects of TiO₂ and Ag Nanoparticles on polyhydroxybutyrate biosynthesis by activated sludge bacteria. *Environmental Science & Technology* 2014; 48: 14712-14720.

- Ratte HT. Bioaccumulation and toxicity of silver compounds: a review. *Environmental Toxicology and Chemistry* 1999; 18: 89-108.
- Rijnaarts HHM, Norde W, Bouwer EJ, Lyklema J, Zehnder AJB. Bacterial adhesion under static and dynamic conditions. *Applied and Environmental Microbiology* 1993; 59: 3255-3265.
- Rijnaarts HHM, Norde W, Lyklema J, Zehnder AJB. The isoelectric point of bacteria as an indicator for the presence of cell-surface polymers that inhibit adhesion. *Colloids and Surfaces B-Biointerfaces* 1995; 4: 191-197.
- Rijnaarts HHM, Norde W, Lyklema J, Zehnder AJB. DLVO and steric contributions to bacterial deposition in media of different ionic strengths. *Colloids and Surfaces B-Biointerfaces* 1999; 14: 179-195.
- Salerno MB, Li X, Logan BE. Adhesion characteristics of two *Burkholderia cepacia* strains examined using colloid probe microscopy and gradient force analysis. *Colloids and Surfaces B-Biointerfaces* 2007; 59: 46-51.
- Sheng ZY, Liu Y. Effects of silver nanoparticles on wastewater biofilms. *Water Research* 2011; 45: 6039-6050.
- Silvestry-Rodriguez N, Bright KR, Slack DC, Uhlmann DR, Gerba CP. Silver as a residual disinfectant to prevent biofilm formation in water distribution systems. *Applied and Environmental Microbiology* 2008; 74: 1639-1641.
- Snowden MJ, Clegg SM, Williams PA, Robb ID. Flocculation of silica particles by adsorbing and nonadsorbing polymers. *Journal of the Chemical Society-Faraday Transactions* 1991; 87: 2201-2207.

- Sondi I, Salopek-Sondi B. Silver nanoparticles as antimicrobial agent: a case study on *E. coli* as a model for gram-negative bacteria. *Journal of Colloid and Interface Science* 2004; 275: 177-182.
- Sotiriou GA, Pratsinis SE. Antibacterial activity of nanosilver ions and particles. *Environmental Science & Technology* 2010; 44: 5649-5654.
- Strand SP, Vandvik MS, Varum KM, Ostgaard K. Screening of chitosans and conditions for bacterial flocculation. *Biomacromolecules* 2001; 2: 126-133.
- Strauss J, Liu YT, Camesano TA. Bacterial adhesion to protein-coated surfaces: an AFM and QCM-D study. *Jom* 2009; 61: 71-74.
- Tufenkji N. Modeling microbial transport in porous media: traditional approaches and recent developments. *Advances in Water Resources* 2007; 30: 1455-1469.
- Tufenkji N, Elimelech M. Breakdown of colloid filtration theory: role of the secondary energy minimum and surface charge heterogeneities. *Langmuir* 2005; 21: 841-852.
- Tuinier R, Rieger J, de Kruif CG. Depletion-induced phase separation in colloid-polymer mixtures. *Advances in Colloid and Interface Science* 2003; 103: 1-31.
- Ubbink J, Schar-Zammaretti P. Colloidal properties and specific interactions of bacterial surfaces. *Current Opinion in Colloid & Interface Science* 2007; 12: 263-270.
- Vadillo-Rodriguez V, Busscher HJ, van der Mei HC, de Vries J, Norde W. Role of lactobacillus cell surface hydrophobicity as probed by AFM in adhesion to surfaces at low and high ionic strength. *Colloids and Surfaces B-Biointerfaces* 2005; 41: 33-41.

- van Loosdrecht MC, Lyklema J, Norde W, Schraa G, Zehnder AJ. The role of bacterial cell wall hydrophobicity in adhesion. *Applied and Environmental Microbiology* 1987; 53: 1893-1897.
- van Loosdrecht MCM, Norde W, Lyklema J, Zehnder AJB. Hydrophobic and electrostatic parameters in bacterial adhesion - dedicated to Werner Stumm for his 65th birthday. *Aquatic Sciences* 1990; 52: 103-114.
- van Oss CJ, Chaudhury MK, Good RJ. Monopolar surfaces. *Advances in Colloid and Interface Science* 1987; 28: 35-64.
- Van Oss CJ, Good RJ, Chaudhury MK. The role of van der Waals forces and hydrogen bonds in "hydrophobic interactions" between biopolymers and low energy surfaces. *Journal of Colloid and Interface Science* 1986; 111: 378-390.
- Vandevivere P, Kirchman DL. Attachment stimulates exopolysaccharide synthesis by a bacterium. *Applied and Environmental Microbiology* 1993; 59: 3280-3286.
- Vanloosdrecht MCM, Norde W, Lyklema J, Zehnder AJB. Hydrophobic and electrostatic parameters in bacterial adhesion. *Aquatic Sciences* 1990; 52: 103-114.
- Vanoss CJ, Gillman CF. Phagocytosis as a surface phenomenon .1. contact angles and phagocytosis of non-opsonized bacteria. *Journal of the Reticuloendothelial Society* 1972; 12: 283-&.
- Velegol SB, Logan BE. Contributions of bacterial surface polymers, electrostatics, and cell elasticity to the shape of AFM force curves. *Langmuir* 2002; 18: 5256-5262.
- Vrij A. Polymers at interfaces and interactions in colloidal dispersions. *Pure and Applied Chemistry* 1976; 48: 471-483.

- Walker SL, Redman JA, Elimelech M. Role of cell surface lipopolysaccharides in *Escherichia coli* K12 adhesion and transport. *Langmuir* 2004; 20: 7736-7746.
- Wood J, Sharma R. How long is the long-range hydrophobic attraction? *Langmuir* 1995; 11: 4797-4802.
- Yang Y, Quensen J, Mathieu J, Wang Q, Wang J, Li M, et al. Pyrosequencing reveals higher impact of silver nanoparticles than Ag⁺ on the microbial community structure of activated sludge. *Water Research* 2014; 48: 317-325.
- Yee N, Fein JB, Daughney CJ. Experimental study of the pH, ionic strength, and reversibility behavior of bacteria-mineral adsorption. *Geochimica Et Cosmochimica Acta* 2000; 64: 609-617.
- Zeng H. *Polymer adhesion, friction, lubrication*. New Jersey: John Wiley & Sons, 2013.

Chapter 3 Effects of Silver NPs on Microbial Community Structure in Activated Sludge

3.1. Introduction

Nanotechnology, emerging in the 1980s, has grown in the 21st century to have the potential to profoundly affect human life. Due to the large surface areas of very small particles, NPs possess unique physical and chemical properties not seen in their macroscopic counterparts. The enhanced strength, durability, flexibility, and performance associated with nanomaterials have been exploited in a multitude of applications, including consumer products, alternative energy, and medicinal uses. Despite bright outlooks for the future of nanotechnology, concerns are expressed over the burgeoning availability of such novel and reactive particles to humans and the environment, particularly the natural aquatic environment (Ju-Nam and Lead, 2008). For instance, with the wide use of NPs in commercial products, it is inevitable that NPs will be released to waste streams. A recent study on the fate of NPs in wastewater treatment systems showed that most NPs are retained in biological wastewater treatment systems (Kiser et al., 2009). Activated sludge, a suspended microbial aggregate, is frequently applied to wastewater to remove organic compounds, biological nutrients (nitrogen and phosphorus), suspended solids, metals, and pathogens through the metabolic reactions of microorganisms. Activated sludge is a collection of biological flocs that consist of microorganisms, extracellular biopolymers, and organic and inorganic compounds (De Clercq et al., 2004; Metcalf and Eddy, 2003). Because many NPs are designed to inhibit

or prevent biological activity, NPs retained in the activated sludge flocs could decrease the effectiveness of contaminant removal.

Among different engineered NPs, the antimicrobial activities of Ag NPs have been studied the most widely because they are commonly used to disinfect appliances in the home, in medical institutions, and in food industries (Konopka et al., 2009; Silvestry-Rodriguez et al., 2008). Various antimicrobial mechanisms of Ag NPs have been examined. For instance, Choi et al. (2008) showed that, due to their small size, Ag NPs can pass through cell membranes and accumulate in the cell causing cell malfunction. Some researchers have suggested that Ag NPs might weaken cell membranes by damaging enzymes.

Previous research has concentrated on the effect of Ag NPs on pure cultured microorganisms, such as *E. coli* cultivated under laboratory conditions (Dror-Ehre et al., 2009; Elechiguerra et al., 2005; Sondi and Salopek-Sondi, 2004; Yoon et al., 2007). The Web of Science database contains a limited number of studies that investigated the impact of Ag NPs or other nanomaterials on complex microorganism communities (Bradford et al., 2009; Fabrega et al., 2011; Nogueira et al., 2012; Sheng and Liu, 2011). To our knowledge, no study has been performed to evaluate the impact of Ag NPs on the microbial communities in wastewater activated sludge, particularly, the impact of activated sludge floc structures on the microbial response to Ag NPs. The overall objective of the present study was to investigate the impact of Ag NPs on the microbial communities in wastewater activated sludge. We hypothesize that the impact of Ag NPs on activated sludge microbial community structures depends on the physical structure of

the activated sludge flocs, the spatial distribution of microorganisms in activated sludge flocs, and the microbial community structures in activated sludge. Molecular biology techniques were employed, and 16S rRNA gene based PCR-DGGE was applied to analyze the microbial community shift after Ag NPs treatment of activated sludge.

3.2. Material and Methods

3.2.1. Activated sludge samples

4 L activated sludge samples were collected into a cylinder with a height of 25 cm and a diameter of 15 cm in February, 2011 (temperature of the collection site was 15°C) from the Gold Bar Wastewater Treatment Plant located in Edmonton, Alberta, Canada. Samples were collected right before each experiment and stored in an ice box during the 30 minutes transport to the laboratory. Samples were processed at 15°C (to simulate a similar environment to that in the activated sludge system in Gold Bar)within 12 hours of arrival at the laboratory. The pH of the wastewater was 6.9 ± 0.1 and the IS was 15.5 mM. Activated sludge samples were allowed to settle by gravity to separate good settleability flocs and poor settleability flocs; the intact activated sludge (samples at time 0 hour) and unsettled activated sludge (intact activated sludge treated by 3 hours gravity-settling) were removed and used for Ag NPs toxicity experiments. Light microscopy was applied to photograph activated sludge samples. A drop (5 μ L) of the sludge sample was placed on the microscope slide, covered with a cover glass, and observed at 10 \times objective under a light microscope. The floc size distribution was determined based on the light microscopy images. The surface structure of microorganisms in the intact sludge and in the unsettled sludge with and without Ag NPs treatment was examined with an SEM

following procedures reported previously (Sheng and Liu, 2011). In order to further examine the presence and distribution of EPS in the activated sludge flocs, EPS and bacterial cells in activated sludge samples were stained using concanavalin A (ConA) conjugated with Taxes Red (Ni et al., 2009) and SYTO 9 green fluorescent nucleic acid dye, respectively, to facilitate fluorescence microscopic observations (20× objective). Each experiment was performed in triplicate.

3.2.2. Preparation and characterization of Ag NPs suspensions

Self-dispersing silver nanopowder was purchased from SkySpring Nanomaterials, Inc. (Houston, USA). The Ag NPs product description stipulated a particle size of less than 15 nm, and a particle composition of 10% silver (99.99% purity) and 90% polyvinylpyrrolidone (PVP), similar to Ag NPs commonly used in commercial products (Brar et al., 2010). Ag NPs stock suspension of 100 mg/L were prepared by dispersion in ultrapure water, mixing by vortex at maximum speed, and sonication for 2 hours. To investigate the impact of wastewater environment on the size stability of Ag NPs, filtered wastewater (filtered through 0.22 µm membranes to remove particulate materials) was used to dissolve Ag NPs. The Ag NPs suspension was then incubated for 24 hours under exactly the same experimental conditions as in the toxicity experiments (15°C, 200 rpm and preserved in the dark). The particle size of the Ag NPs was measured during the 24 hours incubation using dynamic light scattering (DLS).

3.2.3. Ag NPs toxicity experiments

50 mL samples of the intact sludge and unsettled sludge with or without (control samples) Ag NPs at 1 mg/L were incubated in 250 mL flasks at 15°C, 200 rpm, for 24

hours in the dark. All samples were analyzed in triplicate for antimicrobial effects. The effects of 10 mg/L and 200 mg/L Ag NPs on microbial communities in activated sludge were also investigated and compared with 1 mg/L Ag NPs.

3.2.4. Bacterial enumeration using HPC

Bacterial enumeration was performed by HPC using the drop plate method (Liu et al., 2007a). 50 μ L samples were taken at intervals during the 24 hours treatment. A series of 10-fold dilutions of these samples using 1% PBS (pH = 7.0) were performed and 10 μ L of each dilution was plated on R2A agar (Voigt Global Distribution Inc., KS) plates in triplicate. Plates were incubated at 31°C for 24 hours and held at room temperature for another 7 days. Counting was performed after 24 hours (for fast-growing bacteria), after 3 days, and after 7 days (for total number of bacteria) to determine bacterial culturability. The low detection limit was 10^2 CFU/mL.

3.2.5. Activated sludge microbial community analysis using PCR-DGGE

A fragment of the gene that codes for 16S rRNA was analyzed to identify the microbial communities in intact sludge samples and unsettled sludge samples. Details of the PCR-DGGE experiments are provided in the supplementary material. Gel Compar II was used to analyze similarities between DGGE gel lanes.

3.3. Results

3.3.1. Activated sludge characterization

3.3.1.1 Activated sludge floc size distribution

Intact sludge samples and the unsettled sludge samples were observed under a light microscope. Floc size distribution was determined based on the light microscopy images.

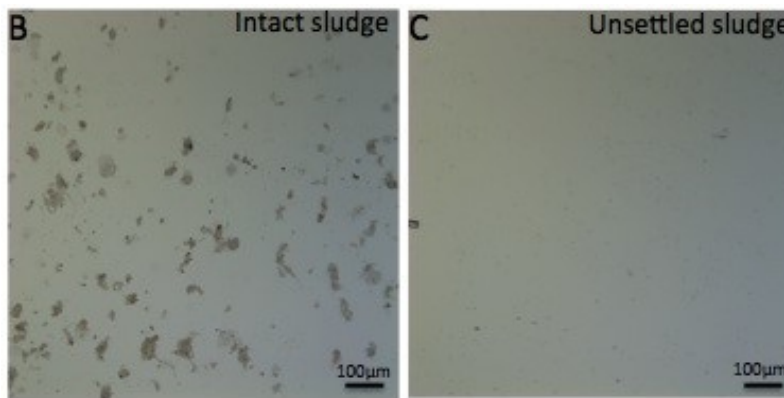
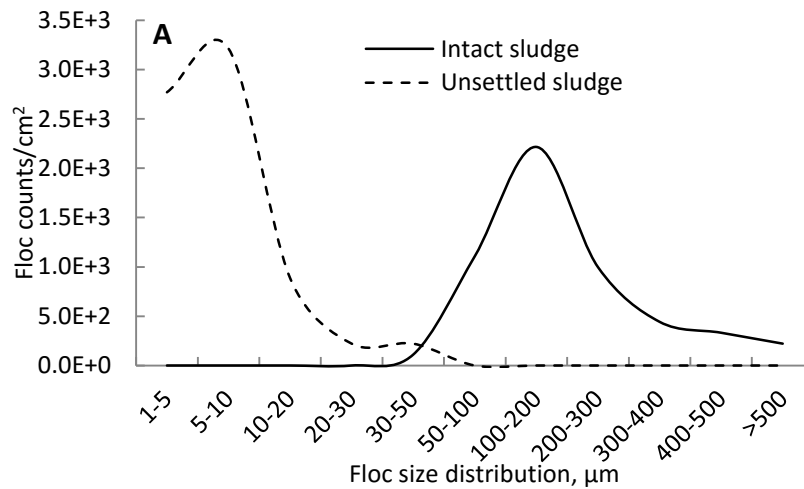


Figure 3.1. Activated sludge floc size distribution and light microscopy images of activated sludge samples: (A) Floc size distribution in intact sludge samples and unsettled sludge samples; (B) Light microscopy image of an intact sludge sample; (C) Light microscopy image of an unsettled sludge sample.

As shown in Figure 3.1A, sizes of flocs in the intact sludge ranged from 10– above 500 µm with most of the flocs being around 100–200 µm. Similar size ranges of activated sludge flocs have been reported (De Clercq et al., 2004; Jorand et al., 1995; Li and Ganczarczyk, 1991; Metcalf and Eddy, 2003). After gravity-settling for 3 hours, the unsettled flocs had a size range of less than 100 µm with most of them being between 1–

10 μm . Intact sludge samples were highly turbid (turbidity = 1800 NTU) and contained visible flocs in a loose flocculating form with highly irregular boundaries (Figure 3.1B). A significant reduction in turbidity was observed in the unsettled sludge samples (turbidity = 7.22 ± 0.026 NTU) (Figure 3.1C), indicating the gravity-settling process can remove a significant amount of activated sludge flocs and therefore affect floc size distribution significantly.

3.3.1.2 Microscopic images of activated sludge samples

Surface structures of microorganisms in intact sludge samples and unsettled sludge samples with and without Ag NPs treatment were observed via SEM and fluorescence microscope. Figures 3.2A and 3.2B show that considerable filamentous bacteria were twisted in a complex EPS matrix in the intact sludge with and without Ag NPs treatment. Badireddy et al. (2010) also found the similar results. After treatment with 1 mg/L Ag NPs for 24 hours, the EPS quantity was reduced significantly and the filamentous cells were more exposed to the environment (Figure 3.2B). Figures 3.2C and 3.2D show that only small EPS-like flocs and no filamentous cells can be seen in unsettled sludge samples. Fluorescence microscopy images presented in Figure S3.1 (supplementary material) reveal that the bacterial cells (green) and EPS (red) were well mixed, and the amount of EPS decreased with Ag NPs treatment. Both SEM and fluorescence microscopy images confirm the presence of EPS, and a decrease in the amount of EPS after Ag NPs treatment.

3.3.2. Ag NPs characterization

The particle size distribution was depicted in Figure S3.2 (supplementary material). The average particle size of 1 mg/L Ag NPs in wastewater solution was 67.89 ± 2.75 nm, which was larger than the product description (< 15 nm). This can be attributed to the aggregation of Ag NPs in the wastewater environment. During the 24 hours incubation, the Ag NPs size did not change significantly ($p = 0.32$) and was 70.85 ± 13.00 nm after 24 hours incubation in wastewater.

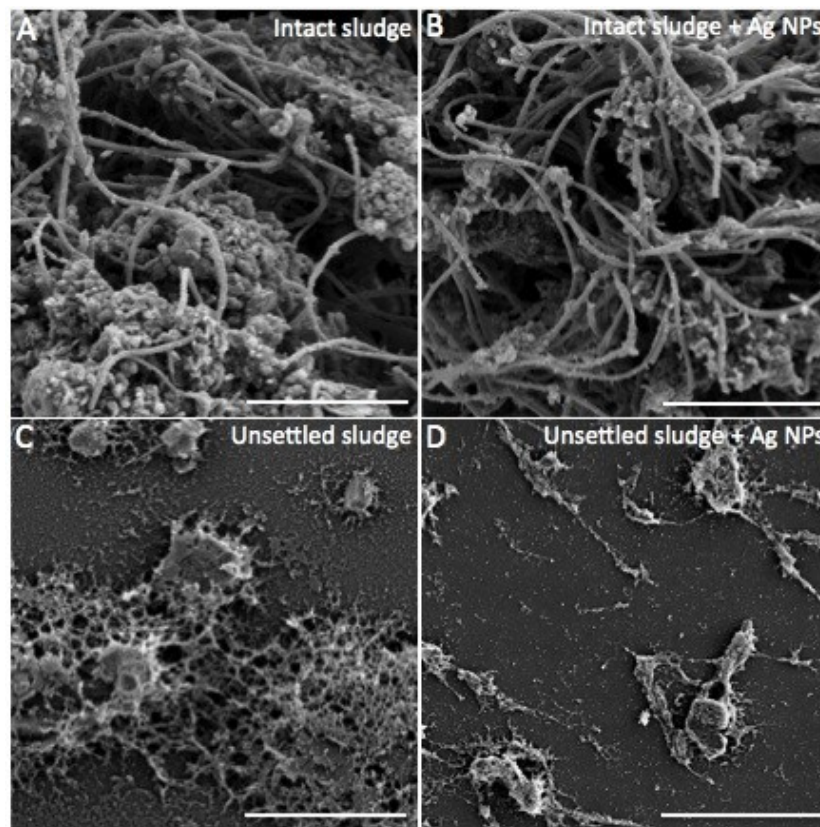


Figure 3.2. Effects of 1 mg/L Ag NPs on the surface structure of activated sludge samples with and without 3 hours gravity-settling: (A) SEM of an intact sludge sample (no Ag NPs treatment); (B) SEM of an intact sludge sample treated with 1 mg/L Ag NPs for 24 hours; (C) SEM of an unsettled sludge sample (no Ag NPs treatment); (D) SEM of an

unsettled sludge sample treated with 1 mg/L Ag NPs for 24 hours. (2000 × magnification,
bar size = 15 μm)

3.3.3. Effects of Ag NPs on heterotrophic cell culturability in activated sludge samples

Figure 3.3 shows the culturability of heterotrophic bacteria in intact sludge samples and unsettled sludge samples. HPCs after 24 hours (Figures 3.3A, 3.3C) indicate the fast-growing heterotrophic bacteria in activated sludge samples. HPCs after 3 days (Figures 3.3B, 3.3D) represent the total viable heterotrophic bacteria in activated sludge samples. HPCs after 7 days (for the total number of bacteria, data not shown) were not significantly different from HPCs results 3 days after plating.

The fast-growing and total bacteria in intact sludge samples were around 1.5×10^7 (Figure 3.3A) and 1.0×10^8 CFU/mL (Figure 3.3B), respectively. Both the number of fast-growing bacteria and the number of total bacteria were reduced by around 1.5 log units in unsettled sludge samples (Figures 3.3C, 3.3D), indicating that around 1.5 log units of heterotrophic bacteria were removed through gravity-settling.

During the 24 hours treatment with 1 mg/L Ag NPs, HPCs showed that the number of fast-growing heterotrophic bacteria in intact sludge samples was maintained at around 1.5×10^7 CFU/mL (Figure 3.3A). Similarly, the total viable heterotrophic bacteria in intact sludge samples stabilized at around 5.0×10^7 CFU/mL (Figure 3.3B). The tendency of untreated control and Ag NPs treated samples was similar during 24 hours of treatment, revealing that 1 mg/L Ag NPs had no impact on the heterotrophic cell culturability of intact sludge samples.

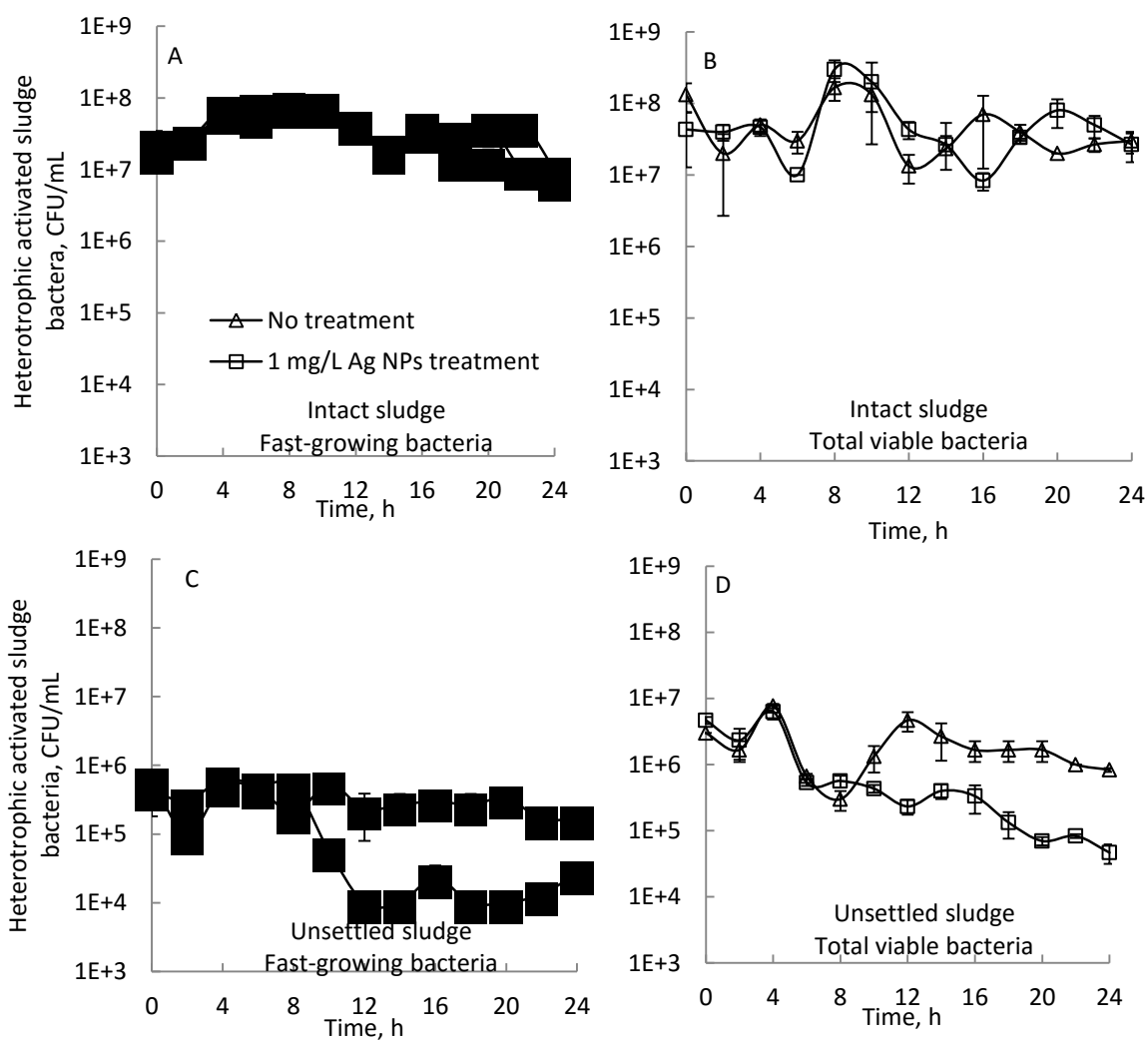


Figure 3.3. Effects of 1 mg/L Ag NPs on heterotrophic cell culturability in activated sludge samples (error bars represent one standard deviation): (A) number of fast-growing heterotrophic bacteria (24 hours after plating) in intact sludge samples with and without 1 mg/L Ag NPs treatment; (B) number of total heterotrophic bacteria (3 days after plating) in intact sludge samples with and without 1 mg/L Ag NPs treatment; (C) number of fast-growing heterotrophic bacteria (24 hours after plating) in unsettled sludge samples with and without 1 mg/L Ag NPs treatment; (D) number of total heterotrophic bacteria (3 days after plating) in unsettled sludge samples with and without 1 mg/L Ag NPs treatment.

Figures 3.3C and 3.3D show the impact of Ag NPs on the HPCs of the unsettled sludge samples. The untreated control stabilized at around 2.0×10^5 CFU/mL during the 24 hours Ag NPs treatment. The presence of 1 mg/L Ag NPs caused about 1.5 log units loss in the fast-growing heterotrophic bacteria number (Figure 3.3C). Figure 3.3D shows that 1 mg/L Ag NPs caused about one log unit loss in the total heterotrophic bacteria number. It should be noted that HPCs started to decrease from around 8 hours, which might be associated with the time taken for Ag NPs to diffuse into the activated sludge flocs. Tiede et al. (2010) also reported that 6 hours contact time was needed for ~ 90% of Ag NPs (initial Ag NPs concentrations: 0.5, 5, and 10 mg/L) to partition into the sewage sludge.

3.3.4. Microbial communities in activated sludge samples

For community diversity analysis, it was assumed that the number of bands in DGGE profiles corresponds to the number of species, with band intensity representing species concentration (Liu et al., 2010; Stamper et al., 2003). Based on the DGGE bands from the intact sludge, a total of 10 strains (WWAS-A~WWAS-J, corresponding to bands A~J, respectively) were identified, which fell into two phyla as shown in Figure 3.4A. Eight of the 10 bands in Figure 3.4B from the intact sludge were sequenced successfully. Identities between each sequence and the corresponding closest homolog from the NCBI nr nucleotide database are shown in Figure 3.4A. Bands B and J were mixtures of DNA from different strains and were not sequenced successfully. Bands A, C, and E were not clustered together with their corresponding homologs because of the presence of too many “N”s in their sequences. Based on the NCBI nr nucleotide database, bands A and E are close to two groups of unknown bacteria affiliating with the phyla *Bacteroidetes* and

Proteobacteria, respectively. The unknown species observed in the activated sludge samples were expected because many microorganisms in environmental samples have not been detected or identified due to the complexity of these samples (Kragelund et al., 2008). The 16S rRNA gene sequence similarities of bands D, E, H, and I were not high enough to confidently identify these four strains because of the presence of too many “N”s in their sequence results. The closest relatives to bands F and G were uncultured *Fluviicola* sp. and uncultured *Rhodocyclaceae bacterium*, respectively, with a sequence similarity of 100% for both strains, and fell into the phyla of *Bacteroidetes* and *Proteobacteria*, respectively.

As shown in Figure 3.4B (lane 1 and lane 3), 3 hours gravity-settling of activated sludge resulted in a significant reduction in the incumbent microbial community. Two bands (A and E) were missing and four bands (B, C, F, and H) were significantly reduced in intensity. Species A and E were observed in intact sludge samples and perhaps settled with the flocs during the 3 hours gravity-settling, while species B, C, F, and H were also removed partially during the gravity-settling indicating that the retained poor settleability flocs were reduced in microbial diversity.

Figure 3.4B (lane 1 and lane 2) shows that the 24 hours Ag NPs treatment caused a significant reduction in intensities of two bands (A and E) in intact sludge samples, suggesting that *Bacteroidetes* and *Proteobacteria* are sensitive to Ag NPs treatment. Since a high intensity of DGGE bands implies a high concentration of species (Liu et al., 2010; Stamper et al., 2003), the increase in intensity of bands C and D after 24 hours Ag

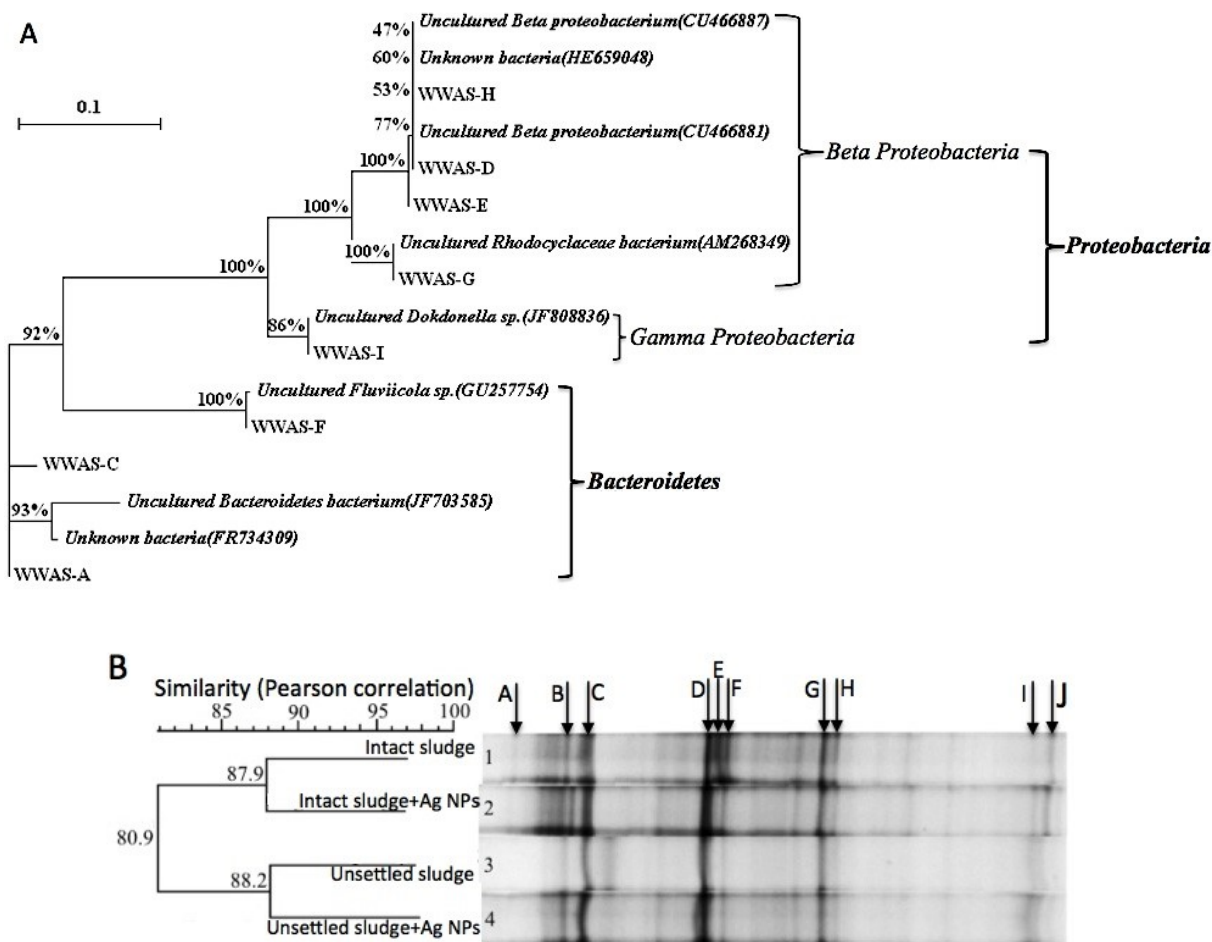


Figure 3.4. Microbial community profile of activated sludge: (A) phylogenetic tree based on DGGE bands; (B) Linkage analysis dendrogram of DGGE profiles of the intact sludge (lane 1), intact sludge treated with 1 mg/L Ag NPs (lane 2), the unsettled sludge (lane 3), and the unsettled sludge treated with 1 mg/L Ag NPs (lane 4).

NPs treatment (lane 2, Figure 3.4B) might be the result of nourishment of certain species by the cell debris of bacteria killed by Ag NPs.

No missing bands were observed in unsettled sludge samples treated with Ag NPs (lane 4, Figure 3.4B), compared to the untreated control (lane 3, Figure 3.4B). The microbial community shift in unsettled sludge samples after treatment with Ag NPs was

not significant. We note that two of the most sensitive strains (bands A and E) toward Ag NPs treatment in intact sludge samples disappeared after 3 hours of gravity-settling; this might explain the low extent of community shifting in the unsettled samples. Nevertheless, HPCs showed that Ag NPs caused around 1 log unit reduction in heterotrophic cells numbers in the unsettled sludge (Figures 3.3C, 3.3D) but no significant reduction ($p = 0.67$) in the intact sludge (Figures 3.3A, 3.3B). Note should be made that HPC is a culture-dependent technique, thus HPCs results need to be interpreted with caution because some bacteria that are killed by Ag NPs may not be detected through HPCs because they might be not culturable.

Although PCR-DGGE is a culture-independent molecular fingerprinting technique to observe microbial diversity and community shifts, it is limited in detecting base sequence differences that are less than 95% (Jackson et al., 2000). Previous studies have showed that DGGE is not sensitive enough to distinguish all sequence changes in 16S rRNA gene fragments (Jackson et al., 2000; Muyzer and Smalla, 1998). Thus, it is possible that the microbial community shifts in the unsettled sludge samples were not detected by DGGE. It is also important to note that some bacteria may be killed by Ag NPs but their DNA are still present in the sample and are subsequently detected by DGGE.

3.3.5. Effects of Ag NPs concentrations on microbial communities in activated sludge

Figure 3.5 shows the impact of Ag NPs concentrations on the DGGE profiles of the unsettled activated sludge (Figure 3.5A) and supernatants of 3 hours gravity-settled activated sludge (Figure 3.5B). Compared to the effects of 1mg/L Ag NPs on both unsettled and 3 hours gravity-settled activated sludge, increasing the concentration to 10

mg/L and 200 mg/L did not cause more reduction in bands intensities in DGGE, although around two log units HPCs reduction were achieved by both 10 mg/L and 200 mg/L Ag NPs treatment (data not shown).

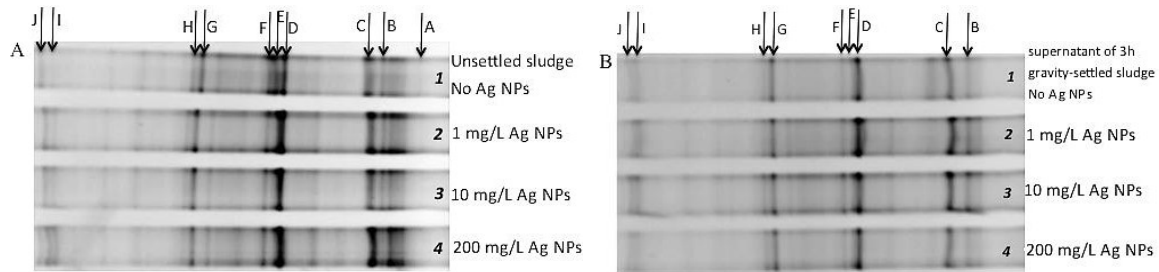


Figure 3.5. Effects of Ag NPs concentrations on the DGGE profiles of the unsettled activated sludge (A) and supernatants of 3 hours gravity-settled

3.4. Discussion

3.4.1. Mechanisms involved in activated sludge susceptibility to Ag NPs

Mechanisms that account for the response of activated sludge microbial community to Ag NPs observed in the current study might include: (i) different microorganisms have different susceptibility to Ag NPs (Gao et al., 2011; Sheng and Liu, 2011); (ii) the physical structure of activated sludge flocs might impact the susceptibility of incumbent microorganisms to Ag NPs (Holbrook et al., 2006).

3.4.1.1 Microbial community structures in activated sludge

It was reported that the toxicity of Ag NPs to bacteria is strain-dependent. Gao et al. (2011) found that 0.5 mg/L Ag NPs can cause 50% growth inhibition in *Pseudokirchneriella subcapitata* but no growth inhibition in microorganisms catalyzing nitrate reduction in sediments. In a separate study, *Thiotrichales* in wastewater rotating

biological contactor (RBC) biofilms were found to be more sensitive than other wastewater microorganisms to Ag NPs (Sheng and Liu, 2011).

Community structures of microorganisms in activated sludge can also impact the response of bacteria to Ag NPs. Our DGGE study suggested that species A and E were more sensitive to Ag NPs than other species present in the activated sludge tested, as shown by a significant reduction in band intensity in the DGGE profile after Ag NPs treatment (lane 1 and lane 2 in Figure 3.4B).

3.4.1.2 Physical structure of activated sludge flocs

Based on mass transfer and adsorption of Ag NPs on the EPS matrix, microbial species distributed on the surface of activated sludge flocs may be exposed to higher toxic levels than species inside the flocs. Previous studies showed that the EPS matrix on the surface of activated sludge flocs or microbial biofilms can trap nanoparticles and prevent their diffusion into the microbial aggregates (Dimkpa et al., 2011). For example, Holbrook et al. (2006) utilized CLSM to examine the fate of quantum dots in biofilms and observed that quantum dots were mainly distributed on the surface of the biofilm. Therefore, species distributed on the surface of activated sludge flocs may be at greater risks of Ag NPs toxicity than species inside the flocs. The relatively more sensitive species (A and E) might have been mainly distributed on the surface of the activated sludge flocs and therefore were inhibited by Ag NPs.

The DGGE results revealed that microbial communities in the intact sludge changed after 24 hours Ag NPs treatment; however, under the same Ag NPs treatment conditions, no significant community structure change was observed for the unsettled sludge. This

behavior implied that the physical structure of the flocs in which bacteria were embedded played an important role in controlling the response of these bacteria to Ag NPs. The DGGE profile showed that two species (A and E) in the intact sludge were significantly inhibited by Ag NPs. It is probable that the good settleability flocs may impair the diffusion of Ag NPs into the central part of the flocs and therefore protect the bacteria present in the middle of these flocs. For instance, Ag NPs may mainly be trapped on the surface of the flocs and threaten only bacteria distributed on the floc surface. There might be areas in the middle of flocs where bacteria are not targeted by Ag NPs (Figure 3.6), corresponding to the microbial diversity reduction in the intact sludge detected in DGGE, although HPCs results suggest that viable heterotrophic bacterial numbers in the intact sludge were not significantly reduced ($p = 0.67$) after the Ag NPs treatment. This may be associated with the fact that the missing microbial species were not cultivable on the R2A agar or the cultivable species were less affected by Ag NPs.

No significant microbial community shift was observed in the unsettled sludge treated with Ag NPs. Perhaps after 3 hours of gravity-settling it became easier for Ag NPs to penetrate poor settleability flocs and diffuse into the entire flocs, resulting in a uniform distribution of Ag NPs and similar threatens to all species present in poor settleability flocs. Therefore no microbial diversity reduction was detected because no pertinent removal of any certain species. It is also possible some bacteria may be killed by Ag NPs but their DNA are still present in the sample and are subsequently detected by DGGE.

Based on a previous report (Dimkpa et al., 2011), and the HPC and DGGE results obtained in the current study, the physical structure of activated sludge flocs and the

diffusion gradient of Ag NPs in activated sludge flocs play important roles in controlling Ag NPs toxicity in activated sludge systems. A schematic of the proposed mechanism is shown in Figure 3.6.

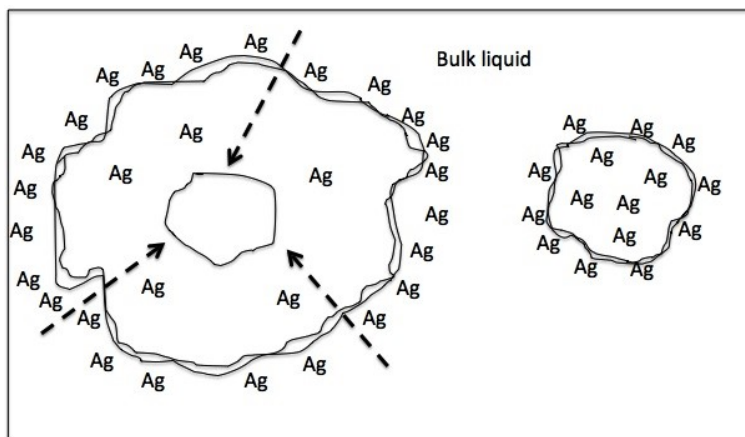


Figure 3.6. Schematic of the physical structure of activated sludge flocs in the intact sludge (left) and the unsettled sludge (right). Dashed lines with arrowheads show the diffusion gradients of Ag NPs in an good settleability activated sludge floc (not to scale).

In Figure 3.6, left, a good settleability floc is represented by a large round-shaped particle. The dashed line with an arrowhead describes the decreasing Ag NPs gradient diffusing from the surface of the floc to the center of the floc. On the right of Figure 3.6, a smaller round-shaped particle represents an activated sludge floc with poor settleability. Its relatively smaller size makes it easier for Ag NPs to penetrate into the entire floc. However, additional studies on the fate, retention, and behavior of Ag NPs in activated sludge flocs should be performed to further verify this hypothesis.

3.4.2. Environmental implications

This study represents one of the first experimental evidences on the impact of Ag NPs on the microbial community in wastewater activated sludge. Both the activated sludge flocs structure and the wastewater conditions were taken into account in this study.

Ag NPs may pose significant threat on the microbial community in wastewater treatment systems. Due to the adsorption and accumulation of NPs in microbial aggregates (e.g. activated sludge flocs and biofilms) (Klaine et al., 2008; Limbach et al., 2008; Ratte, 1999; Tiede et al., 2010), the antimicrobial risks of Ag NPs to the microbial communities in wastewater treatment systems might be increased. Microbial aggregates are considered to be the backbone of the activated sludge system, and any impacts on microbial activities or community structures would cause unanticipated loss of treatment efficiency.

We observed two species of bacteria, present in intact sludge samples and affiliated with *Bacteroidetes* and *Proteobacteria* phyla, that were sensitive to Ag NPs treatment. This may be explained if (1) these two species are relatively more sensitive to Ag NPs than other species present in activated sludge, or/and (2) they present mainly on the good settleability activated sludge flocs or surface of these flocs and therefore are easily targeted by Ag NPs. *Bacteroidetes* and *Proteobacteria* are commonly present in activated sludge samples from both industrial and municipal wastewater treatment plants and have been found to be dominant in activated sludge communities (Larsen et al., 2008; Manz et al., 1994; Wagner et al., 2002). *Bacteroidetes* have roles in sugar degradation and may be responsible for the conversion of LPS and peptidoglycan released by dead cells into N-

acetylglucosamine units, but an abundance of *Bacteroidetes* in activated sludge would lead to sludge bulking or foaming (Kragelund et al., 2008). The beta subclass of *Proteobacteria* were reported to be critical in organic compound degradation and floc formation (Bond et al., 1995) in activated sludge processes. Any unanticipated loss of these major species may cause changes in the characteristics of activated sludge resulting in a reduction in wastewater treatment efficiency (Kragelund et al., 2008). Thus, Ag NPs discharge might lead to a failure of the biological wastewater treatment system, and it is very important to know the impact of Ag NPs on microbial community structures in addition to the total bacterial number. This may provide suggestions to appropriate disposal options of NPs and operational conditions of wastewater treatment processes.

Supplementary Material

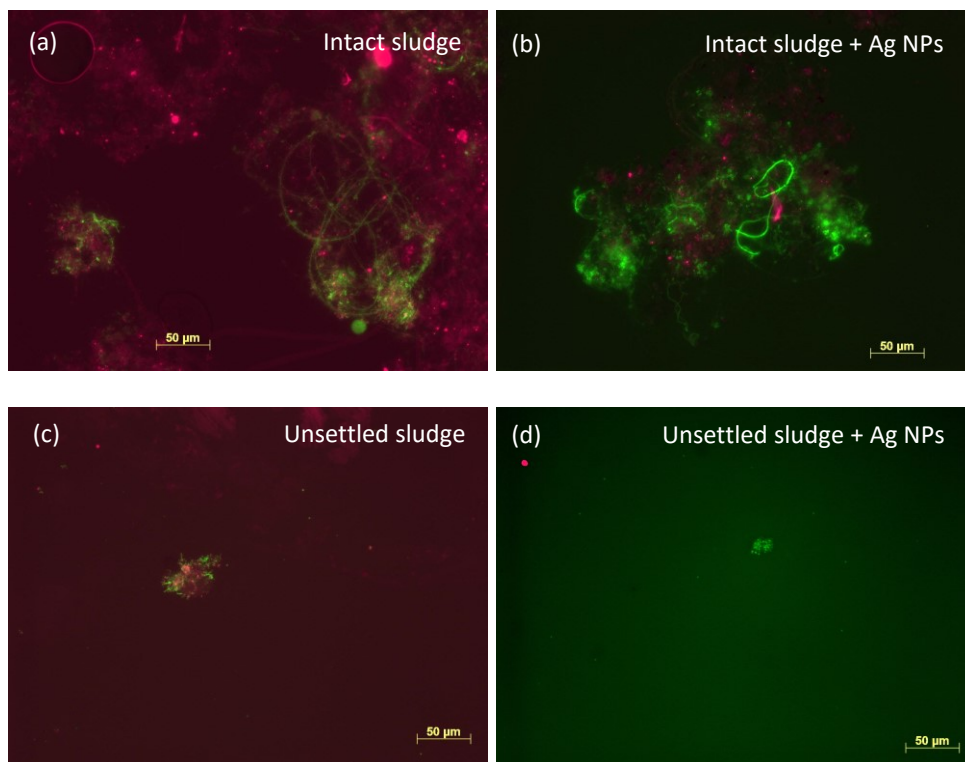


Figure S3.1 Fluorescence microscopy images of activated sludge flocs. Bacterial cells were stained with SYTO 9 green fluorescent nucleic acid dye (green) and EPS were stained with concanavalin A (ConA) conjugated with Texas Red (red): (a) an intact sludge sample (no Ag NPs treatment); (b) an intact sludge sample treated with 1 mg/L Ag NPs for 24 hours; (c) an unsettled sludge sample (no Ag NPs treatment); (d) an unsettled sludge sample treated with 1 mg/L Ag NPs for 24 hours.

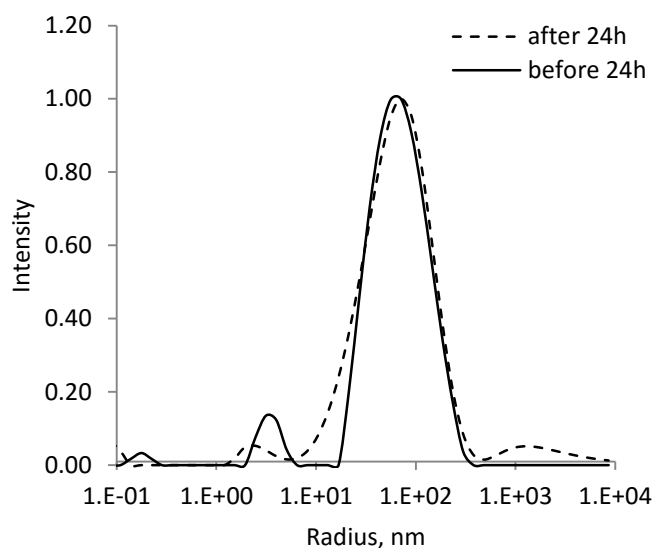


Figure S3.2 Ag NPs size distribution in wastewater environment

Activated sludge community analysis using PCR-DGGE

The gene that codes for 16s rRNA was analyzed to identify the microbial communities in intact activated sludge and the supernatant of 3 hours gravity-settled samples. The Powersoil® DNA Isolation Kit from MO BIO Laboratories, Inc. (Carlsbad, USA) was adopted to extract genomic DNA from each sample. Taq DNA polymerase (Invitrogen Platinum®) was used to amplify a ~ 550 bp fragment of the 16S rRNA gene from each DNA sample. The primer pair 357f (5'-CCT ACGGGA GGC AGC AG -3') and 907r (5'-CCG TCA ATT CCT TTG AGT TT -3') was used. A GC-clamp (5'-CGC CCG CCG CGC GCG GCG GGC GGG GCG GGG GCA CGG GGG G-3') was added to the 5' end of the forward primer. A 50 µL system was used in which the final concentration of each component was as follows: PCR buffer, 1×; MgCl₂, 1.5 mM; dNTPs, 100 µM; Taq, 1.25 U; primer, 0.1 µM each; DNA template, ~ 3 ng. The PCR was run with an initial hot start at 94°C for 5 minutes, followed by 35 cycles of 1 minute at 94°C, 1 minute at 56°C, 40

seconds at 72°C, and a final extension at 72°C for 5 minutes. Polyacrylamide (6.5%) gels (16 cm × 10 cm × 1 mm) were prepared using a gradient delivery system (Model 475, Bio-Rad Laboratories Ltd., Ontario, Canada). A denaturing gradient of 35–55% was adopted to obtain the best separation. DGGE was run using the D-code system (Bio-Rad Laboratories Ltd., Ontario, Canada) at 180 V, 60°C, for 5.5 h in 1 × Tris-acetate-EDTA buffer (TAE). The gels were stained in 0.5 mg/L ethidium bromide for 30 minutes, then destained in deionized water for 30 minutes. Selected bands were excised from the DGGE gel, mashed into Tris-HCl buffer (pH 8.5) and kept at 4°C overnight. 2 µL aliquots of the gel diffusion solution were added as templates into each 50 µL PCR system with the composition previously described. PCR was run in the same conditions. PCR products were purified using an ExoSAP-IT® PCR Product Clean-Up Kit, and sequenced. Each sequence was matched against the NCBI nr nucleotide database using the nucleotide BLAST program. Multiple sequence alignment was built using CLUSTAL W and a phylogenetic tree was calculated and constructed using TREECON.

References

- Andreadakis AD. Physical and chemical-properties of activated-sludge floc. *Water Research* 1993; 27: 1707-1714.
- Badireddy AR, Chellam S, Gassman PL, Engelhard MH, Lea AS, Rosso KM. Role of extracellular polymeric substances in bioflocculation of activated sludge microorganisms under glucose-controlled conditions. *Water Research* 2010; 44: 4505-4516.
- Bond PL, Hugenholtz P, Keller J, Blackall LL. Bacterial community structures of phosphate-removing and non-phosphate-removing activated sludges from sequencing batch reactors. *Applied and Environmental Microbiology* 1995; 61: 1910-1916.
- Bradford A, Handy RD, Readman JW, Atfield A, Muehling M. Impact of silver nanoparticle contamination on the genetic diversity of natural bacterial assemblages in estuarine sediments. *Environmental Science & Technology* 2009; 43: 4530-4536.
- Brar SK, Verma M, Tyagi RD, Surampalli RY. Engineered nanoparticles in wastewater and wastewater sludge - evidence and impacts. *Waste Management* 2010; 30: 504-520.
- Cho M, Chung HM, Choi WY, Yoon JY. Different inactivation behaviors of MS-2 phage and *Escherichia coli* in TiO₂ photocatalytic disinfection. *Applied and Environmental Microbiology* 2005; 71: 270-275.

- Choi O, Deng KK, Kim NJ, Ross L, Surampalli RY, Hu ZQ. The inhibitory effects of silver nanoparticles, silver ions, and silver chloride colloids on microbial growth. *Water Research* 2008; 42: 3066-3074.
- Choi O, Hu ZQ. Size dependent and reactive oxygen species related nanosilver toxicity to nitrifying bacteria. *Environmental Science & Technology* 2008; 42: 4583-4588.
- De Clercq B, Lant PA, Vanrolleghem PA. Focused beam reflectance technique for in situ particle sizing in wastewater treatment settling tanks. *Journal of Chemical Technology and Biotechnology* 2004; 79: 610-618.
- Dimkpa CO, Calder A, Gajjar P, Merugu S, Huang WJ, Britt DW, et al. Interaction of silver nanoparticles with an environmentally beneficial bacterium, *Pseudomonas chlororaphis*. *Journal of Hazardous Materials* 2011; 188: 428-435.
- Dror-Ehre A, Mamane H, Belenkova T, Markovich G, Adin A. Silver nanoparticle-*E. coli* colloidal interaction in water and effect on *E. coli* survival. *Journal of Colloid and Interface Science* 2009; 339: 521-526.
- Elechiguerra JL, Burt JL, Morones JR, Camacho-Bragado A, Gao X, Lara HH, et al. Interaction of silver nanoparticles with HIV-1. *J Nanobiotechnology* 2005; 3: 6.
- Fabrega J, Zhang R, Renshaw JC, Liu WT, Lead JR. Impact of silver nanoparticles on natural marine biofilm bacteria. *Chemosphere* 2011; 85: 961-966.
- Gao J, Wang Y, Hovsepian A, Bonzongo JCJ. Effects of engineered nanomaterials on microbial catalyzed biogeochemical processes in sediments. *J Hazard Mater* 2011; 186: 940-5.

- Gou N, Onnis-Hayden A, Gu AZ. Mechanistic toxicity assessment of nanomaterials by whole-cell-array stress genes expression analysis. *Environmental Science & Technology* 2010; 44: 5964-5970.
- Grijspeerdt K, Verstraete W. Image analysis to estimate the settleability and concentration of activated sludge. *Water Research* 1997; 31: 1126-1134.
- Holbrook RD, Morrow J, Mangel T. Fate of nanoparticles in biological systems — quantum dot behavior in bacterial cells and biofilms. *Microscopy and Microanalysis* 2006; 12(Suppl. 02):618-9.
- Jackson CR, Roden EE, Churchill PF. Denaturing gradient gel electrophoresis can fail to separate 16S rDNA fragments with multiple base differences. 1. *Molecular Biology Today*, 2000, pp. 49-51.
- Jin B, Wilen BM, Lant P. A comprehensive insight into floc characteristics and their impact on compressibility and settleability of activated sludge. *Chemical Engineering Journal* 2003; 95: 221-234.
- Jorand F, Zartarian F, Thomas F, Block JC, Bottero JY, Villemin G, et al. Chemical and structural (2d) linkage between bacteria within activated-sludge flocs. *Water Research* 1995; 29: 1639-1647.
- Ju-Nam Y, Lead JR. Manufactured nanoparticles: An overview of their chemistry, interactions and potential environmental implications. *Science of the Total Environment* 2008; 400: 396-414.
- Kang S, Pinault M, Pfefferle LD, Elimelech M. Single-walled carbon nanotubes exhibit strong antimicrobial activity. *Langmuir* 2007; 23: 8670-8673.

- Kiser MA, Westerhoff P, Benn T, Wang Y, Perez-Rivera J, Hristovski K. Titanium nanomaterial removal and release from wastewater treatment plants. *Environmental Science & Technology* 2009; 43: 6757-6763.
- Klaine SJ, Alvarez PJJ, Batley GE, Fernandes TF, Handy RD, Lyon DY, et al. Nanomaterials in the environment: behavior, fate, bioavailability, and effects. *Environmental Toxicology and Chemistry* 2008; 27: 1825-1851.
- Konopka M, Kowalski Z, Wzorek Z. Disinfection of meat industry equipment and production rooms with the use of liquids containing silver nano-particles. *Archives of Environmental Protection* 2009; 35: 107-115.
- Kragelund C, Levantesi C, Borger A, Thelen K, Eikelboom D, Tandoi V, et al. Identity, abundance and ecophysiology of filamentous bacteria belonging to the Bacteroidetes present in activated sludge plants. *Microbiology-Sgm* 2008; 154: 886-894.
- Larsen P, Nielsen JL, Otzenj D, Nielsen PH. Amyloid-like adhesins produced by floc-forming and filamentous bacteria in activated sludge. *Applied and Environmental Microbiology* 2008; 74: 1517-1526.
- Li DH, Ganczarzyk J. Size distribution of activated-sludge flocs. *Research Journal of the Water Pollution Control Federation* 1991; 63: 806-814.
- Limbach LK, Bereiter R, Mueller E, Krebs R, Gaelli R, Stark WJ. Removal of oxide nanoparticles in a model wastewater treatment plant: influence of agglomeration and surfactants on clearing efficiency. *Environmental Science & Technology* 2008; 42: 5828-5833.

- Liu C, Yang JL, Wu G, Zhang S, Li ZX, Guo JB. Estimation of dominant microbial population sizes in the anaerobic granular sludge of a full-scale UASB treating streptomycin wastewater by PCR-DGGE. *World Journal of Microbiology & Biotechnology* 2010; 26: 375-379.
- Liu GQ, Wang DM, Wang JM, Mendoza C. Effect of ZnO particles on activated sludge: role of particle dissolution. *Science of the Total Environment* 2011; 409: 2852-2857.
- Liu Y, Li J, Qiu XF, Burda C. Bactericidal activity of nitrogen-doped metal oxide nanocatalysts and the influence of bacterial extracellular polymeric substances (EPS). *Journal of Photochemistry and Photobiology a-Chemistry* 2007; 190: 94-100.
- Lok CN, Ho CM, Chen R, He QY, Yu WY, Sun HZ, et al. Proteomic analysis of the mode of antibacterial action of silver nanoparticles. *Journal of Proteome Research* 2006; 5: 916-924.
- Luongo LA, Zhang XQ. Toxicity of carbon nanotubes to the activated sludge process. *Journal of Hazardous Materials* 2010; 178: 356-362.
- Lyon DY, Brown DA, Alvarez PJJ. Implications and potential applications of bactericidal fullerene water suspensions: effect of nC(60) concentration, exposure conditions and shelf life. *Water Science and Technology* 2008; 57: 1533-1538.
- Manz W, Wagner M, Amann R, Schleifer KH. *In-situ* characterization of the microbial consortia active in 2 waste-water treatment plants. *Water Research* 1994; 28: 1715-1723.

- Metcalf and Eddy. Wastewater Engineering: Treatment and Reuse (4th Edition). McGraw-Hill, New York, 2003.
- Morones JR, Elechiguerra JL, Camacho A, Holt K, Kouri JB, Ramirez JT, et al. The bactericidal effect of silver nanoparticles. *Nanotechnology* 2005; 16: 2346-2353.
- Muyzer G, Smalla K. Application of denaturing gradient gel electrophoresis (DGGE) and temperature gradient gel electrophoresis (TGGE) in microbial ecology. *Antonie Van Leeuwenhoek International Journal of General and Molecular Microbiology* 1998; 73: 127-141.
- Ni BJ, Xie WM, Liu SG, Yu HQ, Wang YZ, Wang G, et al. Granulation of activated sludge in a pilot-scale sequencing batch reactor for the treatment of low-strength municipal wastewater. *Water Research* 2009; 43: 751-761.
- Nogueira V, Lopes I, Rocha-Santos T, Santos AL, Rasteiro GM, Antunes F, et al. Impact of organic and inorganic nanomaterials in the soil microbial community structure. *Science of the Total Environment* 2012; 424: 344-350.
- Ratte HT. Bioaccumulation and toxicity of silver compounds: a review. *Environmental Toxicology and Chemistry* 1999; 18: 89-108.
- Sheng ZY, Liu Y. Effects of silver nanoparticles on wastewater biofilms. *Water Research* 2011; 45: 6039-6050.
- Silvestry-Rodriguez N, Bright KR, Slack DC, Uhlmann DR, Gerba CP. Silver as a residual disinfectant to prevent biofilm formation in water distribution systems. *Applied and Environmental Microbiology* 2008; 74: 1639-1641.

- Sondi I, Salopek-Sondi B. Silver nanoparticles as antimicrobial agent: a case study on *E. coli* as a model for gram-negative bacteria. *Journal of Colloid and Interface Science* 2004; 275: 177-182.
- Stamper DM, Walch M, Jacobs RN. Bacterial population changes in a membrane bioreactor for graywater treatment monitored by denaturing gradient gel electrophoretic analysis of 16S rRNA gene fragments. *Applied and Environmental Microbiology* 2003; 69: 852-860.
- Tiede K, Boxall ABA, Wang XM, Gore D, Tiede D, Baxter M, et al. Application of hydrodynamic chromatography-ICP-MS to investigate the fate of silver nanoparticles in activated sludge. *Journal of Analytical Atomic Spectrometry* 2010; 25: 1149-1154.
- Wagner M, Loy A, Nogueira R, Purkhold U, Lee N, Daims H. Microbial community composition and function in wastewater treatment plants. *Antonie Van Leeuwenhoek International Journal of General and Molecular Microbiology* 2002; 81: 665-680.
- Yoon KY, Byeon JH, Park JH, Hwang J. Susceptibility constants of *Escherichia coli* and *Bacillus subtilis* to silver and copper nanoparticles. *Science of the Total Environment* 2007; 373: 572-575.
- Zheng X, Chen Y, Wu R. Long-term effects of titanium dioxide nanoparticles on nitrogen and phosphorus removal from wastewater and bacterial community shift in activated sludge. *Environmental Science & Technology* 2011; 45: 7284-7290.

Zheng X, Su YL, Chen YG. Acute and chronic responses of activated sludge viability and performance to silica nanoparticles. *Environmental Science & Technology* 2012; 46: 7182-7188.

Chapter 4 Flocculation of Bacteria by Depletion Interactions

Due to Rod-shaped CNC

4.1. Introduction

Controlling the stability of colloidal systems is vital in water treatment as well as other wide range of industrial applications, such as paints, coatings, paper making, pharmaceuticals, ceramic manufacturing (Farinato and Dubin, 1999). Bacterial aggregation, resulting in the formation of bioflocs, is one of such key colloidal activity desired to be controlled in water treatment. For instance, the formation of activated sludge flocs in clarifiers, aerated lagoons, or anaerobic sludge blanket bioreactors is critical for the bioreactors to achieve a wide range of remediation results, including nutrient consumption, xenobiotic compound degradation and metal immobilization (Gavrilescu and Macoveanu, 1999; Moharikar et al., 2005; Okunuki et al., 2004). As another example, to gauge dilute concentrations below the detection limit, on line pathogen sensors need to flocculate and phase separate bacteria before the measurement (Johnson et al., 2008).

Microbial aggregation processes are enabled by complex biological and physico-chemical interactions. Flocculation and phase separation of bacteria, like any other inert colloidal systems depend on van der Waals forces, electrostatic forces and steric forces between particles (Liang et al., 2007). The electrostatic repulsive interaction in EDL is the result of negative surface cell potentials and plays a crucial role in the stability of bacterial systems. Steric forces become important if polymers exist in colloidal suspensions. Steric interactions are due to either adsorption or non-adsorption of

polymers onto colloidal particle surfaces. Most of the work to control microbial aggregation and to understand the susceptibility of microbial aggregations investigates the role of adsorbing polymers, which involves the chemical or physical adsorption of macromolecular chains to the bacterial interface. The presence of adsorbed macromolecular chains on bacterial surfaces can destabilize the colloidal system by bridging the particles and promoting the formation of flocs. In bacterial systems, the secretion of EPS is believed to play role in the microbial dispersion stability and floc formation (Flemming and Wingender, 2001a; Flemming and Wingender, 2001b; Kreft and Wimpenny, 2001; Miller and Bassler, 2001). In addition, synthetic cationic or non-ionic polymers are also added into microbial systems to facilitate microbial aggregation, where charge neutralization and inter-particle bridging are the mechanisms play role (Larsen et al., 2009).

Alternatively, non-adsorbing polymers can also cause flocculation through a depletion mechanism (Jenkins and Snowden, 1996). Colloidal instability can be attained not only by bridging or charge reversal of adsorbed polymers but also depletion due to non-adsorbing polymers (Fleer and Scheutjens, 1983). If macromolecular chains are not adsorbing on particle surfaces, they can cause attraction between particles by a mechanism, called depletion. Originally, Traube (1925) observed the phase separation of a natural rubber latex suspension into extremely dilute and very concentrated phases in the presence of plant and seaweed polysaccharides although he did not described the mechanism as depletion. The depletion force between particles due to non-adsorbing polymers was first recognized and described theoretically by Asakura and Oosawa

(1954). Nevertheless, the depletion of non-adsorbing polymers for the aggregation of bacterial suspensions has not been well exploited despite the fact that bacteria can be considered to be a dispersion of negatively charged particles surrounded by non-adsorbing polyelectrolytes—EPS.

Likewise, the addition of repelling NPs into the dispersion of bigger colloidal bacterial particles can also destabilize and flocculate the system by depletion mechanism. According to theoretical prediction, thin rod-shaped particles with a high aspect ratio (L/D) have to be much more effective depletants. Nevertheless, the depletion of charged rod-shaped NPs for the aggregation of bacterial suspensions has not been exploited so far. In this study, the stimulated clustering and phase separation of negatively charged bacteria in the presence of negatively charged nanosized rod-shaped CNC particles as depletants was observed. CNC can be described as 6–10 nm wide and 100–200 nm long particles with negatively charged surfaces (Dong et al., 1998). CNC is expected to be commercially available in the near future.

4.2. Experimental

4.2.1. CNC suspension preparation

CNC sample was received from Alberta Innovates Technology Futures. CNC is prepared by acid hydrolysis of pure cellulose. According to the supplier, cotton pulp is hydrolyzed with 64% sulfuric acid at 50°C for 40 minutes; the mixture is diluted with deionized water to stop the reaction. The suspension is centrifuged, neutralized with Na₂CO₃ and dialyzed to remove the salts. Finally, the suspension is further dispersed in an ultrasonic bath to achieve a 1–2% concentration of stable colloidal suspension. CNC

are obtained in powder form by freeze-drying the suspensions; a detailed preparation method is discussed in elsewhere (Bondeson et al., 2006; Hamad and Hu, 2010). CNC particles in aqueous solutions carry negative electrical charges due to sulfate surface groups. The effective CNC particle size based on the translational diffusion constant was determined by DLS using a Zetasizer Model Nano ZS from Malvern (Worcestershire United Kingdom). The wavelength of the 4 mW He–Ne laser source was 633 nm, and the CNC concentration was 0.1%. The effective size of CNC particles was 90 ± 10 nm which was taken as the particle length. Zeta potential of CNC particles was determined by using the same instrument with electrophoresis mode and cell. pH of the suspension was not adjusted and close to neutral. Zeta potential of CNC was -51.5 ± 0.8 mV in H₂O. All measurements were performed at 25°C. Stock suspension of 1.0% (wt) CNC was prepared for further usage. A weight to volume conversion of the CNC suspension concentration was carried out at 1.5 g/cm³ CNC. Atomic force microscopy (AFM) in the tapping mode was used to obtain CNC pictures. Clean mica substrates (1×1 cm²) were prepared and 5 µL of CNC suspension in water (1.0 mg/mL and 0.5 mg/mL) was deposited on the mica substrate (1 cm²) by spin-coating at 2500 rpm for 40 seconds. The sample surface was observed using a Digital Instruments/Veeco Instruments MultiMode Nanoscope IV AFM equipped with an E scanner. To optimize the height profile in this investigation, silicon cantilevers (MikroMasch USA, Inc.) with low spring constant of 4.5 N/m was used in the tapping mode (TM-AFM). To obtain a clear image of the surface, a low scan rate (1 Hz) and amplitude set point (1 V) were chosen during the measurement. Height images were used to provide the width measurements in nm for the CNC nano

rods. Amplitude images were used to observe the morphology of CNC nano rods. Figure 4.1 shows a micrograph of rod-shaped CNC particles. The average particle width (diameter), determined by image analysis was 8 ± 1 nm.

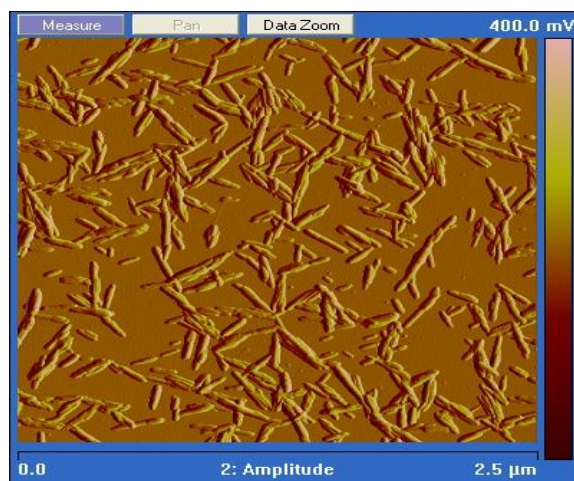


Figure 4.1. An AFM image of CNC particles

4.2.2. Bacterial system

Pseudomonas aeruginosa PAO1 is a Gram-negative bacterium that is present in a diverse range of ecological niches, ranging from water and soil to plant and animal tissues. It is considered the paradigm organism for microbial biofilm study. Figure 4.2 shows an SEM image of *P. aeruginosa* bacteria. On average, *P. aeruginosa* cells are 1.2 μm in length and 0.2 μm in width. The hairy substances on the bacteria are biopolymers (EPS) produced by *P. aeruginosa* during growth. *P. aeruginosa* EPS are generally neutrally charged (Eboigbodin et al., 2005). For each experiment, the stored *P. aeruginosa* PAO1 strains were streaked onto an Luria–Bertani (LB) agar plate and incubated at 37°C overnight. A single colony was then transferred into 10 mL of LB broth and grown in a shaker incubator at 200 rpm and 37°C for 18 hours. Stationary-

phase bacterial cells were harvested by centrifugation at 3000 g and 4°C for 10 minutes. After the supernatant was decanted, the pellets were resuspended in 10 mM of NaCl solution. The centrifugation and resuspension procedure was repeated twice to remove traces of growth media and suspended EPS in solution. The zeta potential of *P. aeruginosa* suspended in 10 mM of NaCl solution is: -29.84 ± 0.6 mV. CNC particles have higher negative zeta potentials than *P. aeruginosa* bacteria. Therefore, the length, aspect ratio, and electrostatically repulsive characters of CNC toward the bacteria make it an ideal bacteria depleting.

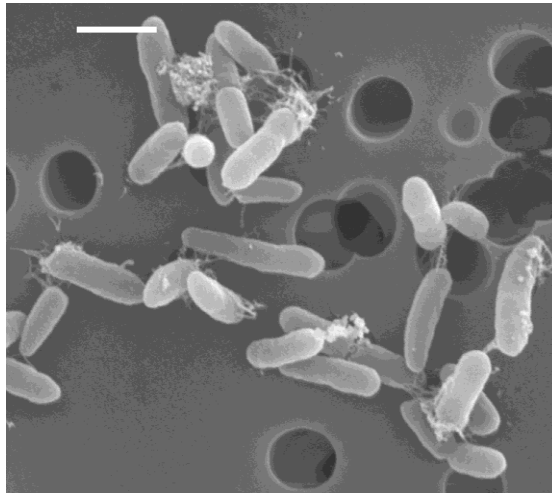


Figure 4.2. An SEM image of *P. aeruginosa* PAO1 (bar = 1 μ m)

4.2.3. Aggregation measurements with CLSM

For the aggregation measurements a *P. aeruginosa* suspension with an initial concentration of 1.0×10^8 cells/mL in 10 mM of NaCl solution was prepared. CNC particles were added to bacterial suspensions at 4.2×10^{-5} mL/mL and 4.2×10^{-2} mL/mL volume fractions which corresponds to bacteria to CNC ratios of 1:100,000 and 1:100 respectively in terms of particle numbers. Bacterial aggregation at bacteria to CNC ratio

of 1:100,000 was examined with CLSM. Bacterial cells and CNC were incubated statically for 20 minutes at room temperature, then bacterial cells were stained using SYTO 9 green fluorescent nucleic acid dye to facilitate microscopic observation.

4.2.4. Jar test for coagulation

In order to calculate the change over time of the percentage of *P. aeruginosa* aggregation, OD₆₀₀ of the original bacterial suspension in 10 mM of NaCl was measured. Samples of the bacterial suspension were taken at intervals over 24 hours incubation (statically at room temperature). Samples were centrifuged at 800g for 2 minutes and the OD₆₀₀ of the supernatant was measured. The aggregation percentage was calculated as:

$$\text{Aggregation Percentage}\% = \frac{OD_{original} - OD_{supernatant}}{OD_{original}} \times 100 \quad 4.1$$

where $OD_{original}$ represents the OD₆₀₀ of the original bacterial suspension untreated with CNC and $OD_{supernatant}$ represents the OD₆₀₀ of the supernatant of an CNC treated sample after settling.

4.3. Results and Discussion

The application of CNC into the bacterial suspension led to the emergence of large bacterial flocs. Figure 4.3 shows CLSM images of the substrate surface. The sidebars in Figure 4.3 show sectional views of the structure along the z-axis. Bacteria in suspension without CNC were well dispersed and flocculate free (Figure 4.3A) and the culture chamber liquid was observed to be turbid. However, after the addition of CNC, large, dense bacterial aggregates were observed in the media (Figure 4.3B). The cluster due to bacterial flocculation covered the whole image frame which is larger than $200 \times 200 \mu\text{m}^2$.

The formation of flocs was accompanied by visible differences in the culture chamber. Although *P. aeruginosa* can spontaneously form flocs, it was determined that flocs were less likely to be formed in the absence of CNC.

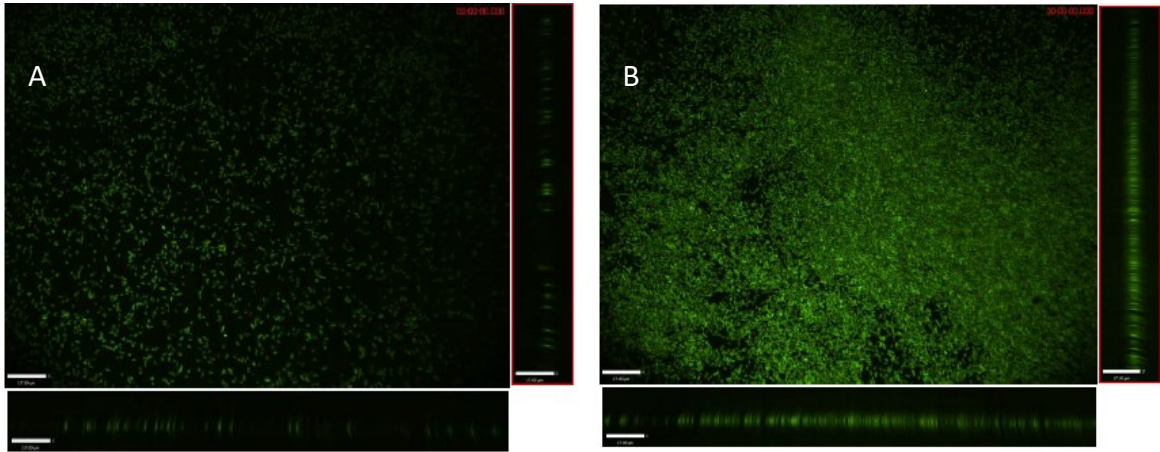


Figure 4.3. Confocal fluorescence slices from the substrate surface and the sidebars illustrate sectional view of the structure along the z-axis. (A) Bacteria without CNC; (B) Bacteria with CNC presence (bacteria to CNC ratio was 1:100,000). (Bar size = 17 μm)

Figure 4.4 shows changes in the *P. aeruginosa* culture aggregation percentage over 24 hours in the absence of CNC and with bacteria:CNC ratios of 1:100,000 and 1:100. In the absence of CNC, *P. aeruginosa* suspension in 10 mM of NaCl appeared turbid and there was no major change in turbidity after 24 hours. This result suggests that bacteria in 10 mM of NaCl solution formed a well dispersed, flocculate free, stable suspension. With the addition of CNC at either 100 or 100,000 times the bacterial number concentrations, a clear solution was formed in the bacterial suspension. The clarification of the bacterial suspension was likely due to the flocculation and phase separation of bacteria by precipitation in the presence of CNC. The decrease in turbidity of the supernatants and

the increase in aggregation percentage with time indicated the formation and settlement of bacterial aggregates in the presence of CNC. The tested CNC concentrations in these experiments were much lower than the concentration (6–8%) where isotropic to nematic phase change occurs. As shown in Figure 4.4, the addition of CNC increased the aggregation percentage significantly during 24 hours incubation: 100% aggregation was achieved in 24 hours when CNC was added to the bacterial suspension in a 100,000:1 ratio compared to around 10% aggregation in the control sample with no CNC. Addition of CNC to the bacterial suspension at a ratio of 100:1 increased the aggregation percentage to 80% in 24 hours compared to the control sample with no CNC. The 15% increase in aggregation in the absence of CNC observed during the 24 hours experimental period may have been caused by a natural process of bacterial aggregation.

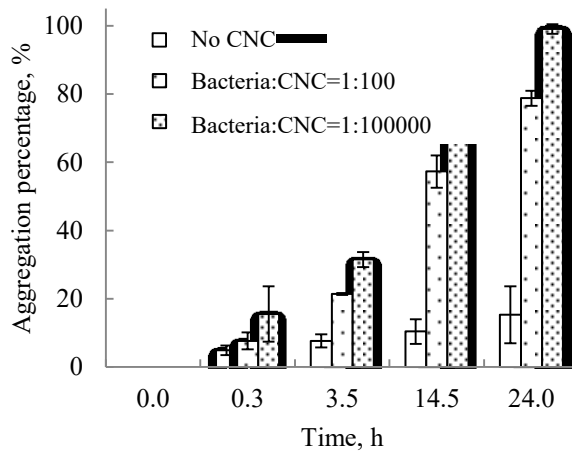


Figure 4.4. Aggregation percentage change over 24 hours of bacterial suspensions with and without CNC (Error bars represent one standard deviation).

Eboigbodin et al. (2005) considered the effect of added non-adsorbing polymers on the

phase behavior of bacteria by depletion. We have shown that the depletion effect is also operational in mixtures of bacteria and CNC rods. Figure 4.5 illustrates schematic pictures of bacteria as large hard cylindrical particles and CNC as small thin rod-shaped particles. Both bacteria and CNC were negatively charged but the CNC had a higher negative zeta potential than the bacteria. As bacteria get close, CNC rods can no longer enter the gap between the big bacterial cells. Then, CNC rods push bacteria together. Hence, CNC particles would be repelled from bacterial cells and could be expected to flocculate bacterial cells by depletion.

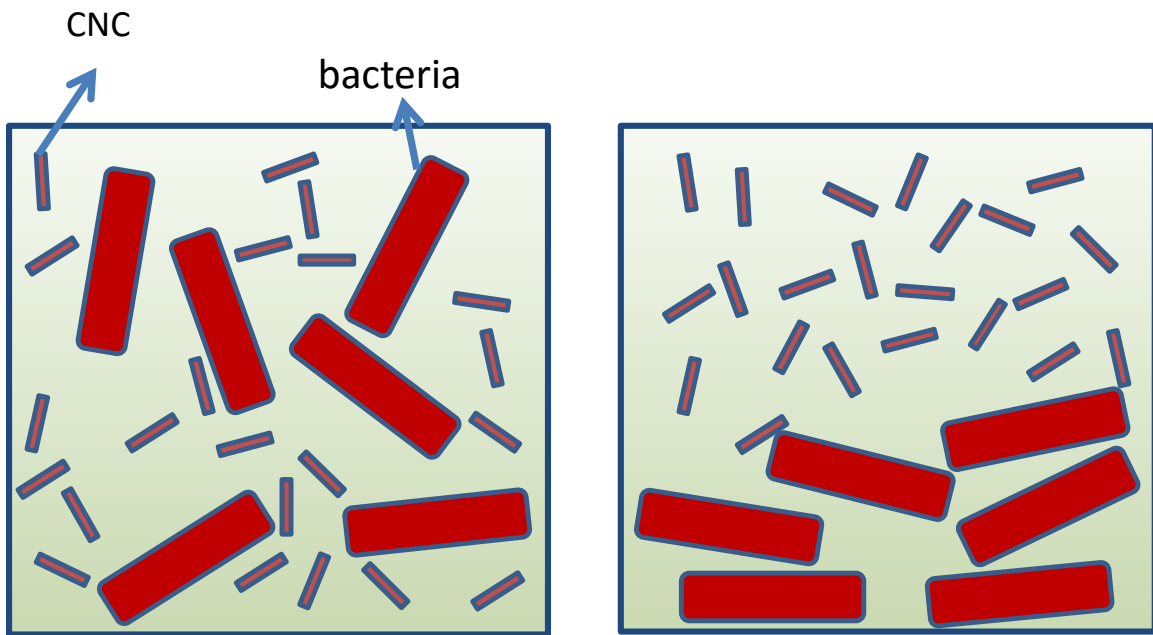


Figure 4.5. Schematic depiction of depletion and phase separation of bacteria due to the presence of rod-shaped NPs (namely, CNC).

Despite the limited number of experiments, the roles of hard spheres, hard rods, and thin disks as depletants have been extensively studied theoretically, as reviewed by Lekkerkerker and Tuinier (2011). The depletion potential W of large hard spheres due to

the presence of small spheres of low density is given by:

$$W(h) = -3k_B T \varphi_s \frac{R}{\sigma} \left(1 - \frac{h}{\sigma}\right)^2 \quad 4.2$$

where k_B is the Boltzmann constant, T is the absolute temperature, φ_s is the volume fraction of small spheres, σ is the diameter of small depletant spheres, R is the radius of the large spheres, and h is the distance between the surfaces of the large spheres. One can estimate the needed depletant concentration if the attraction energy of $-3 k_B T$ is assumed sufficient to induce the phase separation of large particles (Koenderink et al., 1999). As an example, according to equation 4.2, volumetric concentration, φ_s of 0.20 of small spheres with the diameter $\sigma = 100$ nm is needed to phase separate large particles of radius $R = 500$ nm. On the other side, the depletion potential W for the same large colloidal spheres with the radius R in the presence of small rod-shaped particles is given as:

$$W(h) = -\frac{2}{3} k_B T \varphi_r \frac{L}{D} \frac{R}{D} \left(1 - \frac{h}{L}\right)^3 \quad 4.3$$

where L is the length, D is the diameter and φ_r is the volume fraction of rod-shaped particles, R is the diameter and h is the surface to surface distance of bigger spherical colloidal particles. According to equation 4.3, only volume concentration, φ_r of 0.003 of rod-shaped particles with the length, $L = 100$ nm and diameter, $D = 10$ is sufficient to phase separate spherical particles of $R = 500$ nm. As discussed by Koenderink et al. (1999), rod-shaped particles are more efficient depletion agents than spherical particles. Rod-shaped particles can flocculate and phase separate colloids at concentrations lower

than spherical depletants.

It should be noted that CNC concentrations induced bacteria phase separation in the present study were much lower than the critical concentration for colloidal depletion predicted theoretically according to equation 4.3 and reported experimentally (Koenderink et al., 1999). We observed that CNC volume concentration of less than 0.001 produced the flocculation of bacteria. Unlike us, Koenderink et al. (1999) reported that volume concentration of 0.004 silica coated Boehmite (γ -AlOOH) rods with the length $L = 230 \pm 90$ nm and the diameter $D = 9 \pm 2$ nm depleted silica particles with the radius of 370 nm. This result also agrees with the theoretical predictions in equation 4.3. There are few reasons for much better efficiency in our bacteria–CNC mixtures. First of all, our large bacteria are in the form of cylinder shape and clearly do not meet the sphere criterion of equation 4.3. Our system needs to recalculate the interaction between two large cylinders due to hard small rods by using Derjaguin approximation. Nevertheless we still used it to get a rough idea of the volume fraction of rods at which bacteria phase separation may be expected. Secondly, the depletion effect of low concentration of CNC on bacteria can be attributed to the presence of bacterial surface polymers, such as EPS, which vary with different strains. EPS of *P. aeruginosa* are neutrally charged; the primary carbohydrate constituents of *P. aeruginosa* PAO1 EPS are glucose (41.0%), rhamnose (14.3%), and mannose (13.9%) (Liu et al., 2007b). Previous studies showed that bacterial EPS plays significant roles in bacterial aggregation through altering bacterial surface charge density and hydrophobicity (Liu et al., 2010; Flemming and Wingender, 2001a; Flemming and Wingender, 2001b). Therefore our system also does

not meet the hard surface model used in equation 4.3. EPS can also influence cell–cell interactions through causing polymer-mediated repulsive steric interactions or attractive polymer bridging (Eboigbodin et al., 2005; Flemming and Wingender, 2001a; Flemming and Wingender, 2001b).

4.4. Conclusion

Our results showed that rod-shaped NPs cause depletion flocculation of bacteria. Phase separation of bacteria can occur at very low concentrations of rod-shaped CNC particles. The lower end of the concentration range at which phase separation is found is lower than the theoretical estimate. The theoretical estimate is for large hard sphere–small hard rod-shaped particles. In our study, bacteria were large cylindrical particles with hairy and soft surfaces. Nevertheless, our experiments strongly suggest that we have observed entropy-driven fluid–solid phase separation of bacteria in the presence of CNC.

References

- Asakura S, Oosawa F. Interaction between two bodies immersed in a solution of macromolecules. *The journal of physical chemistry* 1954; 1255.
- Asakura S, Oosawa F. Interaction between particles suspended in solutions of macromolecules. *Journal of Polymer Science* 1958; 33: 183-192.
- Bondeson D, Mathew A, Oksman K. Optimization of the isolation of nanocrystals from microcrystalline cellulose by acid hydrolysis. *Cellulose* 2006; 13: 171-180.
- Dogic Z, Purdy KR, Grelet E, Adams M, Fraden S. Isotropic-nematic phase transition in suspensions of filamentous virus and the neutral polymer Dextran. *Physical Review E* 2004; 69.
- Dong XM, Revol JF, Gray DG. Effect of microcrystallite preparation conditions on the formation of colloid crystals of cellulose. *Cellulose* 1998; 5: 19-32.
- Eboigbodin KE, Newton JRA, Routh AF, Biggs CA. Role of nonadsorbing polymers in bacterial aggregation. *Langmuir* 2005; 21: 12315-12319.
- Edgar CD, Gray DG. Influence of dextran on the phase behavior of suspensions of cellulose nanocrystals. *Macromolecules* 2002; 35: 7400-7406.
- Farinato RS, Dubin PL. *Colloid-polymer interactions: from fundamentals to practice*. New York: John Wiley, 1999.
- Fleer GJ, Scheutjens J. Depletion flocculation and stabilization. *Abstracts of Papers of the American Chemical Society* 1983; 186: 65-COLL.

- Flemming HC, Wingender J. Relevance of microbial extracellular polymeric substances (EPSs) - Part I: Structural and ecological aspects. *Water Science and Technology* 2001a; 43: 1-8.
- Flemming HC, Wingender J. Relevance of microbial extracellular polymeric substances (EPSs) - Part II: Technical aspects. *Water Science and Technology* 2001b; 43: 9-16.
- Fuchs M, Schweizer KS. Structure of colloid-polymer suspensions. *Journal of Physics-Condensed Matter* 2002; 14: R239-R269.
- Gavrilescu M, Macoveanu M. Process engineering in biological aerobic wastewater treatment. *Acta Biotechnologica* 1999; 19: 111-145.
- Hamad WY, Hu TQ. Structure-process-yield interrelations in nanocrystalline cellulose extraction. *Canadian Journal of Chemical Engineering* 2010; 88: 392-402.
- Hughes J, Ramsden DK, Symes KC. The flocculation of bacteria using cationic synthetic flocculants and chitosan. *Biotechnology Techniques* 1990; 4: 55-60.
- Jenkins P, Snowden M. Depletion flocculation in colloidal dispersions. *Advances in Colloid and Interface Science* 1996; 68: 57-96.
- Johnson ML, Wan J, Huang S, Cheng Z, Petrenko VA, Kim D-J, et al. A wireless biosensor using microfabricated phage-interfaced magnetoelastic particles. *Sensors and Actuators a-Physical* 2008; 144: 38-47.
- Koenderink GH, Vliegthart GA, Kluijtmans S, van Blaaderen A, Philipse AP, Lekkerkerker HNW. Depletion-induced crystallization in colloidal rod-sphere mixtures. *Langmuir* 1999; 15: 4693-4696.

- Kreft JU, Wimpenny JWT. Effect of EPS on biofilm structure and function as revealed by an individual-based model of biofilm growth. *Water Science and Technology* 2001; 43: 135-141.
- Larsen MU, Seward M, Tripathi A, Shapley NC. Biocompatible nanoparticles trigger rapid bacteria clustering. *Biotechnology Progress* 2009; 25: 1094-1102.
- Lekkerkerker HNW, Tuinier R. *Colloids and Depletion*. Springer 2011; 100.
- Liang Y, Hilal N, Langston P, Starov V. Interaction forces between colloidal particles in liquid: theory and experiment. *Advances in Colloid and Interface Science* 2007; 134-35: 151-166.
- Liu XM, Sheng GP, Luo HW, Zhang F, Yuan SJ, Xu J, Zeng RJ, Wu JG, Yu HQ. Contribution of extracellular polymeric substances (EPS) to the sludge aggregation. *Environmental Science & Technology* 2010; 44: 4355-4360.
- Liu Y, Yang CH, Li J. Influence of extracellular polymeric substances on *Pseudomonas aeruginosa* transport and deposition profiles in porous media. *Environmental Science & Technology* 2007; 41: 198-205.
- Miller M, Bassler B. Quorum sensing in bacteria. *Annual Review of Microbiology* 2001: 165-199.
- Moharikar A, Purohit HJ, Kumar R. Microbial population dynamics at effluent treatment plants. *Journal of Environmental Monitoring* 2005; 7: 552-558.
- Okunuki S, Kawaharasaki M, Tanaka H, Kanagawa T. Changes in phosphorus removing performance and bacterial community structure in an enhanced biological phosphorus removal reactor. *Water Research* 2004; 38: 2433-2439.

Snowden MJ, Clegg SM, Williams PA, Robb ID. Flocculation of silica particles by adsorbing and nonadsorbing polymers. *Journal of the Chemical Society-Faraday Transactions* 1991; 87: 2201-2207.

Chapter 5 Impact of CNC on the Aggregation and Initial Adhesion of *Pseudomonas fluorescens* Bacteria

5.1. Introduction

Bacterial adhesion and biofilm development on solid surfaces is a survival strategy employed by virtually all bacteria. However, biofilm formation in aqueous environments can be detrimental to both human life and industrial processes and should be well controlled (Mattilasandholm and Wirtanen, 1992). For instance, biofilms and bioflocs need to be removed from medical devices to prevent bacterial infection and from drinking water distribution pipes and unit operations to avoid biofouling. It is important to be able to control bacterial attachment and biofilm formation in natural and engineered systems.

The initial attachment of bacteria to a surface is a key preliminary step in biofilm formation because this process has a major impact on subsequent bacterial growth, EPS production, later bacterial adhesion, and biofilm formation. Aggregation and adhesion of bacteria, like that of inert colloids, depend on van der Waals forces, electrostatic interactions, hydrophobic interactions, hydration, steric forces, and other specific forces existant between bacterial cells and surfaces (Liang et al., 2007). The complex and heterogeneous surface structures of bacteria, such as their surface appendages, can complicate the interaction between bacteria and substratum surfaces (Lu et al., 2011). Bacterial surface appendages, such as EPS, are believed to influence bacterial aggregation and adhesion (Bos et al., 1999). Bacterial adhesion to a solid surface consists of two major steps. First, bacterial cell transport to a solid surface is controlled by the size

of the cells and the hydrodynamics of the system. Second, when a cell and a surface are in close proximity, the subsequent interaction can be determined by DLVO-type interactions, hydrophobic, and hydration interactions (Chen and Walker, 2007). Moreover, in the flow regime (simple shear systems), fluid drag effects (shear forces) on bacterial deposition should be taken into account.

Our previous study showed that rod-shaped CNC, even at low concentration (relative to the model prediction), are effective in agglomerating Gram-negative EPS producing bacteria *P. aeruginosa* PAO1 through a depletion mechanism (Sun et al., 2012). It has been suggested that the presence of EPS on *P. aeruginosa* PAO1 cell surfaces contributes to the low CNC concentrations needed to cause bacterial depletion aggregation (Sun et al., 2012). Other physico-chemical factors, such as solution chemistry and the presence of multivalent ion species may also play an important role in bacterial aggregation and adhesion (Chen and Walker, 2007; Otto et al., 1999).

However, it is unclear how CNC-induced bacterial aggregation might depend on the capacity of bacterial cells to produce EPS, and how CNC influence bacterial adhesion in aqueous environments. Hereby, the overall objective of this study was to evaluate the impact of CNC particles on the aggregation and initial adhesion of bacterial cells with different EPS-producing capabilities. The aggregation of bacteria in the absence and presence of CNC was assessed by microscopy and the deposition of bacteria on solid surfaces in the absence and presence of CNC was determined using a batch method and a continuous flow method using a QCM-D. Microscopy was used to quantify cell deposition.

5.2. Material and Methods

5.2.1. Culture and characterization of bacteria

Green fluorescent protein (GFP) labeled Gram-negative strains of *Pseudomonas fluorescens*, wild type (*P. flu* CHA0, with normal EPS production) and the mutant $\Delta gacS$ that can overproduce cellulose in their EPS (*P. flu* CHA19-WS, with increased EPS production; WS [wrinkly spreader] indicates one colony morphology variant from biofilms of the $\Delta gacS$ strain) were selected to perform bacterial aggregation and adhesion experiments. For each experiment, the two strains of *P. flu* CHA0 and *P. flu* CHA19-WS were each streaked onto an LB agar plate and then incubated at 30°C overnight. A single colony from each plate was transferred into 50 mL of LB broth and grown in a shaker incubator at 150 rpm at 30°C overnight. Stationary-phase bacterial cells were harvested by centrifugation at 3000 g at 4°C for 10 minutes. The growth medium was decanted, and the pellets were resuspended in 10 mM of NaCl prepared with reagent grade salt (Fisher Scientific Inc., U.S.) and Milli-Q water (18.2 M Ω , Millipore, Mississauga, ON, Canada) with no pH adjustment (pH 6.0–6.2) and sterilized by autoclave before use. All characterizations and experiments were conducted using this growth medium. Centrifugation and resuspension procedures were repeated two additional times to remove traces of growth media and suspended EPS from the solutions. A final cell density of 1.0×10^8 cells/mL was obtained by measuring the OD₆₀₀ with a UV spectrophotometer (Varian Inc., U.S.). SEM was employed to characterize the size and morphology of the bacterial cells. The zeta potential and average hydrodynamic size of each strain were determined by DLS (Malvern Zetasizer Nano-ZS. Model: ZEN3600,

Malvern Instruments Ltd, Worcestershire, UK) at 25°C. Zeta potential and particle size measurements were repeated in five independent experiments.

5.2.2. CNC suspension: preparation and characterization

A stock suspension of 1.0% (wt) CNC was prepared right before each experiment by suspending CNC particles in 10 mM of NaCl (pH 6.0–6.2), and sonicating the solution for 5 minutes in a ultrasonic bath to disperse the CNC particles. The CNC suspension was then filtered through a 0.45 µm membrane (Acrodisc® Syringe Filters with GHP Membrane, Pall Corporation, US) and used directly in bacterial aggregation and adhesion experiments. The morphology of CNC particles was assessed by TEM. The size and zeta potential of CNC particles were assessed by DLS measurements in 10 mM of NaCl at 25°C. The size was then qualitatively compared with images from TEM.

5.2.3. Bacterial aggregation experiments

In the aggregation experiment, 1 mL 1.0% (wt) CNC suspension was added to 1 mL of the bacterial suspension to achieve a volume fraction of 3.3×10^{-3} mL/mL (detailed calculations of volume fraction are provided in the supplementary material). Treatment controls without added CNC were also prepared. The whole system was incubated statically at 24°C for 30 minutes before bacterial cells were dropped on clean microscopy glass slides (Fisher Scientific) (the cleaning protocol is provided in the supplementary material) to facilitate fluorescent microscopic observations. Microscopic visualization of the slides was carried out under fluorescent light using an Axio Imager M2 microscope (Carl Zeiss, Germany) with a Zeiss LD Plan-NEOFLUAR 40× objective. At least 10 randomly chosen areas of each slide were imaged; the number and size (radius) of

bacterial aggregates in each area were obtained through counting the aggregates in 10 areas and averaging the results. These experiments were conducted in triplicate in at least five independent experiments.

5.2.4. Bacterial initial adhesion experiments: batch method

To evaluate and quantify the impact of CNC on bacterial initial adhesion, a batch method (Lu et al., 2011) was employed by immersing a clean microscopy glass cover slip (Fisher Scientific) in each bacterial suspension. For each adhesion experiment, fresh *P. flu* CHA0 and *P. flu* CHA19-WS bacterial suspensions (1.0×10^8 cells/mL in 10 mM of NaCl) were prepared. 1 mL was distributed in each well of a 24-well plate (Corning Inc., U.S.) and then 1 mL of 1.0% (wt) CNC suspension (in 10 mM of NaCl) was added to each well to achieve a volume fraction of 3.3×10^{-3} mL/mL. The cleaned glass cover slips were completely submerged in the bacterial suspensions, the whole system was placed in a shaker incubator for 30 minutes at 24°C and 120 rpm. The glass cover slips were removed from the bacterial suspensions and rinsed with 10 mM of NaCl solution to remove loosely attached cells. To observe the difference before and after CNC treatment of each strain, the cells attached to the slides were visualized and quantified by fluorescence microscopy. Briefly, after each adhesion test, the bacteria coated slides were placed on clean microscope slides. At least 50 randomly chosen areas on each slide were imaged with fluorescent light with a 40× objective. The size of each image was 3.7632×10^{-4} cm². The cell density (cells/cm²) on each slide was obtained through counting the cells in each area, then taking the average of all of the area cell counts. Batch bacterial adhesion experiments were conducted in duplicate in at least five independent

experiments. The variance of bacterial adhesion was analyzed with a one-way analysis of variance (ANOVA) and was reported as p-values. p-values of less than 0.05 suggested that differences were statistically significant.

5.2.5. Bacterial initial adhesion experiments: continuous flow method

To mimic environmentally relevant flow conditions, and to evaluate real-time bacteria–surface interactions, a continuous flow method was applied using a QCM-D. QCM-D is an advanced technology for the study of surface interactions and provides real-time, label-free measurements of molecular adsorption and/or interactions taking place on surfaces. Based on the piezoelectric effect, the frequency change (ΔF) of a quartz crystal sensor corresponds to the mass loaded on the quartz surface; the dissipation change (ΔD) indicates the energy dissipation response of the freely oscillating sensor and corresponds to the viscoelastic properties of molecular layers as they build up or are otherwise changed on the quartz surface. The QCM-D technique is sensitive to nanograms of mass and can be applied to in situ structural arrangements, thus it is a useful technique to investigate the mechanisms and strength of cell adhesion to surfaces (Marcus et al., 2012; Olsson et al., 2010; Olsson et al., 2011; Strauss et al., 2009).

Deposition of bacteria on silica coated quartz surfaces (with a fundamental resonant frequency of approximately 5 MHz, QSX-303, Q-sense AB, Gothenburg, Sweden) was studied using a QCM-D (Q-sense E4, Biolin Scientific, Sweden). All QCM-D experiments were performed under flow-through conditions, using a digital peristaltic pump (ISMATEC, IPC high precision multichannel dispenser) operating in pushing mode, with the studied solutions injected into the sensor crystal chamber at 0.15 mL/min

(Gutman et al., 2013; Vanoyan et al., 2010); the temperature within each flow module was maintained at 24°C. According to the manufacturer, such a flow rate results in laminar flow through each flow module. Prior to each experiment, the cleaned silica surface was equilibrated by pumping 10 mM of NaCl solution through it. The 1.0% CNC suspension, the bacterial suspension, and the bacterial suspension supplemented with CNC (5 mL bacteria suspension in 10 mM of NaCl plus 5 mL 1.0 % CNC in 10 mM of NaCl) were then each injected for 30 minutes to assess the bacterial deposition behavior. Following the injection, silica surfaces were eluted with 10 mM of NaCl to assess bacterial adhesion stability.

To further investigate the impact of CNC on bacterial deposition, QCM-D experiments were also conducted using CNC coated silica surfaces. Prior to each experiment, the cleaned silica surface was equilibrated by pumping 10 mM of NaCl solution through it. The 1.0% CNC suspension was then injected for 20 minutes to coat the silica surface. Following the injection, silica surfaces were eluted with 10 mM of NaCl to assess CNC deposition stability. Bacterial suspension was then injected for 20 minutes to assess the bacterial deposition behavior. QCM-D experiments were repeated in at least five independent experiments, and representative results were presented in results section.

Microscopy images of the silica surfaces were captured after the QCM-D adhesion experiments to quantify adhered cell numbers. The cell density (cells/cm²) on the silica surfaces was calculated based on the microscopy images. In contrast to the batch systems, QCM-D experiments allow continuous, noninvasive monitoring of bacterial adhesion, which reflects the natural environment where the organisms reside.

5.2.6. DLVO interaction energy calculations

The initial adhesion of bacteria to solid substrata in aquatic systems is considered to be similar to the deposition of colloidal particles. Thus, classic DLVO theory has been widely applied to explain bacterial adhesion behavior (Abu-Lail and Camesano, 2003b; Bayouhd et al., 2009; Walker et al., 2004). Classic DLVO theory describes the total energy ΔG^{TOT} between bacteria and substratum in solution as a balance between attractive Lifshitz-van der Waals ΔG^{LW} and electrostatic interaction free energies ΔG^{EL} as a function of separation distance d (Derjaguin and Landau, 1993; Smith, 1983; Verwey, 1947), as expressed in equation 5.1.

$$\Delta G^{TOT}(d)_{classic} = \Delta G^{LW}(d) + \Delta G^{EL}(d) \quad 5.1$$

Sphere-plate geometry was assumed when calculating the interaction energies between the bacteria and surface (the cells are assumed to be spherical, with radius of a , approaching a semi-infinite plate). The free energies— $\Delta G^{LW}(d)$ and $\Delta G^{EL}(d)$ —involved in this process are expressed in equation 5.2:

$$\Delta G^{LW}(d) = -\frac{A_{123}a}{6d} \quad 5.2$$

$$\Delta G^{EL}(d) = \pi\epsilon a(\zeta_1^2 + \zeta_2^2) \left[\frac{2\zeta_1\zeta_2}{\zeta_1^2 + \zeta_2^2} \ln \frac{1 + \exp(-\kappa d)}{1 - \exp(-\kappa d)} + \ln\{1 - \exp(-2\kappa d)\} \right]$$

A_{123} , ϵ , ζ , and κ^{-1} are the un-retarder bacterium-water-substratum Hamaker constant in water, the permittivity of the medium, the zeta potential, and the Debye length, respectively. d is the separation distance between the bacterium and the substratum. The input parameters needed to describe the electrostatic and van der Waals forces for

bacterium-silica and CNC-silica interactions are provided in Table S5.1 in the supplementary material.

5.3. Results

5.3.1. Characterization of bacterial cells and CNC particles

The wild type strain *P. flu* CHA0 is reported to have normal EPS production, whereas the mutant strain *P. flu* CHA19-WS has increased EPS production. As shown in Figure 5.1, both strains are rod-shaped and equipped with thread-like EPS appendages. More EPS coverage was observed on *P. flu* CHA19-WS (Figure 5.1B) than on *P. flu* CHA0 (Figure 5.1A). The results are consistent with the fact that *P. flu* CHA19-WS cells overproduce cellulose in their EPS (Workentine et al., 2008). DLS measurements showed that the hydrodynamic diameter of *P. flu* CHA0 cells, $1.76 \pm 0.07 \mu\text{m}$, corresponding to an equivalent radius of $0.44 \mu\text{m}$ (Table 5.1), was longer than that of *P. flu* CHA19-WS cells, $1.44 \pm 0.03 \mu\text{m}$, which corresponded to an equivalent radius of $0.41 \mu\text{m}$ (Table 5.1), a finding that was confirmed by SEM images (Figure 5.1). In addition, under the experimental conditions of 10 mM of NaCl, pH 6.0–6.2, the two strains displayed statistically different ($p = 1.9 \times 10^{-4}$) negative zeta potential values, $-18.78 \pm 1.31 \text{ mV}$ and $-16.22 \pm 0.89 \text{ mV}$ for *P. flu* CHA0 and *P. flu* CHA19-WS, respectively.

Figure 5.2 shows a TEM image of rod-shaped CNC particles with a length of 100–200 nm and a width (diameter) of around 10 nm; the hydrodynamic diameter (length) of the CNC particles measured using DLS was $114 \pm 2.13 \text{ nm}$, which corresponds to an equivalent radius of $0.020 \mu\text{m}$ (Table 5.1). The zeta potential of the CNC particles in 10 mM of NaCl, pH 6.0–6.2, was $-42.3 \pm 1.07 \text{ mV}$, indicating negatively charged surfaces

that can be attributed to the sulfate ester groups introduced by the esterification reaction during hydrolysis.

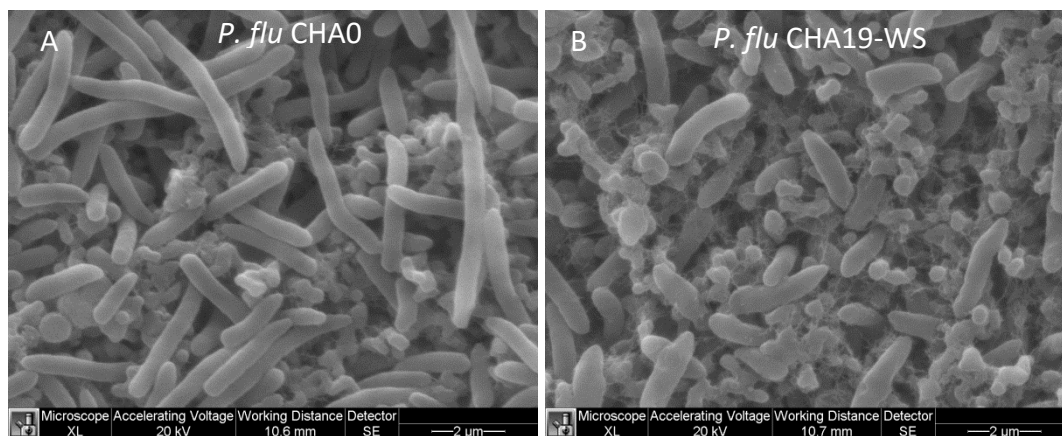


Figure 5.1. Representative SEM micrographs of (A) *P. flu* CHA0 and (B) *P. flu* CHA19-WS

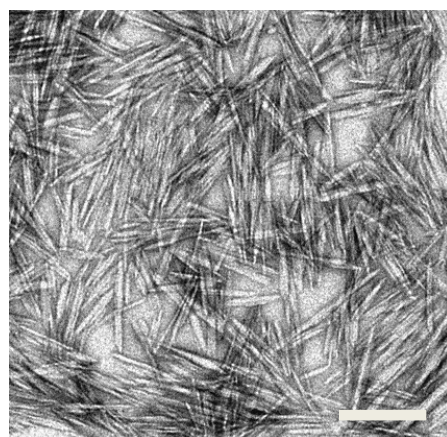


Figure 5.2. A TEM image of CNC particles (Bar size = 200 nm)

5.3.2. Bacterial aggregation

Without CNC, the two strains were well dispersed (Figures S5.1A and C), free of flocculate (average radius = 0.44 μm and 0.41 μm for *P. flu* CHA0 and *P. flu* CHA19-WS, respectively, calculated based on DLS measurements), and the culture chamber

liquid was observed to be turbid. With the addition of CNC, *P. flu* CHA19-WS showed significant aggregation and formed large, dense bacterial aggregates (estimated average radius = 4.5 μm) (Figure S5.1D), while *P. flu* CHA0 formed small, loose bacterial aggregates (estimated average radius = 2 μm) (Figure S5.1B). The results indicate that, although bacterial cells can spontaneously form flocs, bacterial flocs were unlikely to form without CNC application under the experimental conditions tested here.

Table 5.1. Key parameters used in DLVO calculations and interaction energies as calculated by DLVO theory

Sample	Size ^a (μm)		Zeta potential ^b (mV)	$\Phi_{1\text{min}}$ ^c (kT)	Φ_{max} ^d (kT)	$\Phi_{2\text{min}}$ ^e (kT)
	DLS	Equivalent Radii				
<i>P. flu</i> CHA0	1.76±0.07	0.44	-18.78±1.31	-860	202	-4.6
<i>P. flu</i> CHA0+CNC	N/A	2.0	-18.78±1.31	-3907	920	-20.9
<i>P. flu</i> CHA19-WS	1.44±0.03	0.41	-16.22±0.89	-847	118	-4.6
<i>P. flu</i> CHA19-WS+CNC	N/A	4.5	-16.22±0.89	-9293	1299	-50
CNC	0.114±0.002	0.020	-42.30±1.07	-319.0	10.0	-1.9

- The average particle hydrodynamic size, determined by DLS. (Aggregates size of *P. flu* CHA0, and *P. flu* CHA19-WS after addition of CNC was determined by microscopy)
- Zeta potential was tested in 10 mM of NaCl solution (pH 6.0–6.2).
- The depth of the primary energy minimum, calculated by DLVO theory.
- The height of the primary energy barrier, calculated by DLVO theory.
- The depth of the secondary energy minimum, calculated by DLVO theory.

To determine the interaction between bacterial cells and CNC particles, zeta potential distributions of bacteria, of CNC, and of a mixture of bacteria and CNC were measured under the same physico-chemical conditions. The measurement of zeta potential distributions of individual components and their combination to study particle interactions follows the work of Xu et al. (2003). As shown in Figure S5.2A, samples

with only CNC particles exhibited single modal zeta potential distributions, with peaks at ~ -40 mV. Samples with only bacterial strains also exhibited single modal zeta potential distributions, with peaks at ~ -17 mV and ~ -15 mV for *P. flu* CHA0 (Figure S5.2B) and *P. flu* CHA19-WS (Figure S5.2C), respectively. A bimodal zeta potential distribution was observed for samples with a mixture of CNC and bacterial cells, with a peak at ~ -40 mV representing CNC particles and a peak at ~ -17 mV representing *P. flu* CHA0 (Figure S5.2D), a peak at ~ -15 mV representing *P. flu* CHA19-WS (Figure S5.2E). The zeta potential distribution results suggest that bacterial cells and CNC have no direct contact with each other under the conditions tested. This observation implies that depletion interactions play a key role in the observed bacterial aggregation in the presence of CNC. However, the impact of physico-chemical factors (e.g., pH, IS) on CNC-induced bacterial aggregation deserves further research.

5.3.3. Batch bacterial initial adhesion

Figure 5.3 illustrates the enumeration of the cell density of each strain deposited on glass cover slips, determined from microscopic observations. As can be seen in Figure 5.3, in the absence of CNC, *P. flu* CHA19-WS showed a slightly higher ($p = 0.049$) adhesion capability (average $1.02 \times 10^6 \pm 3.85 \times 10^5$ cells/cm²) than did *P. flu* CHA0 (average $7.40 \times 10^5 \pm 1.84 \times 10^5$ cells/cm²), which might be explained by the fact that *P. flu* CHA19-WS is less negatively charged than the wild type *P. flu* CHA0. It should also be noted that the higher EPS coverage of the *P. flu* CHA19-WS strain, in comparison to its wild type strain, might play an important role in controlling its initial adhesion to glass surfaces. In a bacterial adhesion kinetic study using a radial stagnation point flow

system, Chen and Walker (2007) indicated that a greater bacterial adhesion to a quartz surface resulted from more EPS coverage.

After the addition of CNC, deposition of *P. flu* CHA0 (average 2.07×10^5 cells/cm²) and *P. flu* CHA19-WS (average 8.69×10^4 cells/cm²) on glass cover slips was significantly ($p = 7.72 \times 10^{-8}$ and 4.49×10^{-7} , respectively) inhibited, and achieved about 0.6 (~ 72%) and 1.1 log-unit reduction (~ 91.5%) in cell density, respectively.

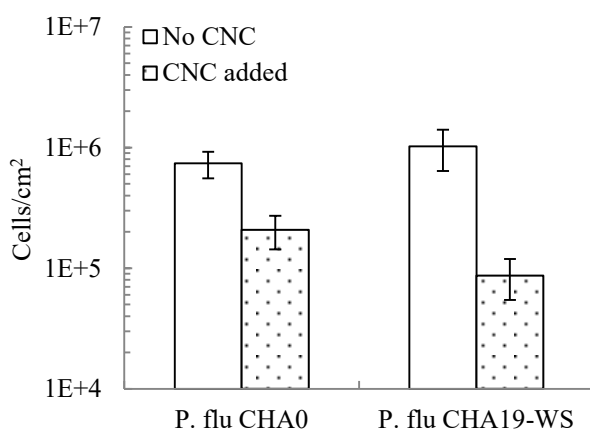


Figure 5.3. Enumeration of batch bacterial adhesion studies. Each data point represents the average of three measurements for one sample. Error bars represent the standard deviation.

5.3.4. Bacterial initial adhesion under continuous flow conditions

Bacterial initial adhesion under continuous flow conditions (flow rate = 0.15 mL/min) was studied using a QCM-D coupled with a fluorescence microscope. QCM-D frequency shifts (ΔF) and dissipation changes (ΔD) with time were monitored, where a large ΔF suggests a large mass load on silica surfaces and a large ΔD suggests a soft mass load on silica surfaces.

As shown in Figure 5.4A, adsorption began as soon as the sample solution made contact with the silica surface. In the absence of bacteria, CNC adsorption on silica reached a plateau of around 1.75 Hz about 50 minutes post-CNC injection.

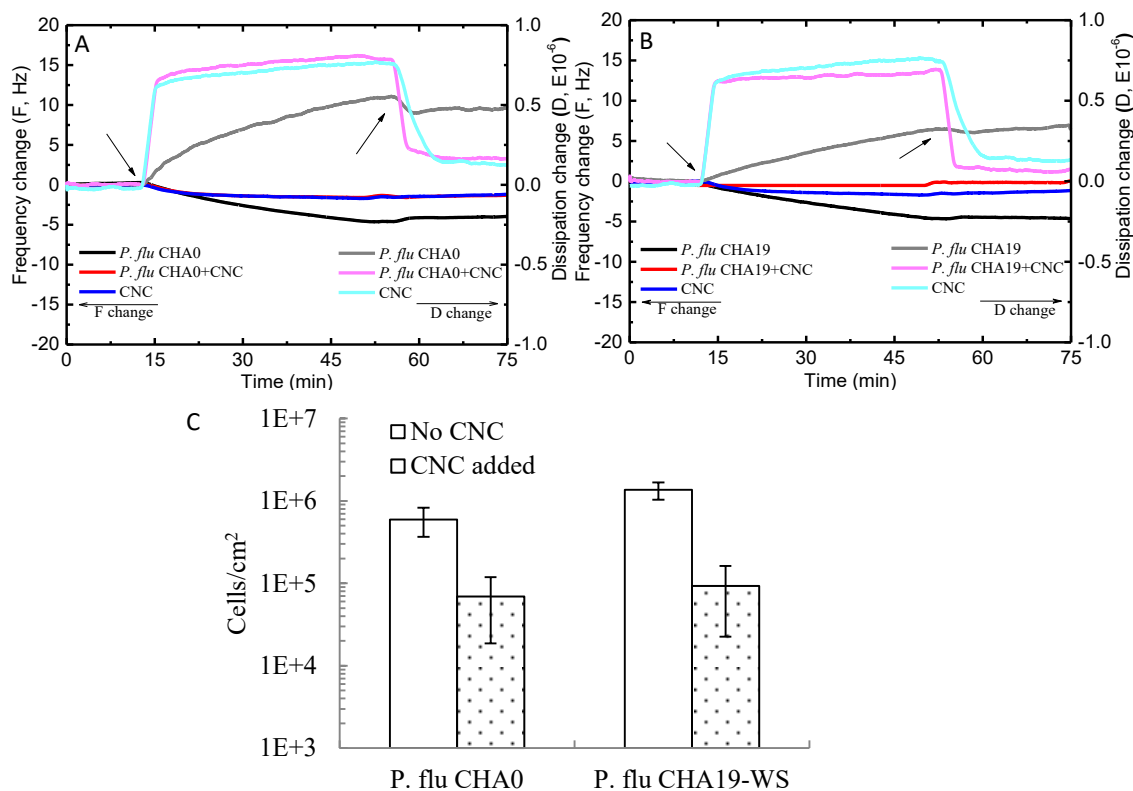


Figure 5.4. Representative QCM-D adhesion results (The frequency change ΔF and dissipation change ΔD responses for the adsorption of CNC, bacteria with CNC and bacteria respectively obtained from QCM-D measurements. Solutions were sequentially pumped through the SiO₂ sensor surface in the following order: 10 mM of NaCl (0–10 minutes, flat line in the figure), samples (CNC, mixture of bacteria and CNC, bacteria) in 10 mM of NaCl (starting from the arrowed position), and 10 mM of NaCl (starting from the arrowed position) at 0.15 mL/min.) (A) Adsorption profile of *P. flu* CHA0 with and without CNC; (B) Adsorption profile of *P. flu* CHA19-WS with and without CNC; (C)

Cell density (cells/cm²) on silica surface after QCM-D adhesion experiments. Each data point represents the average of three measurements for one sample. Error bars represent the standard deviation.

In approximately 55 minutes, *P. flu* CHA0 achieved a ΔF of around 4.5 Hz without CNC and a ΔF of 1.75 Hz with CNC, a value the same as that of CNC alone. The finding that the ΔF of *P. flu* CHA0 supplemented with CNC was lower than that of *P. flu* CHA0 alone, indicates that *P. flu* CHA0 adhesion to a silica surface was inhibited by CNC. Adsorbed CNC and *P. flu* CHA0 supplemented with CNC desorbed slightly upon rinsing with 10 mM of NaCl. In the absence of CNC, adsorbed *P. flu* CHA0 desorbed significantly and reached a final ΔF of around 4 Hz. The desorption of *P. flu* CHA0 suggests that these bacteria had been reversibly deposited on the silica surface.

Similarly, the ΔD began to change as soon as the sample made contact with the silica surface (Figure 5.4A). It should be noted that dissipation occurs when the driving voltage to the crystal is shut off and the energy from the oscillating crystal dissipates from the system. ΔD indicates the energy dissipation (loss of energy/damping) response of the freely oscillating sensor, which corresponds to the viscoelastic properties of the adsorbed molecular layers on the quartz surface (equation S5.4 in the supplementary material). A final ΔD of around 0.15×10^{-6} for both CNC and *P. flu* CHA0 supplemented with CNC was achieved. The final ΔD of *P. flu* CHA0 was around 0.5×10^{-6} . This suggests that the binding of attached *P. flu* CHA0 cells to the silica surface was relatively more flexible than the binding of *P. flu* CHA0 supplemented with CNC, where the cell might not be

coupled so closely to the surface, highlighting the viscoelastic nature of the attached bacterial cells (Poitras and Tufenkji, 2009).

The adsorption of *P. flu* CHA19-WS achieved a final ΔF around 5 Hz (Figure 5.4B), and desorbed only slightly upon rinsing with 10 mM of NaCl. Consistent with the batch adhesion results (Figure 5.3), *P. flu* CHA19-WS (Figure 5.4B) showed a slightly higher adhesion capability than that of *P. flu* CHA0 (Figure 5.4A) under the same hydrodynamic flow condition. ΔF of the *P. flu* CHA19-WS supplemented with CNC was around 0.2 Hz and decreased to around 0 Hz when rinsed with 10 mM of NaCl, indicating that few *P. flu* CHA19-WS cells were adsorbed on the silica surface and that the adsorption was loose.

A final ΔD of about 0.35×10^{-6} was achieved with *P. flu* CHA19-WS and a final ΔD of about 0 was observed for *P. flu* CHA19-WS supplemented with CNC. This suggests a relatively more rigid binding of attached *P. flu* CHA19-WS cells supplemented with CNC to the silica surface, compared with *P. flu* CHA19-WS cells only.

Because it is difficult to directly link ΔF in QCM-D to the numbers of the attached bacterial cells (Gutman et al., 2013; Marcus et al., 2012; Olsson et al., 2011), microscopy was employed to quantify cell numbers of bacteria adhered to the silica surfaces to support ΔF results in QCM-D bacterial adhesion studies. Microscopy images of the silica surfaces were captured after each QCM-D adhesion experiment, and the cell density on silica surfaces was calculated (Figure 5.4C) based on the microscopy images. As shown in Figure 5.4C, adhesion of *P. flu* CHA0 ($\sim 5.96 \times 10^5$ cells/cm²) on silica surfaces was significantly ($p < 0.05$) inhibited by CNC (to $\sim 6.87 \times 10^4$ cells/cm², or $\sim 88.5\%$

inhibition), which was consistent with the *P. flu* CHA0 QCM-D adhesion results (shown in Figure 5.4A). The cell density of *P. flu* CHA19-WS on the silica surface ($\sim 1.36 \times 10^6$ cells/cm²) was higher than that of *P. flu* CHA0 ($\sim 5.96 \times 10^5$ cells/cm²), which is consistent with the batch (Figure 5.3) and QCM-D adhesion results (Figures 5.4A and 5.4B). In the presence of CNC, adsorption of *P. flu* CHA19-WS was also significantly ($p < 0.05$) hindered (to $\sim 9.25 \times 10^4$ cells/cm², or $\sim 93.2\%$ inhibition), as determined from microscopic observations (Figure 5.4C), although the final ΔF of the *P. flu* CHA19-WS supplemented with CNC was about 0 in QCM-D experiments (Figure 5.4B), which might be associated with the presence of EPS and surface hydrophobicity, as these factors have been reported to lead to a reduced ΔF in QCM-D results (Gutman et al., 2013; Marcus et al., 2012). Therefore, it is necessary to use direct microscopy to support ΔF results in QCM-D bacterial adhesion studies (Gutman et al., 2013; Marcus et al., 2012; Olsson et al., 2011).

5.3.5. Classic DLVO interactions

Experimentally measured equivalent radii and zeta potential values were used in the DLVO interaction energy calculations (Table 5.1). The calculated primary energy minimum ($\Phi_{1\min}$), the primary energy barrier (Φ_{\max}), and the secondary energy minimum ($\Phi_{2\min}$) are presented in Table 5.1. The DLVO energy profiles are depicted in Figure S5.3 in the supplementary material. A negative Φ at the primary energy minimum or secondary energy minimum indicates attractive forces that contribute to colloidal attachment whereas a positive Φ suggests a repulsive force that promotes colloidal stability or mobility. Although an idealized DLVO approach was applied by assuming

bacterial cells and CNC particles were smooth spheres, the energy calculations can be considered to capture the qualitative trends of the samples.

Figure S5.3 shows the energy sum of the electrostatic and van der Waals interactions, both of which decay with separation distance. Without CNC, the strong positive repulsive energy barriers of *P. flu* CHA0 (202 kT) and *P. flu* CHA19-WS (118 kT) to the silica surface indicate that the adhesion of both cell types to the silica surface was unfavorable. This was expected because the surface of both bacterial cells and silica surface were negatively charged under most physiological conditions, giving rise to repulsive electrostatic interactions on close approach. Previous studies reported that bacterial adhesion to solid surfaces (for instance, sand grains) occurred in the presence of sizable calculated primary energy barriers up to 1000 kT, likely due to the local surface charge heterogeneities on collector surfaces, which are not accounted for by classic DLVO theory (Redman et al., 2004; Truesdail et al., 1998). Additionally, the presence of shear force in both batch and QCM-D systems in the current study might also contribute to an unfavorable condition for bacterial deposition. In the present study, bacterial adhesion occurred under both batch (Figure 5.3) and hydrodynamic flow (Figure 5.4) conditions, suggesting bacterial adhesion studied here might be attributed to the primary minima. Of note, the secondary minima of both bacterial strains were around -4.6 kT, which are higher than the average thermal energy of the Brownian particles themselves (~ 1.5 kT) (Hahn and O'Melia, 2004). Thus, deposition in secondary minima for both strains was not negligible. The depths of primary minima and secondary minima of both bacteria were close to each other, suggesting that the theoretical DLVO energy profiles (Figure S5.3)

could not explain the observed difference in adhesion abilities of the two bacterial strains (Figures 5.3 and 5.4). The presence of shear force and different EPS coverage (*P. flu* CHA19-WS has increased EPS production than *P. flu* CHA0, Figure 1) might explain the different adhesion abilities. *P. flu* CHA0 cells with a hydrodynamic diameter of $1.76 \pm 0.07 \mu\text{m}$, corresponding to an equivalent radius of $0.44 \mu\text{m}$ (Table 5.1), were bigger than *P. flu* CHA19-WS cells with a hydrodynamic diameter of $1.44 \pm 0.03 \mu\text{m}$, corresponding to an equivalent radius of $0.41 \mu\text{m}$ (Table 5.1); thus, *P. flu* CHA0 cells may experience a larger shear force and thus be less easily deposited than *P. flu* CHA19-WS cells. Zeta potential values indicate that *P. flu* CHA0 cells ($-18.78 \pm 1.31 \text{ mV}$) were more negatively charged than *P. flu* CHA19-WS cells ($-16.22 \pm 0.89 \text{ mV}$) under the tested conditions in this study, thus, *P. flu* CHA0 cells attached less than *P. flu* CHA19-WS cells.

With the addition of CNC, DLVO predicted deep primary minima (-9293 kT for *P. flu* CHA19-WS and -3907 kT for *P. flu* CHA0) and secondary minima (-50 kT for *P. flu* CHA19-WS and -20.9 kT for *P. flu* CHA0) for both bacterial cells to the silica surface, indicating that more cell deposition was expected than was observed in our adhesion results. This deviation might be explained by the fact that the larger-sized bacterial aggregates formed in the presence of CNC could experience reduced convective-diffusive transport to the solid surface, resulting in their reduced deposition on the surface.

In the case of CNC particles only, a positive energy barrier about 10 kT was predicted. Although CNC particles and the silica surface were both negatively charged, it is possible for some CNC particles to deposit on the silica surface irreversibly in the primary minimum due to the small primary energy barrier. The QCM-D study showed an obvious

deposition of CNC on the silica surface, and those previously deposited CNC was only partially removed after Milli-Q water injection (Figure S5.4), indicating that CNC adhesion was mainly attributed to the primary minimum, and CNC might also interact with the silica surface at a small separation distance (around 15 nm), due to the presence of the reversible secondary minimum (-1.9 kT).

Bacterial cells may also experience steric, hydration, and hydrodynamic forces when approaching a silica surface. Surface roughness or surface charge heterogeneity (Johnson and Tong, 2006; Li et al., 2008; Vanoyan et al., 2010; Walker et al., 2004) of both bacterial and silica surfaces may represent other explanations for deviation of the observed bacterial adhesion behaviors from predicted DLVO curves. Furthermore, the zeta potential of the silica surface might have changed due to the deposition of CNC. However, it is challenging to evaluate the distribution of CNC on the silica surface, and the reference zeta potential values used in the classic DLVO interaction calculations are likely to be inaccurate.

5.4. Discussion

5.4.1. Impact of CNC on bacterial aggregation

Our studies showed that CNC particles induce bacterial aggregation mainly through depletion interactions. Based on the depletion mechanism (Vrij, 1976), the addition of repulsive CNC particles into a dispersion of bigger colloidal bacterial cells might destabilize the system. Theoretical calculations of the depletion potential W for bacterial cells in the presence of rod-shaped CNC particles are given as (detailed calculations are provided in the supplementary material):

$$W(h) = -\frac{2}{3}k_B T \varphi_r \frac{L}{D} \frac{R}{D} \left(1 - \frac{h}{L}\right)^3 \quad 5.3$$

where k_B is the Boltzmann constant, T is the absolute temperature, L is the length, D is the diameter, φ_r is the volume fraction of rod-shaped particles (CNC particles), R is the diameter, and h is the surface-to-surface distance of bigger spherical colloidal particles (bacterial cells). The result indicates that under the test conditions in this study, depletion aggregation was unlikely to occur due to the low CNC concentration in the system (3.3×10^{-3} mL/mL); based on the model prediction, a volume fraction φ_r of 1×10^{-2} mL/mL is needed for aggregation. There are three possible explanations for the observed deviation of the aggregation from predicted depletion potentials.

First, the formula (equation 5.3) used in the depletion potential calculations is ideal for large spherical particles in the presence of small, rod-shaped particles, whereas the bacterial cells in the current study were cylindrically shaped. Second, the deviation might be explained by the presence of bacterial EPS which could impose polymer-mediated steric interactions such as polymer bridging that were not considered in the predicted depletion potentials. Eboigbodin et al. (2005) showed that EPS were involved in a depletion attractive mechanism, which induced bacterial aggregation and phase separation of *E. coli* cells. Previous studies (Eboigbodin et al., 2005; Tsuneda et al., 2004) have shown that EPS surrounding the bacterial cells can trigger a depletion interaction among the bacterial cells. Repulsive interactions between like-charged bacterial cells can lead to depletion, whereas the presence of EPS can impose polymer bridging (Strand et al., 2001), resulting in more significant aggregation of the more EPS-

covered strain (*P. flu* CHA19-WS in our study). As polymer induced forces are sensitive to the IS of the solution (Kim et al., 2009; Kim et al., 2010), the impact of polymer bridging on bacterial adhesion in the presence of CNC under different IS conditions should be investigated. Third, the surface charge of bacterial cells might play an important role in bacterial aggregation (Wang et al., 2011). In a previous study (Sun et al., 2012), CNC induced much more significant aggregation of *P. aeruginosa* PAO1 than was observed in the two *P. fluorescens* strains in the current study. The *P. aeruginosa* PAO1 used in the previous study was more negatively charged (−29.84 mV in 10 mM of NaCl, pH 6.0–6.2) than the *P. fluorescens* strains (−18.78 and −16.22 mV for *P. flu* CHA0 and *P. flu* CHA19-WS, respectively in 10 mM of NaCl, pH 6.0–6.2) used in this study.

5.4.2. Impact of CNC on bacterial initial adhesion

In the presence of CNC, a significant reduction in bacterial initial adhesion on glass surfaces was observed using both batch and continuous flow methods, suggesting that CNC is capable of reducing bacterial initial adhesion to a solid surface. It was also observed that the extent of CNC-induced reduction in bacterial initial adhesion varied depending on the bacterial surface EPS coverage. There are several potential explanations for the above observations.

First, compared to single bacterial cells, the larger-sized bacterial aggregates formed in the presence of CNC could experience reduced convective-diffusive transport to the solid surface, resulting in their reduced deposition on the surface. Based on the dimensions and flow rates employed in the QCM-D flow cell, the *Pe* number was estimated to be 0.001

(Vanoyan et al., 2010), indicating that the bacteria in the QCM-D flow cell effectively experienced a diffusion-dominated flow regime (Elimelech et al., 1995; Quevedo and Tufenkji, 2009). Therefore, the decrease in diffusion coefficient with increasing colloid size that led to reduced bacterial deposition in the presence of CNC, could also hold true for the QCM-D flow cell.

The extent of bacterial deposition reduction varied depending on the bacterial surface EPS coverage. In the presence of CNC, bacteria with more EPS formed relatively larger flocs compared to bacteria with less EPS (Figures S5.1 D and B), resulting less bacterial initial adhesion under both batch (Figure 5.3) and continuous flow conditions (Figure 5.4C).

Second, in the presence of CNC, larger bacterial aggregates experience greater shear force along the solid surface than do nonaggregated cells; an increased shear force might lead to a greater detachment rate. The shear force under hydrodynamic flow conditions likely sweeps attached secondary minimum associated bacteria from the system (Johnson and Tong, 2006).

Third, adsorption of negatively charged CNC particles on silica surfaces contributes repulsive electrostatic and steric forces that can reduce the deposition of bacterial cells and enhance the reentrainment of deposited bacterial cells to the bulk liquid. CNC adsorption on silica surfaces increased the surface negativity (-42.3 ± 1.07 mV and -36.3 ± 0.15 mV in 10 mM of NaCl, pH 6.0–6.2, for CNC and the silica surface, respectively). Deposition of bacterial cells might be hindered due to the enhanced repulsive forces between the bacterial cells and the CNC coated silica surfaces. This hypothesis was

supported by our QCM-D study that showed no more bacterial adhesion on CNC coated silica surface (Figure S5.4).

Fourth, the presence of CNC may lead to a bacterial EPS conformational change that inhibits EPS interaction with solid surfaces. Chen and Walker (2007) reported that due to the presence of certain ions, bacterial surface polymers may become more rigid and thus be inhibited from interacting with a quartz surface. This rigidity minimized the ability of the polymers to reconfirm to and interact directly with a solid surface. In our study, the antibacterial adhesion effects of CNC were more pronounced for bacterial cells with greater EPS coverage, indicating that EPS play a significant role in controlling bacterial interactions with CNC and other bacteria. However, further experiments that test the impact of CNC on bacterial surface polymers are needed to evaluate this hypothesis.

Other potential mechanisms should also be considered. For instance, with an increase of bacterial size, gravitational settling probably increases resulting in more bacterial deposition on silica surfaces. A previous study showed that gravitational dominance can be expected for particles greater than 1 μm in diameter (Chen et al., 2010). In the present study, the equivalent spherical diameter of bacterial cells increased from $\sim 0.8 \mu\text{m}$ in the absence of CNC to 4 μm and 9 μm in the presence of CNC for *P. flu* CHA0 and *P. flu* CHA19-WS, respectively. Our results indicate that gravitational sedimentation did not play a significant role in controlling bacterial initial adhesion under the conditions in this study. Other interaction forces, such as the shear force may play a more important role and lead to reduced bacterial adhesion in the presence of CNC. Further research on the impact of flow conditions (such as flow rate) and physico-chemical factors (such as pH

and IS) on bacterial adhesion in the presence of CNC will provide better understanding of the mechanisms in CNC-reduced bacterial initial adhesion.

5.5. Conclusion

This study indicates that CNC can induce bacterial aggregation, and thus inhibit subsequent bacterial initial adhesion on solid surfaces. Under the batch and hydrodynamic flow conditions applied, the effect of CNC on bacterial aggregation caused a significant reduction in bacterial initial adhesion to silica surfaces. Thus, CNC might be an excellent candidate for creation and manipulation of bacterial flocs and for preventing bacterial initial adhesion and subsequent biofilm development. Artificial formation of bioflocs and control of the development of biofilms are of interest in many applications involving in biodegradation or bioremediation (Kumar et al., 2011).

Supplementary Material

CNC volume fraction calculations:

Density of CNC is 1.5 g/cm^3 (Sun et al., 2012).

$$1.0\% \text{ (wt) CNC volume fraction} = \frac{1\%}{\text{Density of CNC}} = \frac{0.01 \text{ g/mLH}_2\text{O}}{1.5 \text{ g/cm}^3} = 6.6 \times 10^{-3} \text{ cm}^3 / \text{mLH}_2\text{O} = 6.6 \times 10^{-3} \text{ mL} / \text{mLH}_2\text{O}$$

In the current study, 1 mL 1.0% (wt) CNC suspension was added to 1 mL of the bacterial suspension, thus CNC weight concentration was 0.5%.

$$0.5\% \text{ (wt) CNC volume fraction} = \frac{6.6 \times 10^{-3} \text{ mL} / \text{mL}}{2} = 3.3 \times 10^{-3} \text{ mL/mL}$$

Microscopy glass slides/glass cover slips cleaning protocol:

Prior to each experiment, the slide pieces were thoroughly rinsed with deionized (DI) water to remove visible impurities (large particles). Subsequently, the slides were immersed in 1N HCl and sonicated for 10 minutes to remove grease. After sonication, the slides were rinsed with sterilized ultrapure water, 70% ethanol, and sterilized ultrapure water successively. Finally, the drying process was achieved in a biosafety cabinet (CLASS II Type A2, Microzone Cor., Canada). The clean slides were reserved as slides used in the bacterial aggregation and initial adhesion experiments (Hwang et al., 2012).

Zeta potential measurements of glass slides:

To determine the surface charge of glass slide surfaces, silicon dioxide particles (approx. 99%; particle size 0.5–10 μm with 80% being between 1–5 μm . Sigma–Aldrich) were used. Zeta potential of silicon dioxide particles was measured in 10 mM of NaCl solution with no pH adjustment (pH 6.0–6.2) using a Malvern Zetasizer Nano-ZS

(Model: ZEN3600, Malvern Instruments Ltd, Worcestershire, UK) at 25°C. Zeta potential of glass slides is reported to be -36.3 ± 0.15 mV in this study.

Depletion potential calculations:

The depletion potential W for the same colloidal spheres with the radius R in the presence of rod-shaped particles is given as:

$$W(h) = -\frac{2}{3}k_B T \varphi_r \frac{L}{D} \frac{R}{D} \left(1 - \frac{h}{L}\right)^3 \quad 5.3$$

where k_B is the Boltzmann constant, T is the absolute temperature, L is the length, D is the diameter, φ_r is the volume fraction of rod-shaped particles (CNC particles here), R is the diameter and h is the surface-to-surface distance of bigger spherical colloidal particles (bacterial cells here). One can estimate the needed depletant concentration if the attraction energy of $-3 k_B T$ is assumed sufficient to induce the phase separation of large particles (Lekkerkerker and Tuinier, 2011).

Parameters used in the current study:

$$L = 100 \text{ nm}$$

$$D = 10 \text{ nm}$$

$R = 440$ and 410 nm (Equivalent Radii) for *P. flu* CHA0 and *P. flu* CHA19-WS cells respectively

$$\varphi_r = 3.3 \times 10^{-3} \text{ mL/mL}$$

According to equation 5.3, the depletion potential $W(h)$ was about $-1 k_B T$, which is less than $-3 k_B T$. Therefore, the depletion aggregation was unfavorable in the current study.

Dissipation change (ΔD) in QCM-D experiments:

ΔD is defined by the following equation S5.5:

$$\Delta D = \frac{E_{lost}}{2\pi E_{stored}} \quad \text{S5.4}$$

where E_{lost} is the energy lost during one oscillation cycle, E_{stored} is the total energy stored in the oscillator. ΔD represents the sum of all processes that induce energy losses in the oscillating system (Rodahl et al., 1995).

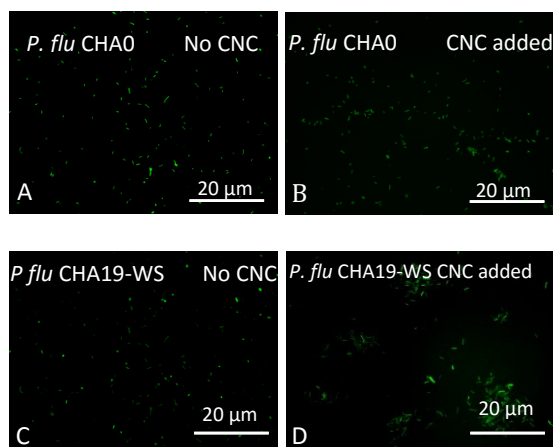


Figure S5.1. Representative fluorescent microscopy images of bacterial aggregation. *P. flu* CHA0 without (A) and with CNC (B); *P. flu* CHA19-WS without (C) and with CNC (D).

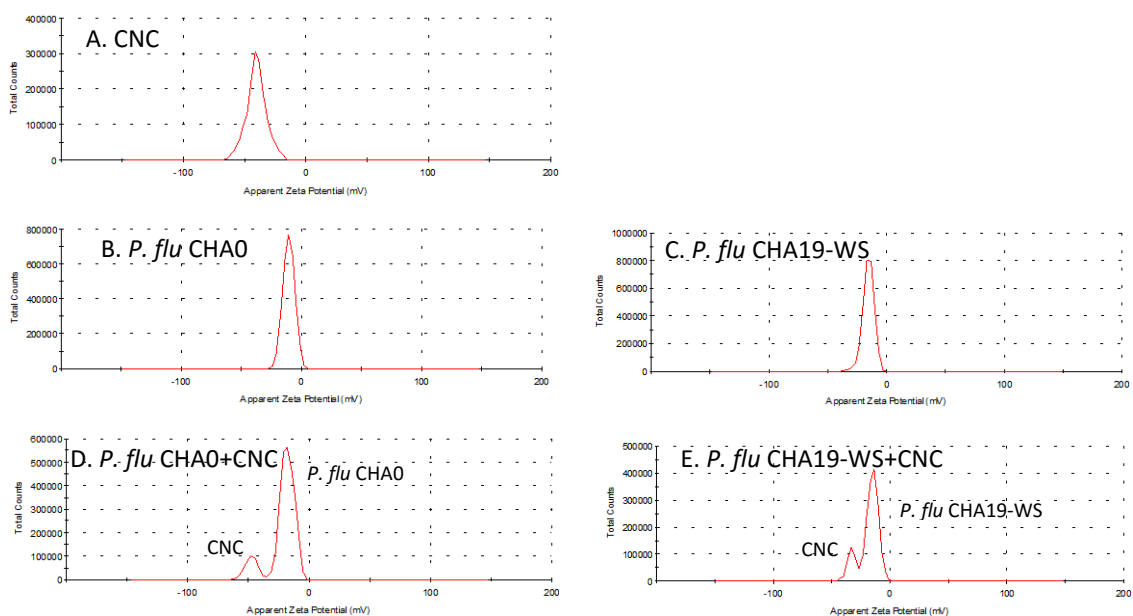


Figure S5.2. Representative zeta potential distribution (in 10 mM of NaCl solution with no pH adjustment). (A) CNC; (B) *P. flu* CHA0; (C) *P. flu* CHA19-WS; (D) *P. flu* CHA0 and CNC mixture; (E) *P. flu* CHA19-WS and CNC mixture.

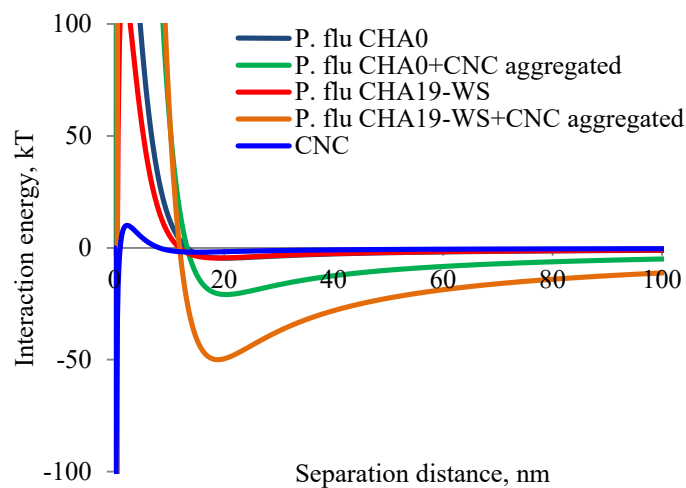


Figure S5.3. Theoretical DLVO interaction energies between bacteria and the silica surface with and without CNC, and DLVO interaction energies between CNC particles and the silica surface.

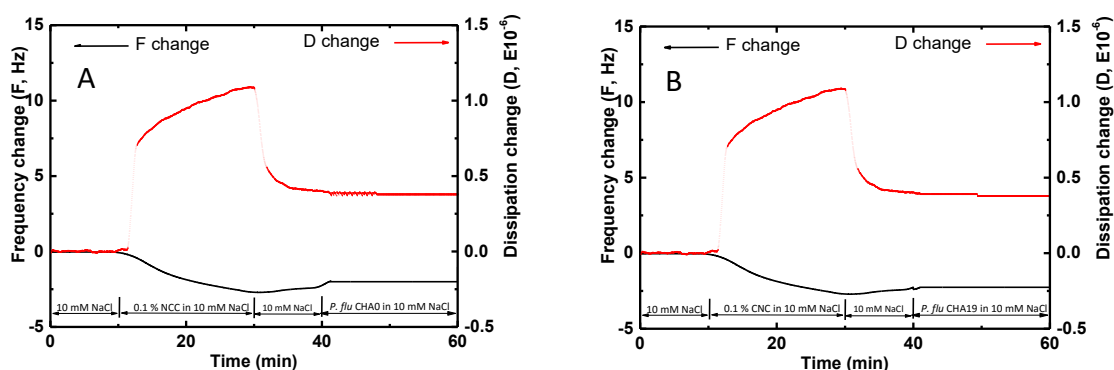


Figure S5.4. QCM-D study on bacterial adsorption onto CNC coated silica surfaces. (A) *P. flu* CHA0; (B) *P. flu* CHA19-WS

Table S5.1. Input parameters used in the DLVO calculations

Symbol	Value used
a_1 , equivalent radius of <i>P. flu</i> CHA0 cells (m)	4.4×10^{-7}
a_2 , equivalent radius of <i>P. flu</i> CHA19-WS cells (m)	4.1×10^{-7}
a_3 , equivalent radius of CNC particles (m)	2.04×10^{-8}
ζ_1 , zeta potential of <i>P. flu</i> CHA0 (mv)	-18.78
ζ_2 , zeta potential of <i>P. flu</i> CHA19-WS (mv)	-16.22
ζ_3 , zeta potential of CNC (mv)	-42.30
ζ_4 , zeta potential of glass surface/silica crystal surface (mv)	-36.30
A_{123} , bacterium-water-silica Hamaker constant (J)	6.16×10^{-21} (Rijnaarts et al., 1995a; Rijnaarts et al., 1995b)
A_{123} , CNC-water-silica Hamaker constant (J)	4.4×10^{-20}
relative permittivity of water (20°C)	80.1
vacuum permittivity	8.854×10^{-12}
κ^{-1} , Debye length (m)	3.04×10^{-9}

Note:

1. In NaCl solution, the EDL Debye length κ^{-1} is given by $\kappa^{-1} = \frac{0.304}{\sqrt{[NaCl]}}$ nm where [NaCl]

in the unit of M (Lu et al., 2011).

2. The Hamaker constant for CNC-water-silica is calculated based on the equation

$A_{132} = (\sqrt{A_{11}} - \sqrt{A_{33}})(\sqrt{A_{22}} - \sqrt{A_{33}})$, where A_{11} is Hamaker's constant for cellulose particles, A_{22} is Hamaker's constant for silica, and A_{33} is Hamaker's constant for water. Hamaker's constants for cellulose, silica, and water used in this study were 1.1×10^{-20} J (Boluk et al., 2012), 2.0×10^{-20} J (Lombay et al., 2011), and 3.7×10^{-20} J (Lerner et al., 2012), respectively.

References

- Abu-Lail NI, Camesano TA. Role of lipopolysaccharides in the adhesion, retention, and transport of *Escherichia coli* JM109. *Environmental Science & Technology* 2003; 37: 2173-2183.
- Asakura S, Oosawa F. Interaction between particles suspended in solutions of macromolecules. *Journal of Polymer Science* 1958; 33: 183-192.
- Bayoudh S, Othmane A, Mora L, Ben Ouada H. Assessing bacterial adhesion using DLVO and XDLVO theories and the jet impingement technique. *Colloids and Surfaces B-Biointerfaces* 2009; 73: 1-9.
- Boluk Y, Zhao LY, Incani V. Dispersions of nanocrystalline cellulose in aqueous polymer solutions: structure formation of colloidal rods. *Langmuir* 2012; 28: 6114-6123.
- Bos R, van der Mei HC, Busscher HJ. Physico-chemistry of initial microbial adhesive interactions - its mechanisms and methods for study. *Fems Microbiology Reviews* 1999; 23: 179-230.
- Chen GX, Hong YS, Walker SL. Colloidal and bacterial deposition: role of gravity. *Langmuir* 2010; 26: 314-319.
- Chen GX, Walker SL. Role of solution chemistry and ion valence on the adhesion kinetics of groundwater and marine bacteria. *Langmuir* 2007; 23: 7162-7169.
- Derjaguin B, Landau L. Theory of the stability of strongly charged lyophobic sols and of the adhesion of strongly charged-particles in solutions of electrolytes. *Progress in Surface Science* 1993; 43: 30-59.

- Eboigbodin KE, Newton JRA, Routh AF, Biggs CA. Role of nonadsorbing polymers in bacterial aggregation. *Langmuir* 2005; 21: 12315-12319.
- Elimelech M, Jia X, Gregory J, Williams R. Particle deposition and aggregation: measurement, modelling and simulation. Oxford, UK.: Butterworth-Heinemann, 1995.
- Gutman J, Walker SL, Freger V, Herzberg M. Bacterial attachment and viscoelasticity: physicochemical and motility effects analyzed using quartz crystal microbalance with dissipation (QCM-D). *Environmental Science & Technology* 2013; 47: 398-404.
- Hahn MW, O'Melia CR. Deposition and reentrainment of Brownian particles in porous media under unfavorable chemical conditions: some concepts and applications. *Environmental Science & Technology* 2004; 38: 210-220.
- Hwang G, Kang S, El-Din MG, Liu Y. Impact of an extracellular polymeric substance (EPS) precoating on the initial adhesion of *Burkholderia cepacia* and *Pseudomonas aeruginosa*. *Biofouling* 2012; 28: 525-538.
- Johnson WP, Tong MP. Observed and simulated fluid drag effects on colloid deposition in the presence of an energy barrier in an impinging jet system. *Environmental Science & Technology* 2006; 40: 5015-5021.
- Kim HN, Hong Y, Lee I, Bradford SA, Walker SL. Surface characteristics and adhesion behavior of *Escherichia coli* O157:H7: role of extracellular macromolecules. *Biomacromolecules* 2009; 10: 2556-2564.

- Kim HN, Walker SL, Bradford SA. Macromolecule mediated transport and retention of *Escherichia coli* O157:H7 in saturated porous media. *Water Research* 2010; 44: 1082-1093.
- Kumar A, Mortensen NP, Mukherjee PP, Retterer ST, Doktycz MJ. Electric field induced bacterial flocculation of enteroaggregative *Escherichia coli* 042. *Applied Physics Letters* 2011; 98: 253701.
- Lekkerkerker HNW, Tuinier R. *Colloids and Depletion*. Springer 2011; 100.
- Lerner RN, Lu QY, Zeng HB, Liu Y. The effects of biofilm on the transport of stabilized zerovalent iron nanoparticles in saturated porous media. *Water Research* 2012; 46: 975-985.
- Li YS, Wang YG, Pennell KD, Abriola LM. Investigation of the transport and deposition of fullerene (C60) nanoparticles in quartz sands under varying flow conditions. *Environmental Science & Technology* 2008; 42: 7174-7180.
- Liang Y, Hilal N, Langston P, Starov V. Interaction forces between colloidal particles in liquid: theory and experiment. *Advances in Colloid and Interface Science* 2007; 134-35: 151-166.
- Lombay G, Sundararajan S, Wang KJ, Subramaniam S. A test method for determining adhesion forces and Hamaker constants of cementitious materials using atomic force microscopy. *Cement and Concrete Research* 2011; 41: 1157-1166.

- Lu QY, Wang J, Faghijnejad A, Zeng HB, Liu Y. Understanding the molecular interactions of lipopolysaccharides during *E. coli* initial adhesion with a surface forces apparatus. *Soft Matter* 2011; 7: 9366-9379.
- Marcus IM, Herzberg M, Walker SL, Freger V. *Pseudomonas aeruginosa* attachment on QCM-D sensors: the role of cell and surface hydrophobicities. *Langmuir* 2012; 28: 6396-6402.
- Mattilasandholm T, Wirtanen G. Biofilm formation in the industry - a review. *Food Reviews International* 1992; 8: 573-603.
- Olsson ALJ, van der Mei HC, Busscher HJ, Sharma PK. Novel analysis of bacterium-substratum bond maturation measured using a quartz crystal microbalance. *Langmuir* 2010; 26: 11113-11117.
- Olsson ALJ, van der Mei HC, Busscher HJ, Sharma PK. Acoustic sensing of the bacterium-substratum interface using QCM-D and the influence of extracellular polymeric substances. *Journal of Colloid and Interface Science* 2011; 357: 135-138.
- Otto K, Elwing H, Hermansson M. Effect of ionic strength on initial interactions of *Escherichia coli* with surfaces, studied on-line by a novel quartz crystal microbalance technique. *Journal of Bacteriology* 1999; 181: 5210-5218.
- Poitras C, Tufenkji N. A QCM-D-based biosensor for *E. coli* O157:H7 highlighting the relevance of the dissipation slope as a transduction signal. *Biosensors & Bioelectronics* 2009; 24: 2137-2142.

- Quevedo IR, Tufenkji N. Influence of solution chemistry on the deposition and detachment kinetics of a CdTe quantum dot examined using a quartz crystal microbalance. *Environmental Science & Technology* 2009; 43: 3176-3182.
- Redman JA, Walker SL, Elimelech M. Bacterial adhesion and transport in porous media: role of the secondary energy minimum. *Environmental Science & Technology* 2004; 38: 1777-1785.
- Rijnaarts HH, Norde W, Bouwer EJ, Lyklema J, Zehnder AJ. Reversibility and mechanism of bacterial adhesion. *Colloids and Surfaces B: Biointerfaces* 1995a: 5-22.
- Rijnaarts HHM, Norde W, Lyklema J, Zehnder AJB. The isoelectric point of bacteria as an indicator for the presence of cell-surface polymers that inhibit adhesion. *Colloids and Surfaces B-Biointerfaces* 1995b; 4: 191-197.
- Rodahl M, Hook F, Krozer A, Brzezinski P, Kasemo B. Quartz-crystal microbalance setup for frequency and q-factor measurements in gaseous and liquid environments. *Review of Scientific Instruments* 1995; 66: 3924-3930.
- Smith MCW. microbial adhesion to surfaces - BERKELEY, RCW. *Journal of the American Chemical Society* 1983; 105: 2510-2510.
- Strand SP, Vandvik MS, Varum KM, Ostgaard K. Screening of chitosans and conditions for bacterial flocculation. *Biomacromolecules* 2001; 2: 126-133.
- Strauss J, Liu YT, Camesano TA. Bacterial adhesion to protein-coated surfaces: an AFM and QCM-D study. *Jom* 2009; 61: 71-74.

- Sun X, Danumah C, Liu Y, Boluk Y. Flocculation of bacteria by depletion interactions due to rod-shaped cellulose nanocrystals. *Chemical Engineering Journal* 2012; 198: 476-481.
- Truesdail SE, Lukasik J, Farrah SR, Shah DO, Dickinson RB. Analysis of bacterial deposition on metal (hydr)oxide-coated sand filter media. *Journal of Colloid and Interface Science* 1998; 203: 369-378.
- Tsuneda S, Aikawa H, Hayashi H, Hirata A. Significance of cell electrokinetic properties determined by soft-particle analysis in bacterial adhesion onto a solid surface. *Journal of Colloid and Interface Science* 2004; 279: 410-417.
- Vanoyan N, Walker SL, Gillor O, Herzberg M. Reduced bacterial deposition and attachment by quorum-sensing inhibitor 4-Nitro-pyridine-N-oxide: the role of physicochemical effects. *Langmuir* 2010; 26: 12089-12094.
- Verwey EJW. Theory of the stability of lyophobic colloids. *Journal of Physical and Colloid Chemistry* 1947; 51: 631-636.
- Vrij A. Polymers at interfaces and interactions in colloidal dispersions. *Pure and Applied Chemistry* 1976; 48: 471-483.
- Walker SL, Redman JA, Elimelech M. Role of cell surface lipopolysaccharides in *Escherichia coli* K12 adhesion and transport. *Langmuir* 2004; 20: 7736-7746.
- Wang H, Sodagari M, Chen YJ, He X, Newby BMZ, Ju LK. Initial bacterial attachment in slow flowing systems: effects of cell and substrate surface properties. *Colloids and Surfaces B-Biointerfaces* 2011; 87: 415-422.

Workentine ML, Harrison JJ, Tran V, Stenroos PU, Weljie AM, Zhang P, et al. K-160. metabolic and physiological characterization of phenotypic variants obtained from *Pseudomonas Fluorescens* missing the GacS sensor kinase. 2012, 2008.

Xu ZH, Liu JJ, Choung JW, Zhou ZA. Electrokinetic study of clay interactions with coal in flotation. International Journal of Mineral Processing 2003; 68: 183-196.

Chapter 6 Impact of CNC on the Aggregation and Initial Adhesion to a Solid Surface of *Escherichia coli* K12: Role of Solution Chemistry

6.1. Introduction

Bacterial adhesion to exposed surfaces is inevitable in all natural and industrial aquatic systems, and may lead to the development of a complex biofilm. Biofilm development starts with the adhesion to a surface of single cells or cell aggregates. Attached cells multiply, building complex surface communities that can be detrimental to human health and industrial processes. Biofilms often cause pathogen contamination, biocorrosion, and biofouling in engineered systems (Kumar and Anand, 1998; Mattilasandholm and Wirtanen, 1992). Conversely, the immobilization of bacteria on surfaces can be advantageous when it is employed in bioreactors to remove contaminants, degrade xenobiotic compounds, and immobilize metals (Habash and Reid, 1999; Salerno et al., 2007). In both cases it is essential to control bacterial aggregation and adhesion.

Our previous studies demonstrated that CNC can (1) induce bacterial aggregation through a depletion mechanism, and (2) hinder bacterial initial adhesion to a solid surface (Sun et al., 2012; Sun et al., 2014). CNC are much smaller than bacterial cells in size, based on depletion mechanism, when nanosized CNC are added to a bacterial culture, the gaps between bacterial cells and the bulk solution experience a difference in osmotic pressure which leads to the exclusion of CNC particles from the gaps between bacterial cells and attractive force between bacterial cells (Sun et al., 2012).

Solution chemistry such as pH and IS can significantly impact interactions between bacterial cells and between bacteria and a surface. For instance, the surface of a bacterial

cell is less negatively charged at lower pH (due to the protonation of chemical groups, such as carboxyl and phosphate (Elzinga et al., 2012; Rijnaarts et al., 1995b)) and higher IS (due to suppression of the EDL). The lower negative charge results in a decreased electrostatic repulsion between bacterial cells and between bacteria and a surface. The reduced repulsive electrostatic forces may lead bacterial cells to approach each other or a solid surface. When a sufficient proximity is reached such that van der Waals attraction may overcome the repulsive energy barrier between two negatively charged surfaces, bacterial aggregation or adhesion is facilitated (Chen and Walker, 2007; Jiang et al., 2011). Classic DLVO theory describes the balance between electrostatic repulsion and van der Waals attraction and can be used to explain the impact of solution chemistry on bacterium–bacterium and bacterium–solid surface interactions (Hwang et al., 2012; Hwang et al., 2013).

Information on effective pH and IS ranges for CNC application in inducing bacterial aggregation and reducing bacterial adhesion on solid surfaces is lacking. The objective of this study was to evaluate bacterial aggregation and adhesion to a solid surface in the presence of CNC under different solution pH and IS conditions. The aggregation of bacteria in the absence and presence of CNC was assessed by microscopy; the deposition of bacteria on solid surfaces in the absence and presence of CNC was determined using a batch method. Microscopy was used to quantify cell deposition.

6.2. Material and Methods

6.2.1. Culture and characterization of bacterial cells

Aggregation and adhesion experiments were performed with Gram-negative *E. coli* K12. For each experiment, bacteria were streaked onto an LB agar plate, then incubated at 37°C overnight. A single colony from the plate was transferred into 50 mL of LB broth and grown in a shaker incubator at 150 rpm at 37°C for 16 hours. Stationary-phase bacterial cells were harvested by centrifugation at 3000 g at 4°C for 10 minutes. Pellets were resuspended in NaCl solutions of variable pH and IS prepared with reagent grade salt (Fisher Scientific Inc., U.S.) and Milli-Q water (18.2 MΩ, Millipore, Mississauga, ON, Canada) and sterilized by autoclave before use. Centrifugation and resuspension procedures were repeated two additional times to remove traces of growth media and suspended EPS from the solutions. A final cell density of 1.0×10^8 cells/mL was obtained by measuring the OD₆₀₀ with a UV spectrophotometer (Varian Inc., U.S.). SEM was employed to characterize the morphology of the bacterial cells. The zeta potential of *E. coli* K12 cells versus pH and IS was determined at 25°C with a DLS spectrophotometer (Malvern Zetasizer Nano ZS. Model: ZEN3600, Malvern Instruments, UK). The average hydrodynamic size of *E. coli* K12 cells was also determined by DLS. Bacterial suspensions were prepared in NaCl solutions of interest and each measurement was repeated with at least three different samples.

6.2.2. CNC suspension preparation and characterization

Stock suspensions of 1.0% (wt) CNC in NaCl solution at different IS and pH were prepared following the protocol in our previous study (Sun et al., 2012). The zeta potential of CNC as a function of IS and pH was assessed by DLS measurements at 25°C.

CNC suspensions were prepared in the NaCl solutions of interest and each measurement was repeated with at least three different samples.

6.2.3. Bacterial aggregation experiment

In the aggregation experiment, 1 mL of 1.0% (wt) CNC suspension was added to 1 mL of a bacterial suspension (with pH adjustments) to achieve a volume fraction of 3.3×10^{-3} mL/mL. Controls without CNC were also prepared. Samples were incubated statically at 24°C for 30 minutes and stained with SYTO[®] 9 green fluorescent nucleic acid dye for another 15 minutes before the bacterial suspensions were dropped on clean microscopy glass slides and visualized under fluorescent light using an Axio Imager M2 microscope (Carl Zeiss, Germany) with a Zeiss LD Plan-NEOFLUAR 40× objective. At least 50 images of randomly chosen areas on each slide were taken. The images were analyzed using AxioVision 4.8; the size (the equivalent spherical radius of one bacterial cluster) of each bacterial aggregate on each image was measured and then averaged to get the average size before and after CNC treatment. These experiments were conducted in triplicate in at least five independent experiments.

6.2.4. Bacterial initial adhesion to a silica surface

For each adhesion experiment, fresh *E. coli* K12 bacterial suspensions (1.0×10^8 cells/mL in NaCl solutions at various IS) were prepared as described in section 6.2.1. 1 mL of bacterial suspension was distributed in each well of a 24-well plate (Corning Inc., U.S.), then 1 mL of 1.0% (wt) CNC suspension was added to each well, followed by pH adjustments with 1 M NaOH/1 N HCl. The cleaned glass slides (diameter 1.2 cm, Fisher Scientific Inc., U.S.) were completely submerged in the bacterial suspension for 30

minutes at 24°C in a static state to allow the bacteria to attach to the surfaces. Then the bacterial suspension was removed and the glass slides were carefully washed three times with NaCl solution to remove loosely attached bacteria. To observe the difference before and after CNC treatment, the slides were visualized with fluorescent microscopy and cells attached to slides were quantitated. Briefly, after each adhesion test, the bacteria coated slides were placed on clean microscope slides and stained with SYTO[®] 9 green fluorescent nucleic acid dye for 15 minutes. Thereafter, fluorescent light and a 40× objective were used to take a minimum of 50 randomly chosen fields of view of each slide. The size of each image was $3.7632 \times 10^{-4} \text{ cm}^2$. The number of bacteria in each image was obtained through counting the bacteria in five areas (4 corners plus the center) of the image, then averaging. Bacterial adhesion experiments were conducted in triplicate in at least five independent experiments. The variance of bacterial adhesion was analyzed with a one-way analysis of variance (ANOVA) and was reported as p-values. p-values of less than 0.05 suggest significant differences.

6.2.5. Theoretical interaction energy calculations for bacterial aggregation

Classic DLVO theory of colloid stability, simulating bacteria–bacteria interactions, was applied to explain bacterial aggregation behavior in this study. Classic DLVO theory describes total energies ΔG^{TOT} between bacteria and bacteria in solution as a balance between attractive Lifshitz-van der Waals ΔG^{LW} (equation 6.1 (Hogg et al., 1966)) and electrostatic ΔG^{EL} (equation 6.2 (Hogg et al., 1966)) interaction energies as a function of separation distance d . Sphere-sphere geometry was assumed when calculating the

interaction energies between bacteria (the bacterial cells are assumed to be spherical, with an equivalent spherical radius of a , approaching another sphere).

$$\Delta G^{LW}(d) = -\frac{A_{121}aa}{6d(a+a)} \quad 6.1$$

$$\Delta G^{EL}(d) = \frac{\varepsilon a \zeta^2}{2} \ln[1 + \exp(-\kappa d)] \quad 6.2$$

$$\kappa^{-1} = \left(\frac{2000e^2 N_A}{\varepsilon k_B T} \times \frac{1}{2} \sum_i M_i z_i^2 \right)^{-\frac{1}{2}} \quad 6.3$$

where A_{121} , ε , ζ , and κ^{-1} are the bacterium-water-bacterium Hamaker constant in water, the dielectric constant of the water, the surface potential (the experimentally determined zeta potentials of the bacteria were used in the place of surface potentials in DLVO calculations), and the Debye length, respectively. d is the separation distance between bacterium and bacterium, a is the radius of bacteria. κ^{-1} can be calculated from equation 6.3 (Bradford and Torkzaban, 2008). The input parameters needed to describe the DLVO interaction are provided in Table S6.1 in the supplementary material. After CNC particles were added to the bacterial suspension, the depletion potential $\Delta G^{Dep}(d)$ (equation 6.4 (Koenderink et al., 1999; Mao et al., 1995)) was calculated to evaluate the effect of CNC on the interactions between bacteria.

$$\Delta G^{Dep}(d) = -\frac{2}{3} k_B T \varphi_r \frac{L}{D} \frac{R}{D} \left(1 - \frac{d}{L}\right)^3 \quad 6.4$$

where k_B is the Boltzmann constant, T is the absolute temperature, L is the length, D is the diameter, φ_r is the volume fraction of CNC particles, R is the diameter of bacterial cells and d is the separation distance between bacterial cells.

6.3. Results and Discussion

6.3.1. Characterization of bacterial cells and CNC particles

As shown in Figure 6.1, *E. coli* K12 cells were rod-shaped and equipped with thread-like EPS appendages. Based on DLS measurements, the average hydrodynamic size of an *E. coli* K12 cell was $4.8 \pm 0.5 \mu\text{m}$, which was taken as the cell length. The resulting equivalent spherical radius of one *E. coli* K12 cell was $0.6 \mu\text{m}$, which was used in the interaction energy calculations.

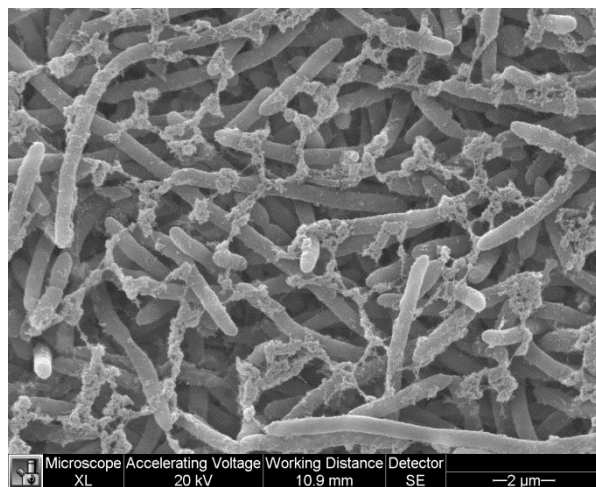


Figure 6.1. An SEM micrograph of *E. coli* K12

Zeta potential values of CNC and *E. coli* K12 cells as a function of the pH and IS of the NaCl solution are shown in Figure 6.2. Both CNC and *E. coli* K12 cells exhibited negatively charged surfaces over the tested pH and IS ranges. Both pH and IS play significant roles in zeta potential changes of *E. coli* K12. As shown in Figure 6.2A, the zeta potential of *E. coli* K12 decreased from $-6.48 \pm 0.995 \text{ mV}$ to $-22.6 \pm 0.351 \text{ mV}$ when the pH of the NaCl solution increased from 2.7 to 7.2. The surface of the cells was more negatively charged at higher pH due to the deprotonation of chemical groups, e.g.,

carboxyl groups ($-\text{COOH}$) or phosphate (HPO_4^{2-}) (Elzinga et al., 2012; Rijnaarts et al., 1995b). As shown in Figure 6.2B, the zeta potential of *E. coli* K12 cells increased from -26 ± 2.28 mV to -10 ± 0.836 mV when the IS of the NaCl solution increased from 1 mM to 50 mM (Figure 6.2B). The IS of the medium is an important factor affecting the electrostatic interactions. Based on EDL theory, an increase in IS will suppress the EDL resulting in a decrease in the zeta potential of a colloidal particle (Berg, 2010).

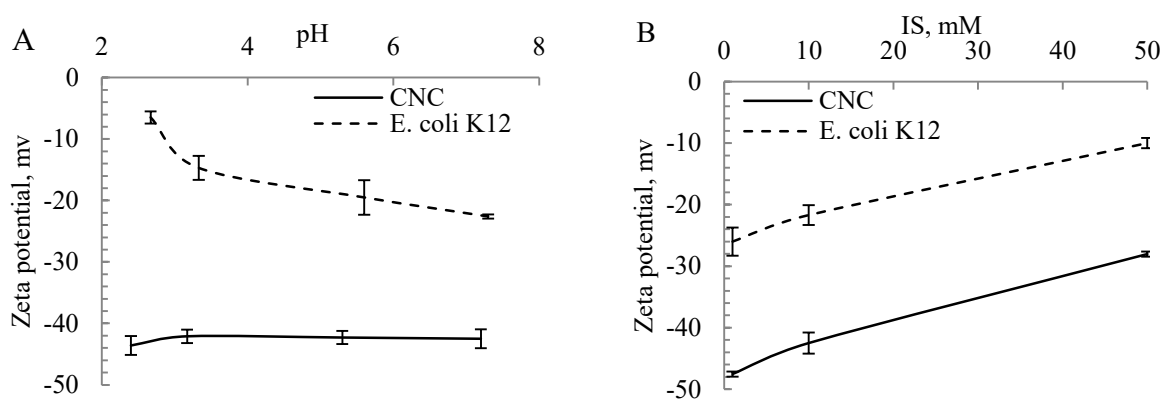


Figure 6.2. Zeta potential of CNC and *E. coli* K12 as a function of pH (in 10 mM of NaCl) (A) and IS (at pH = 7.2) (B). Each data point represents the average of three measurements for one sample. Error bars represent the standard deviation.

The zeta potential of CNC in 10 mM of NaCl remained relatively constant at about -43 mV with pH increasing from 2.4 to 7.2, indicating a stable CNC suspension in the pH range tested in this study. Similar results were reported by Zhong et al. (2012) who demonstrated that CNC suspensions can be stable at a wide pH range from 2 to 11. With an increase in IS, the zeta potential of the CNC particles became less negative at pH 7.2 (Figure 6.2B), a change that can be explained by EDL theory (Berg, 2010). It was observed that with increasing IS, the CNC suspension destabilized. The average CNC size

increased from about 100 nm to 250 nm when the IS was increased from 1 mM to 50 mM (Figure S6.1 in the supplementary material).

6.3.2. Impact of IS on bacterial aggregation and initial bacterial adhesion (pH = 7.2)

Figure 6.3 shows the average size of *E. coli* K12 aggregates (Figure 6.3A), classic DLVO interaction energy profiles (Figure 6.3B), depletion interaction energy profiles (Figure 6.3C), and bacterial adhesion (Figure 6.3D) in 1, 10, and 50 mM of NaCl (pH = 7.2), in the absence and presence of CNC. Figure 6.3A shows the average size of aggregates before and after CNC addition. In the absence of CNC, *E. coli* K12 were well dispersed and suspensions were flocculate free in all three IS conditions. The equivalent spherical radius of one *E. coli* K12 cell was 0.6 μm , which was taken as the average aggregate size before CNC addition. In the presence of CNC, *E. coli* K12 in 10 mM of NaCl showed significant aggregation and formed dense bacterial clusters with an average size (the equivalent spherical radius of one bacterial cluster) of $\sim 8.3 \mu\text{m}$ (Figure 6.3A, and Figure S6.2 in the supplementary material), as calculated from microscopy images. Several large *E. coli* K12 clusters (the equivalent spherical radius of one bacterial cluster was approximately 6.8 μm) also emerged in 50 mM of NaCl (as shown in Figure 6.3A, and Figure S6.2). No aggregation was apparent in 1 mM of NaCl (Figure 6.3A, and Figure S6.2). Although bacterial cells can spontaneously form agglomerates, it appears that without CNC application bacterial agglomerates were unlikely to form in the 1 mM, 10 mM, and 50 mM of NaCl conditions tested.

Figure 6.3B shows the classic DLVO energy curves, which predict decreasing energy barriers from 17 kT to 8 kT with increasing IS from 1 mM to 10 mM, and no energy

barrier at 50 mM. This is in good agreement with EDL theory (the zeta potential of bacteria became less negative with increasing IS from 1 mM to 50 mM, as shown in Figure 6.2A). Thus, the affinity of bacterium to bacterium should increase with an increase in salt concentration. However, before CNC addition, there was no bacterial aggregation observed even at an IS of 50 mM (Figure 6.3A, and Figure S6.2), although there was no energy barrier shown in the theoretical DLVO calculation. This discrepancy may be attributed to the presence of other interactions, such as polymer-mediated steric repulsion due to the presence of bacterial surface polymers, which is not considered in the classic DLVO theory but inhibits bacterial aggregation. Previous studies reported that steric interactions dominate at high IS in bacteria–bacteria/bacteria–surface interactions, due to the conformational change of polymers outside the cell surface. For example, the polymers might become more brushlike and protrude further than the EDL, and can therefore interact with each other (Cai et al., 2013; Hwang et al., 2012; Hwang et al., 2013; Kim et al., 2009; Lerner et al., 2012; Rijnaarts et al., 1999). Chen and Walker (2007) also indicated that the presence of ions among the polymers could lead to more rigid polymers; as a result, polymer rigidity might enhance steric interactions. It should be noted that other interactions, such as hydrophobic and hydration interactions (Chen and Walker, 2007), might exist in a bacterial suspension. Xu and Logan (2005) reported that the protein in EPS can be compressed and folded into a denser core at high IS;

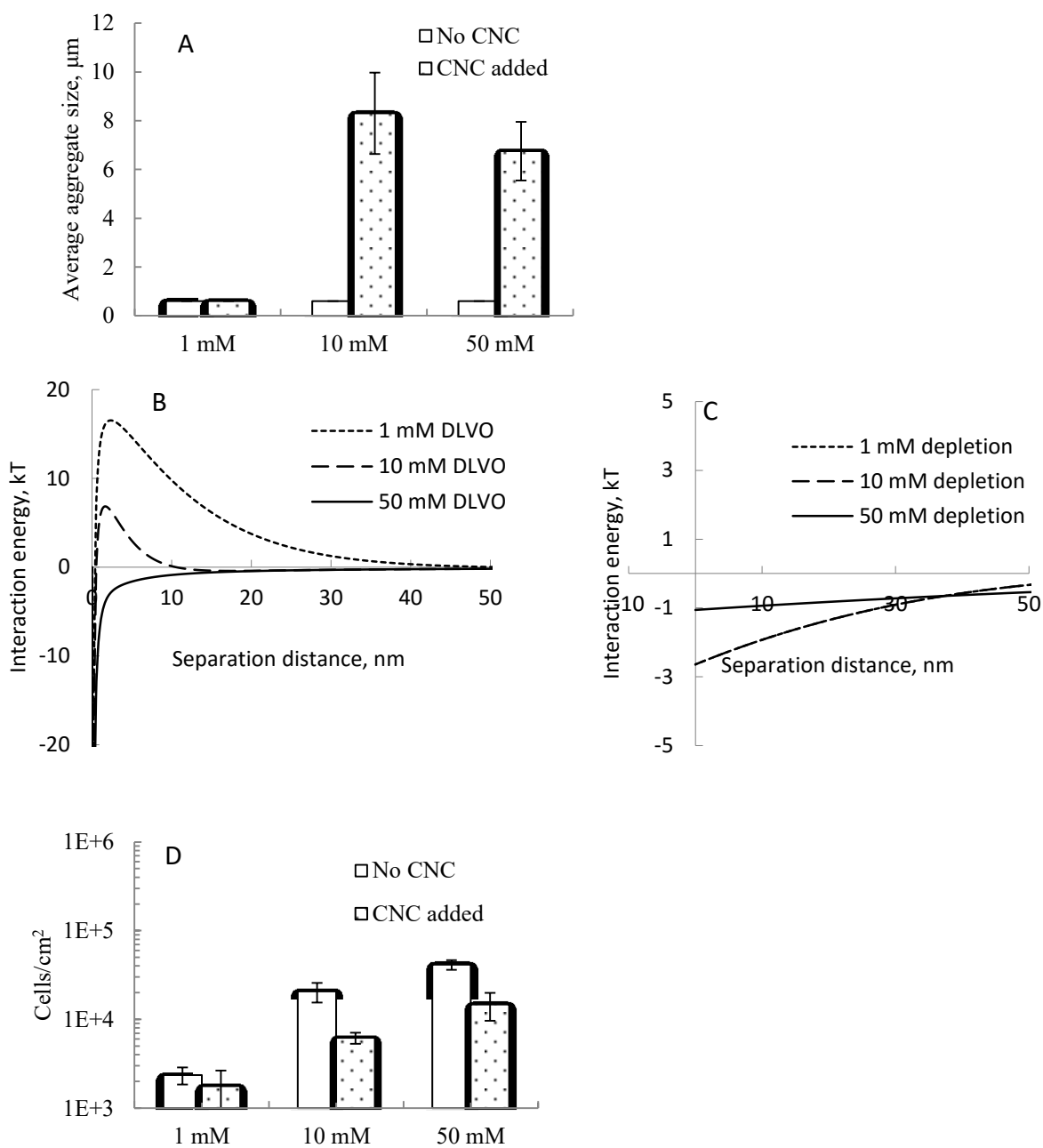


Figure 6.3. Impact of IS on *E. coli* K12 aggregation and adhesion with and without CNC. (A) Average aggregates size (the equivalent spherical radius of one bacterial cluster); (B) DLVO interaction energy profiles; (C) Depletion interaction energy profiles; (D) Average adhesion cell density (error bars represent one standard deviation) (pH = 7.2).

hydrophobic sites on the bacterial surfaces were thus reduced resulting in reduced hydrophobic attraction between bacterial cells.

Bacterial aggregation was observed only after CNC were added to the bacterial suspension at 10 mM and 50 mM of NaCl. Because of the small size of CNC particles, CNC could induce bacterial aggregation through the depletion mechanism (Sun et al., 2012; Sun et al., 2014). Figure 6.3C shows the depletion energy profiles in the presence of CNC. Based on the theoretical calculation of depletion potential (equation 6.4), the depletion potential depends on the size of CNC particles, the size of bacterial cells, and the volume fraction of CNC to bacteria. The theoretically calculated depletion attraction was the same from 1 mM to 10 mM IS (Figure 6.3C) because the CNC suspension was stable and the CNC size did not change from 1 mM to 10 mM IS. However, when the IS increased to 50 mM, the CNC suspension became unstable and the CNC size used in the calculations increased because of CNC aggregation (Figure S6.1 in the supplementary material), resulting in a less effective depletion attraction (Figure 6.3C). When the IS was increased from 1 mM to 50 mM, the zeta potential of both bacteria and CNC became less negative (Figure 6.2B), which indicates that the electrostatic repulsion between bacteria and CNC became weaker, leading to less effective depletion attraction between bacteria and bacteria. A previous study reported that screening repulsive electrostatic interactions inhibit the depletion mechanism and weaken the effective colloid-colloid attraction (Buzzaccaro et al., 2010).

Overall, an increase in IS decreased both the contribution of DLVO repulsion and the contribution of depletion attraction between bacteria. As a result, the extent of bacterial

aggregation in solutions of different IS was not proportional to the IS, but bacterial aggregation was optimal at 10 mM IS. At 1 mM IS, DLVO repulsion was the strongest and, although depletion attraction was also strong, depletion attraction was not able to overcome the DLVO repulsion, so the bacterial suspension was stable against aggregation. DLVO repulsion was weakest at 50 mM IS, but depletion attraction was also weaker at 50 mM IS than at 10 mM IS, so there was some bacterial aggregation, but not as much as that at 10 mM IS. DLVO repulsion at 10 mM IS was not strong enough to overcome the depletion attraction at 10 mM IS, resulting in the highest degree of bacterial aggregation observed in these experiments.

Figure 6.3D illustrates the cell densities of *E. coli* K12 deposited on glass slides in solutions of different IS with and without CNC, determined from fluorescence microscopy observations. In the absence of CNC, bacterial adhesion to the silica surface increased with an increase in IS; this result is supported by EDL theory and previous studies (Redman et al., 2004; Yang et al., 2012a; Yang et al., 2012b; Yang et al., 2013). The EDL is suppressed at higher IS, resulting in a decrease in the zeta potential (the zeta potential becomes less negative) of bacterial cell surfaces and solid surfaces. As the repulsion between cells and the surface decreased, the cell adhesion capacity was enhanced, in agreement with classic DLVO theory. After CNC addition, bacterial adhesion was inhibited at high IS (10 mM and 50 mM of NaCl). Among the three IS conditions tested (1, 10, and 50 mM of NaCl), the deposition of *E. coli* K12 on glass slides was the most significantly ($p = 0.008$) inhibited in 10 mM of NaCl, and achieved about a 0.52 log-unit reduction (~ 70%) in cell density. In 50 mM of NaCl, deposition of

E. coli K12 on glass slides was also significantly ($p = 0.03$) inhibited by 0.44 log-units (~64%). However, the presence of CNC did not significantly ($p > 0.05$) reduce the deposition of *E. coli* K12 on glass slides in 1 mM of NaCl. The above phenomenon is possibly due to bacterial aggregation in the presence of CNC at 10 and 50 mM. Large cell aggregates have a lower diffusion coefficient than single bacterial cells and will experience reduced convective-diffusive transport to the silica surface, resulting in lower deposition on the surface (Elimelech et al., 1995). Similar results were reported in a previous study (Sun et al., 2014).

6.3.3. Impact of pH on bacterial aggregation and initial bacterial adhesion (IS = 10 mM)

Relatively mild pH conditions (3.5–7.2) were selected in the current study to reduce the potential impact of pH on bacterial physiology. Microscopy showed that cells were intact during the experiments. Figure 6.4 shows the average size of *E. coli* K12 aggregates (Figure 6.4A), classic DLVO interaction energy profiles (Figure 6.4B), depletion interaction energy profiles (Figure 6.4C), and adhesion (Figure 6.4D) at different pH (in 10 mM of NaCl).

In the absence of CNC, *E. coli* K12 suspensions were flocculate free at all three pH conditions (pH 3.5, 5.2, and 7.2) (Figure 6.4A, and Figure S6.3 in the supplementary material), although the DLVO interaction energy profiles (Figure 6.4B) predict a minor energy barrier (0.65 kT) at pH 3.5, and minor secondary minima at all three pH conditions (−0.51 kT, −0.44 kT, −0.41 kT at pH 3.5, 5.2, and 7.2, respectively). Figure 6.4B indicates that secondary minima associated bacterial aggregation was expected at all three pH conditions (a primary minimum associated bacterial aggregation might exist at

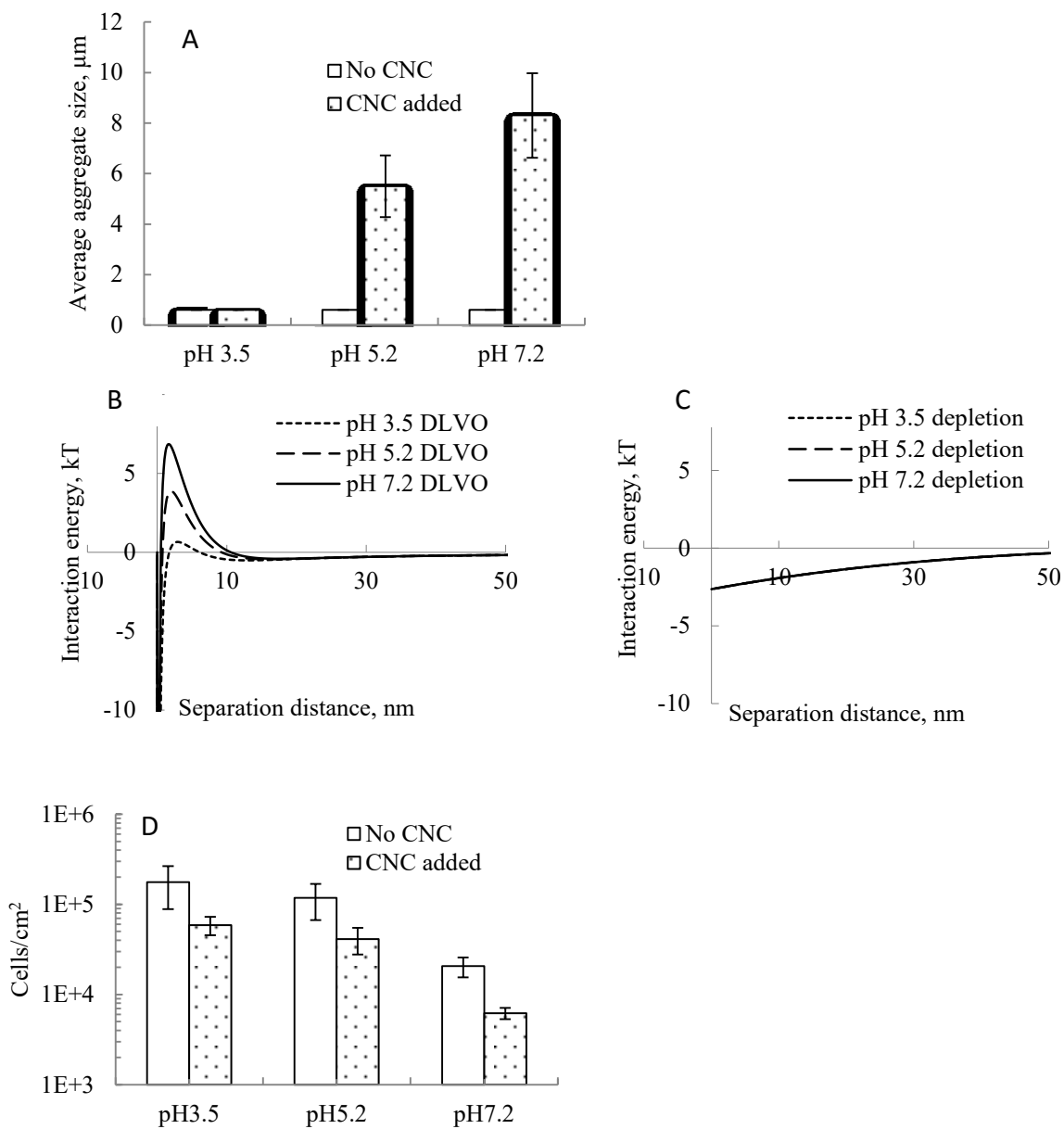


Figure 6.4. Impact of pH on bacterial aggregation and adhesion with and without CNC. (A) Average aggregates size (the equivalent spherical radius of one bacterial cluster); (B) classic DLVO interaction energy profiles; (C) Depletion interaction energy profiles; (D) Average adhesion cell density (error bars represent one standard deviation) (IS = 10 mM).

pH 3.5 due to the minor energy barrier). The presence of other interactions, such as steric interactions might explain this deviation.

E. coli K12 showed aggregation to average clump sizes of $\sim 5.5 \mu\text{m}$ at pH 5.2 and $\sim 8.3 \mu\text{m}$ at pH 7.2 after CNC addition, but aggregation was not observed at pH 3.5 (Figure 6.4A, and Figure S6.3 in the supplementary material). At pH 3.5, steric repulsion was likely stronger than depletion attraction, thus the bacterial system was stable against aggregation. CNC induced depletion attraction overcame DLVO repulsion and steric repulsion, as a result, bacterial aggregation was observed at pH 5.2 and pH 7.2. Note should be made that the zeta potential of CNC used in this study was stabilized at about -43 mV in 10 mM of NaCl when the pH increased from 3.5 to 7.2 (Figure 6.2A), also the CNC size was stable when the pH increased from 3.5 to 7.2. Thus, the contribution of CNC induced depletion attraction was the same at the three pH conditions tested here (Figure 6.4C). However, the bacteria zeta potential became more negative with increasing pH, increasing the electrostatic repulsion between bacteria and CNC and leading to enhanced depletion attraction. Therefore, more aggregation was observed at pH 7.2 than at pH 5.2. Buzzaccaro et al. (2010) also reported the enhancement of depletion attraction by electrostatic repulsion.

Figure 6.4D illustrates *E. coli* K12 cells deposited on a silica surface at different pH in 10 mM of NaCl with and without CNC. In the absence of CNC, the bacterial adhesion capacity decreased with an increase in pH, in accordance with previous studies (Elzinga et al., 2012; Jiang et al., 2011). After CNC addition, deposition of *E. coli* K12 on the

silica surface was significantly ($p = 0.008$) inhibited (0.52 log-unit reduction) at pH 7.2; whereas CNC did not significantly inhibit bacterial deposition at pH 3.5 ($p = 0.08$) and pH 5.2 ($p = 0.06$). The adhesion results correlate with the aggregation results (Figure 6.4A), in which CNC induced more aggregation of *E. coli* at higher pH than at lower pH. This effect is likely a result of reduced convective-diffusive transport to the silica surface due to the larger sized bacterial aggregates formed in the presence of CNC at higher pH.

6.4. Conclusion

Bacterial aggregation and adhesion to solid surfaces can be significantly affected by the surrounding solution chemistry. In the present study, the roles of pH and IS in *E. coli* K12 aggregation and deposition on silica surfaces were investigated in NaCl solutions in the absence and presence of CNC. Theoretical classic DLVO interaction energy and depletion interaction energy were calculated to explain bacterial aggregation in solutions containing bacteria and CNC. In the presence of CNC at pH 5.2–7.2 and IS 10–50 mM, depletion was the dominant mechanism, inducing bacterial aggregation which could consequently result in decreased convective-diffusive transport to the silica surface.

Bacteria are ubiquitous in all aquatic systems and are often a nuisance in industrial processes and detrimental to human health. Control of bacterial adhesion and biofilm formation is possible only when the effects of solution chemistry on biofilm formation and bacterial adhesion to surfaces are understood. Natural aquatic systems contain a wide range of dissolved organic matters, thus, future work on the aggregation and adhesion of bacteria over a broad range of environmentally relevant conditions is needed.

Supplementary Material

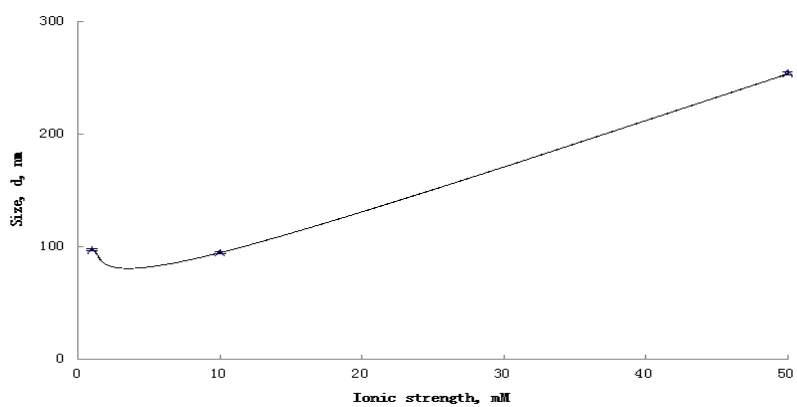


Figure S6.1. Changes of particle size of CNC versus IS (pH = 7.2). (Error bars represent one standard deviation)

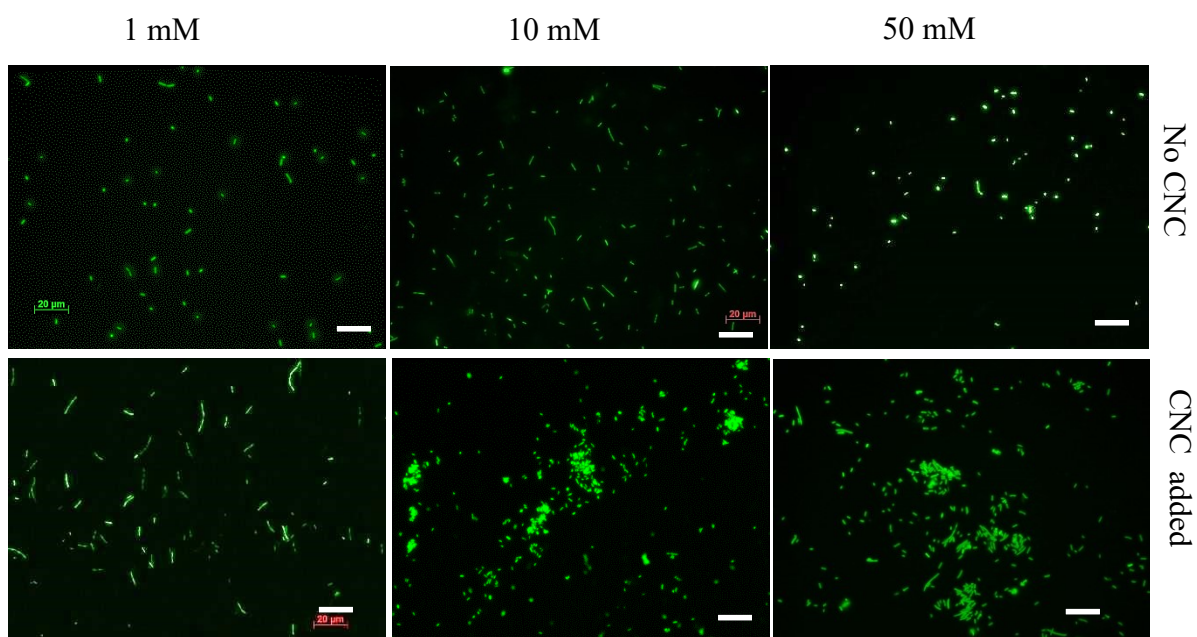


Figure S6.2. Representative microscopy images of *E. coli* K12 aggregation with and without CNC in different IS (pH = 7.2). Bar size=20 μ m.

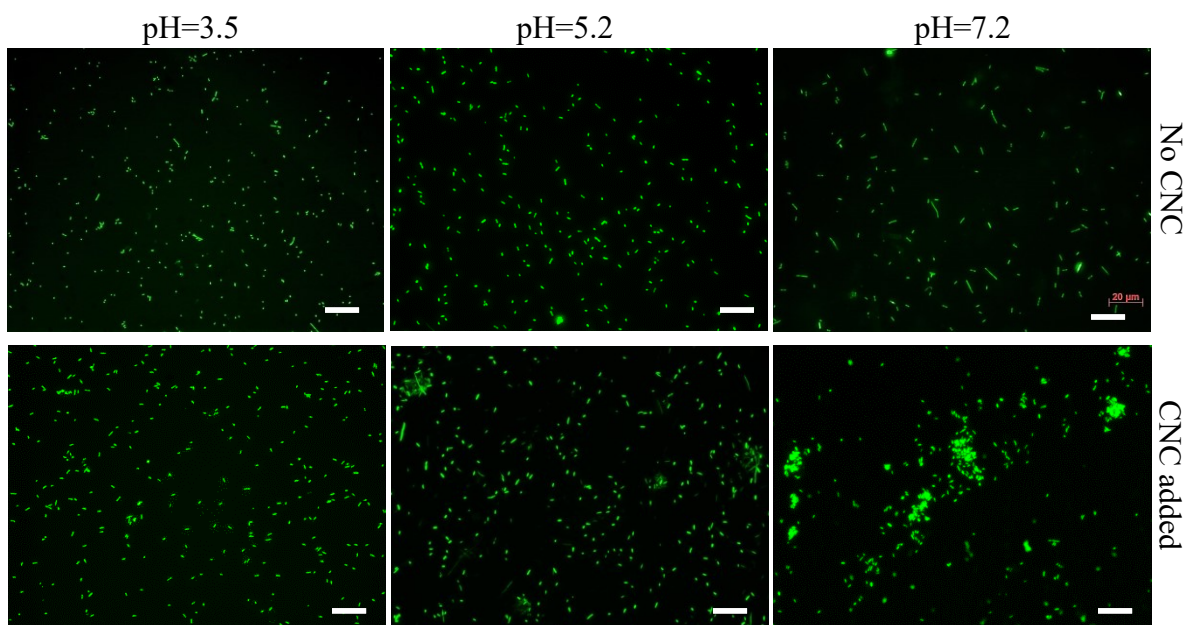


Figure S6.3. Representative microscopy images of *E. coli* K12 aggregation with and without CNC at different pH (IS = 10 mM). Bar size = 20 μm .

Table S6.1. Input parameters in DLVO calculations

Symbol	Value used	
a, equivalent spherical radius of bacterial cells	0.6 μm	
ζ_1 , zeta potential of <i>E.coli</i> K12 (mv)	-26.00	1 mM pH7.2
	-22.60	10 mM pH7.2
	-10.00	50 mM pH7.2
	-14.70	10 mM pH3.5
	-19.50	10 mM pH5.2
	-22.60	10 mM pH7.2
A_{121} , bacterium-water-bacterium Hamaker constant (J)	7.2×10^{-22}	
ϵ_r relative permittivity of water (20°C)	80	
ϵ_0 vacuum permittivity (F/m)	8.854×10^{-12}	
ϵ water dielectric constant	$80.1 \times (8.854 \times 10^{-12})$	
k_B , Boltzmann constant ($\text{m}^2\text{kgs}^{-2}\text{K}^{-1}$)	1.38×10^{-23}	
T, Temperature (K)	298	
NA, Avogadro's number (molecules/mole)	6.02×10^{23}	
Mi, molar concentration of electrolyte (mol/L)	0.01	
e, electron charge (C)	1.602×10^{-19}	
z, electrolyte valence	1	

Note: the Hamaker constant for bacterium-water-bacterium is calculated based on the equation $A_{121} = (\sqrt{A_{11}} - \sqrt{A_{22}})(\sqrt{A_{11}} - \sqrt{A_{22}})$, where A_{11} is Hamaker's constant for

bacteria, and A_{22} is Hamaker's constant for water. Hamaker's constants for bacteria, and water used in this study were 4.8×10^{-20} J (Lerner et al., 2012), and 3.7×10^{-20} J (Lerner et al., 2012), respectively.

References

- Berg JC. An introduction to interfaces & colloids The bridge to Nanoscience. New Jersey: World Scientific, 2010.
- Bradford SA, Torkzaban S. Colloid transport and retention in unsaturated porous media: a review of interface-, collector-, and pore-scale processes and models. *Vadose Zone Journal* 2008; 7: 667-681.
- Buzzaccaro S, Piazza R, Colombo J, Parola A. Enhancement of depletion forces by electrostatic depletant repulsion. *Journal of Chemical Physics* 2010; 132.
- Cai P, Huang Q, Walker SL. Deposition and survival of *Escherichia coli* O157:H7 on clay minerals in a parallel plate flow system. *Environmental Science & Technology* 2013; 47: 1896-1903.
- Chen GX, Walker SL. Role of solution chemistry and ion valence on the adhesion kinetics of groundwater and marine bacteria. *Langmuir* 2007; 23: 7162-7169.
- Elimelech M, Jia X, Gregory J, Williams R. Particle deposition and aggregation: measurement, modelling and simulation. Oxford, UK.: Butterworth-Heinemann, 1995.
- Elzinga EJ, Huang J-H, Chorover J, Kretzschmar R. ATR-FTIR spectroscopy study of the influence of pH and contact time on the adhesion of *Shewanella putrefaciens* bacterial cells to the surface of hematite. *Environmental Science & Technology* 2012; 46: 12848-12855.
- Habash M, Reid G. microbial biofilms: their development and significance for medical device-related infections. *Journal of Clinical Pharmacology* 1999; 39: 887-898.

- Hogg R, Healy TW, Fuersten.Dw. Mutual coagulation of colloidal dispersions. Transactions of the Faraday Society 1966; 62: 1638-&.
- Hwang G, Kang S, El-Din MG, Liu Y. Impact of an extracellular polymeric substance (EPS) precoating on the initial adhesion of *Burkholderia cepacia* and *Pseudomonas aeruginosa*. Biofouling 2012; 28: 525-538.
- Hwang G, Liang J, Kang S, Tong M, Liu Y. The role of conditioning film formation in *Pseudomonas aeruginosa* PAO1 adhesion to inert surfaces in aquatic environments. Biochemical Engineering Journal 2013; 76: 90-98.
- Jiang L, Wang JF, Liang SZ, Cai J, Xu ZN. Control and optimization of *Clostridium tyrobutyricum* ATCC 25755 adhesion into fibrous matrix in a fibrous bed bioreactor. Applied Biochemistry and Biotechnology 2011; 165: 98-108.
- Kim HN, Hong Y, Lee I, Bradford SA, Walker SL. surface characteristics and adhesion behavior of *Escherichia coli* O157:H7: role of extracellular macromolecules. Biomacromolecules 2009; 10: 2556-2564.
- Koenderink GH, Vliegthart GA, Kluijtmans S, van Blaaderen A, Philipse AP, Lekkerkerker HNW. Depletion-induced crystallization in colloidal rod-sphere mixtures. Langmuir 1999; 15: 4693-4696.
- Kumar CG, Anand SK. Significance of microbial biofilms in food industry: a review. International Journal of Food Microbiology 1998; 42: 9-27.
- Lerner RN, Lu QY, Zeng HB, Liu Y. The effects of biofilm on the transport of stabilized zerovalent iron nanoparticles in saturated porous media. Water Research 2012; 46: 975-985.

- Mao Y, Cates ME, Lekkerkerker HNW. Depletion stabilization by semidilute rods. *Physical Review Letters* 1995; 75: 4548-4551.
- Mattilasandholm T, Wirtanen G. Biofilm formation in the industry - a review. *Food Reviews International* 1992; 8: 573-603.
- Redman JA, Walker SL, Elimelech M. Bacterial adhesion and transport in porous media: role of the secondary energy minimum. *Environmental Science & Technology* 2004; 38: 1777-1785.
- Rijnaarts HHM, Norde W, Lyklema J, Zehnder AJB. The isoelectric point of bacteria as an indicator for the presence of cell-surface polymers that inhibit adhesion. *Colloids and Surfaces B-Biointerfaces* 1995; 4: 191-197.
- Rijnaarts HHM, Norde W, Lyklema J, Zehnder AJB. DLVO and steric contributions to bacterial deposition in media of different ionic strengths. *Colloids and Surfaces B-Biointerfaces* 1999; 14: 179-195.
- Salerno MB, Li X, Logan BE. Adhesion characteristics of Two *Burkholderia cepacia* strains examined using colloid probe microscopy and gradient force analysis. *Colloids and Surfaces B-Biointerfaces* 2007; 59: 46-51.
- Sun X, Danumah C, Liu Y, Boluk Y. Flocculation of bacteria by depletion interactions due to rod-shaped cellulose nanocrystals. *Chemical Engineering Journal* 2012; 198-199: 476-481.
- Sun X, Lu Q, Boluk Y, Liu Y. The impact of cellulose nanocrystals on the aggregation and initial adhesion of *Pseudomonas fluorescens* bacteria. *Soft Matter* 2014; 10: 8923-8931.

- Xu LC, Logan BE. Interaction forces between colloids and protein-coated surfaces measured using an atomic force microscope. *Environmental Science & Technology* 2005; 39: 3592-3600.
- Yang H, Kim H, Tong M. Influence of humic acid on the transport behavior of bacteria in quartz sand. *Colloids and Surfaces B-Biointerfaces* 2012a; 91: 122-129.
- Yang H, Tong M, Kim H. Influence of bentonite particles on representative gram negative and gram positive bacterial deposition in porous media. *Environmental Science & Technology* 2012b; 46: 11627-11634.
- Yang H, Tong M, Kim H. Effect of carbon nanotubes on the transport and retention of bacteria in saturated porous media. *Environmental Science & Technology* 2013; 47: 11537-11544.
- Zhong L, Fu S, Peng X, Zhan H, Sun R. Colloidal stability of negatively charged cellulose nanocrystalline in aqueous systems. *Carbohydrate Polymers* 2012; 90: 644-649.

Chapter 7 Impact of CNC on the Aggregation of *Pseudomonas aeruginosa*: Role of EPS and Organic Matters

7.1. Background

EPS is one of the main bacterial surface polymers, which makes bacterial surfaces more complicated than other colloidal particles' surfaces. Typically, the EPS matrix consists of a mixture of macromolecules, including proteins, polysaccharides, nucleic acids, humic substances, lipids, and other polymeric compounds (Hwang et al., 2012). It is believed that EPS has profound effects on bacterial adhesion and the subsequent biofilm formation (Frank and Belfort, 2003). Previous studies into these effects mainly focused on the EPS bound to the bacterial surface promoting bacterial adhesion on solid substratum. However, very few studies concerned the effect of isolated EPS on bacterial aggregation and bacterial adhesion. In reality, EPS would exist as a part of dissolved organic matter, and it would probably mediate bacterium–bacterium/bacterium–surface interactions. However, the exact role of EPS on bacterial aggregation has not been elucidated and more research to this end is needed. *Pseudomonas aeruginosa* EPS are generally neutrally charged (Eboigbodin et al., 2005). As the predominant component of EPS monosaccharides, glucose is usually used as the model monosaccharide in bacterial EPS (Sebastiao et al., 2013). Humic acid (HA) is the major humic substance in aqueous environments (Amal et al., 1992), and is therefore used as the model humic substance in bacterial EPS and the model organic matter in environment. The objective of this study is to evaluate the role of isolated EPS on bacterial aggregation in the presence of CNC. The impact of glucose and HA is also studied.

7.2. Experimental

7.2.1. Cellulose nanocrystals (CNC)

CNC was received from Alberta Innovates Technology Futures. CNC is prepared by acid hydrolysis of pure cellulose. A detailed preparation method is discussed in Sun et al. (2012). CNC particles in aqueous solutions carry negative electrical charges due to sulfate surface groups generated during the hydrolysis process. The hydrodynamic size of the CNC particles was determined by DLS using a Zetasizer Model Nano ZS from Malvern (Worcestershire, United Kingdom), which was 90 ± 10 nm taken as the particle length. Zeta potential of CNC particles was determined using the same instrument with the electrophoresis mode and cell. The pH of the suspension was not adjusted, and was close to neutral. Zeta potential of CNC was -42.3 ± 1.07 mV in 10 mM of NaCl (pH not adjusted). All measurements were performed at 25°C. Stock suspension of 1.0% (wt) CNC in 10 mM of NaCl (pH not adjusted) was prepared for further use.

7.2.2. Bacterial system

Pseudomonas aeruginosa PAO1 is a Gram-negative bacterium. For each experiment, the -80°C stored *P. aeruginosa* PAO1 strains were streaked onto a LB agar plate and incubated at 37°C overnight. A single colony was then transferred into 10 mL of LB broth and grown in a shaker incubator at 200 rpm and 37°C for 18 hours. Stationary phase bacterial cells were harvested by centrifugation at 3000 g and 4°C for 10 minutes. After the supernatant was decanted, the pellets were resuspended in 10 mM of NaCl solution. The centrifugation and resuspension procedure was repeated twice to remove traces of growth media in the solution. A final concentration of 1.0×10^8 cells/mL in 10 mM of

NaCl solution was prepared for future use. The zeta potential of *P. aeruginosa* cells suspended in 10 mM of NaCl solution (pH not adjusted) was measured to -29.84 ± 0.6 mV.

7.2.3. EPS isolation

The isolation of EPS from *P. aeruginosa* PAO1 is summarized below (Hwang et al., 2012). Harvested bacterial cells were washed twice with an isotonic solution (0.9% NaCl), then the pellet was suspended in ultrapure water and heated for 10 minutes at 80°C. After this treatment, the samples were centrifuged at 15000 g at 4°C for 15 minutes, and the supernatants were collected as EPS extracts. The EPS were further filtered through a 0.22 µm membrane filter, and stored at -20°C for further use.

7.2.4. Preparation of glucose and HA suspension

A total of 4.5 mg/L glucose in 10 mM of NaCl was prepared by simply dissolving D-glucose in 10 mM of NaCl. A total of 0.1 g/L HA (Suwannee River humic acid standard (II), International Humic Substances Society, Atlanta, GA) in 10 mM of NaCl was prepared by simply dissolving HA powder in 10 mM of NaCl, and stirring it for 24 hours in darkness. The stock solution was then filtered through 0.45 µm membrane filters to remove any un-dissolved HA. Glucose and HA suspension were prepared right before each experiment run.

7.2.5. Experimental protocols

All samples are prepared and listed in Table 7.1. Prepared samples were incubated in a shaker incubator (37°C, 200 rpm) for 30 minutes, then dyed with SYTO 9 green fluorescent nucleic acid stain before the bacterial suspensions were dropped on clean

microscopy glass slides and visualized under fluorescent light using an Axio Imager M2 microscope (Carl Zeiss, Germany) with a Zeiss LD Plan-NEOFLUAR 40× objective. At least 50 images of randomly chosen areas on each slide were taken. The images were analyzed using AxioVision 4.8; the size (the equivalent spherical radius of one bacterial cluster) of each bacterial aggregate on each image was measured, and then the average size was calculated. These experiments were conducted in triplicate in at least five independent experiment runs.

7.3. Results and Discussion

Table 7.1. Samples and average size of bacterial flocs in each sample

Sample	Average bacterial
A. 0.5 mL bacterial suspension+1 mL NaCl	No flocs found
B. 0.5 mL bacterial suspension+0.5 mL NaCl+0.5 mL CNC	30
C. 0.5 mL bacterial suspension+0.5 mL NaCl+0.5 mL EPS	20
D. 0.5 mL bacterial suspension+0.5 mL EPS+0.5 mL CNC	10
E. 0.5 mL bacterial suspension+0.5 mL NaCl+0.5 mL glucose	30
F. 0.5 mL bacterial suspension+0.5 mL CNC+0.5 mL glucose	5
G. 0.5 mL bacterial suspension+0.5 mL NaCl+0.5 mL HA	5
H. 0.5 mL bacterial suspension+0.5 mL CNC+0.5 mL HA	50

The average size of bacterial flocs was estimated based on microscopy images, and is listed in Table 7.1. Figure 7.1 shows representative microscopy images of bacterial aggregation. Consistent with the previous study (Sun et al., 2012), *P. aeruginosa* PAO1 suspension (in 10 mM of NaCl, pH not adjusted) was stable against aggregation (Figure 7.1A), the presence of CNC induced *P. aeruginosa* PAO1 aggregation (to an average floc

size of 30 μm , Figure 7.1B) through depletion mechanism. Similarly, the presence of EPS, glucose and HA also encouraged *P. aeruginosa* PAO1 aggregation to a different extent

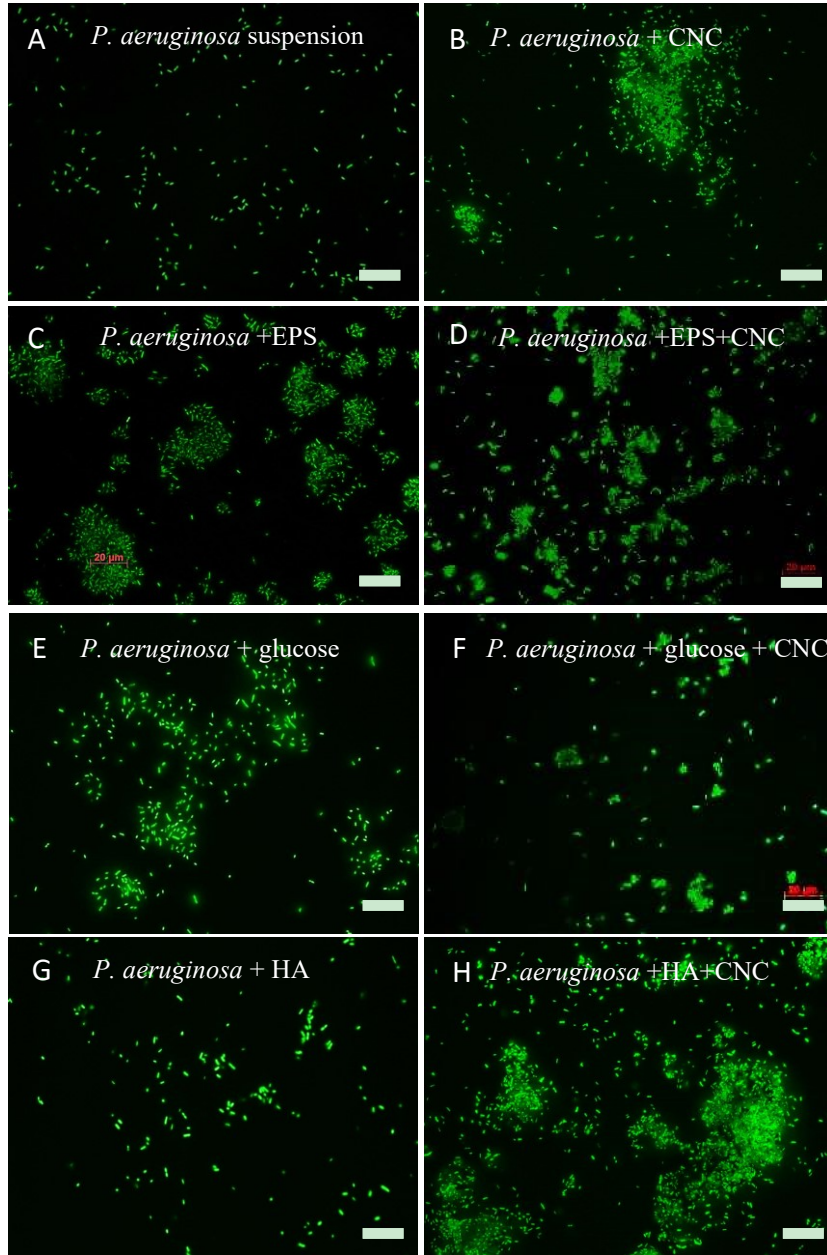


Figure 7.1. Representative images of bacterial aggregation with and without CNC. (Bar size = 20 μm)

(the average sizes were 20 μm (Figure 7.1C), 30 μm (Figure 7.1E), and 5 μm (Figure 7.1G), respectively). The possible mechanisms involved in bacterial aggregation observed in this study include depletion attraction and steric interactions. Steric interactions consist of steric attraction (bridging) and repulsion (Lu et al., 2011). The presence of glucose triggers the most significant bacterial aggregation, which might be associated with steric attraction due to the presence of glucose. As the main component of *P. aeruginosa* EPS monosaccharides, glucose plays a key role in EPS-mediated bacterial aggregation. EPS contain various functional groups such as carboxylic, phosphoric, amino, and hydroxyl that can interact with surfaces and mediate bacterium–bacterium interactions (Adoue et al., 2007)—for instance, to facilitate bacterial aggregation. HA results in the least bacterial aggregation. HA is usually found to adsorb on colloid surfaces (Qu et al., 2010), and can potentially adsorb on bacterial surfaces; thus, the presence of HA on bacterial surfaces might enhance steric repulsion between bacterial cells. Besides, negatively charged HA on bacterial surfaces might enhance the electrostatic repulsion between bacterial cells, resulting in less bacterial aggregation.

After adding CNC to the bacterial suspension, bacterial aggregation was hindered in the presence of both CNC and EPS (the average floc size of 10 μm , Figure 7.1D) when compared with bacterial suspensions to which only EPS (the average floc size of 20 μm , Figure 7.1C) or only CNC (the average floc size of 30 μm , Figure 7.1B) had been added. This difference can likely be attributed to steric hindrance due to the presence of both CNC and EPS. EPS might adsorb on bacterial surfaces and CNC surfaces and promote the steric repulsion between bacterial cells. EPS might deplete CNC and reduce depletion

attraction between bacterial cells. Compared with results observed in the presence of glucose only (Figure 7.1E), the presence of both CNC and glucose (Figure 7.1F) appears to significantly reduce bacterial aggregation (the average floc size reduced from 30 μm to 5 μm). Glucose might reduce CNC-induced depletion attraction between bacterial cells through steric repulsion. On the contrary, bacterial aggregation was promoted significantly in the presence of both CNC and HA (average floc size 50 μm , Figure 7.1H), compared with aggregation observed in the presence of HA only (average floc size 5 μm , Figure 7.1G). HA has a heterogeneous structure with hydrophobic backbones and hydrophilic side chains (Qu et al., 2010). Negatively charged HA could potentially adsorb to CNC surfaces, thus increasing the electrostatic repulsion between bacteria and CNC and leading to enhanced depletion attraction. Therefore, more aggregation was observed in the bacterial suspension when both CNC and HA were present. Buzzaccaro et al. (2010) also reported the enhancement of depletion attraction by electrostatic repulsion.

It should be noted that the average floc size estimated from microscopy images represents the degree of bacterial aggregation. Other factors, such as the density of the flocs, also impact the analysis and comparison of bacterial aggregation. Unfortunately, it is challenging to evaluate the density of bacterial flocs.

References

- Adoue M, Bacchin P, Lorthois S, Combes D, Schmitz P, Mercier-Bonin M. Experimental methodology for analysing macromolecular interactions in the context of marine bacterial adhesion to stainless steel. *Chemical Engineering Research & Design* 2007; 85: 792-799.
- Amal R, Raper JA, Waite TD. Effect of fulvic-acid adsorption on the aggregation kinetics and structure of hematite particles. *Journal of Colloid and Interface Science* 1992; 151: 244-257.
- Eboigbodin KE, Newton JRA, Routh AF, Biggs CA. Role of nonadsorbing polymers in bacterial aggregation. *Langmuir* 2005; 21: 12315-12319.
- Frank BP, Belfort G. Polysaccharides and sticky membrane surfaces: critical ionic effects. *Journal of Membrane Science* 2003; 212: 205-212.
- Hwang G, Kang S, El-Din MG, Liu Y. Impact of an extracellular polymeric substance (EPS) precoating on the initial adhesion of *Burkholderia cepacia* and *Pseudomonas aeruginosa*. *Biofouling* 2012; 28: 525-538.
- Lu QY, Wang J, Faghihnejad A, Zeng HB, Liu Y. Understanding the molecular interactions of lipopolysaccharides during *E. coli* initial adhesion with a surface forces apparatus. *Soft Matter* 2011; 7: 9366-9379.
- Qu X, Hwang YS, Alvarez PJJ, Bouchard D, Li Q. UV irradiation and humic acid mediate aggregation of aqueous fullerene (nC(60)) nanoparticles. *Environmental Science & Technology* 2010; 44: 7821-7826.

Sebastiao FdA, Pilarski F, Franco Lemos MV. Composition of extracellular polymeric substances (EPS) produced by *Flavobacterium columnare* isolated from tropical fish in Brazil. Brazilian Journal of Microbiology 2013; 44: 861-864.

Sun X, Danumah C, Liu Y, Boluk Y. Flocculation of bacteria by depletion interactions due to rod-shaped cellulose nanocrystals. Chemical Engineering Journal 2012; 198: 476-481.

Chapter 8 Conclusions

This thesis presents the application of two types of NPs in microbial systems. First, the toxic effects of Ag NPs on wastewater activated sludge biomass are investigated. Second, the impact of CNC on bacterial aggregation and adhesion is studied. Implications of applying each type of NP in microbial systems are reported.

8.1. Impact of Ag NPs on Wastewater Activated Sludge and Their Environmental Implications

This study represents the first experimental evidence on the impact of activated sludge flocs structure (floc size) on the response of the microbial community structure in wastewater activated sludge to Ag NPs. According to the results obtained through this study, 1 mg/L Ag NPs may pose a significant threat to the microbial viability and diversity in wastewater activated sludge biomass, but this highly depends on the sludge flocs' size and the spatial distribution of microbial communities. Microbial communities are regarded as the backbone of the wastewater activated sludge system; any side effects on microbial activities or community structures would decline the contaminant removal efficiency. With more and more NPs being released into the waste streams as a result of their increasing use, NPs will potentially accumulate in the biomass of wastewater treatment systems (e.g., activated sludge flocs and biofilms). Therefore, there is potentially a high risk that Ag NPs might increasingly compromise the microbial communities in wastewater treatment systems. This study suggests appropriate disposal options for NPs are necessary and recommends improvements to the operational

conditions of wastewater treatment processes to cope with the increasing presence of Ag NPs in wastewater.

It is worthwhile to notice that the response of activated sludge microorganisms to Ag NPs is dependent on the activated sludge floc size and structures. Further studies should be performed to evaluate the potential impact of the activated sludge floc size and structures on their responses toward Ag NPs. Because the floc concentration might play an important role in controlling the microbial response to Ag NPs, the direct impact of floc concentrations on the toxicity of Ag NPs should be investigated in a future study.

Furthermore, since only one kind of NP was tested under aerobic conditions in the current study, future studies on the implications of NPs in conditions relevant to engineering systems are needed. The exact concentration of engineered NPs retained in the biological wastewater treatment systems also deserves future study.

8.2. Impact of CNC on Bacterial Aggregation/Adhesion and Their Environmental Implications

Compared to Ag NPs, rod-shaped CNC particles are environmentally friendly NPs. This study represents the first experimental evidence on the nanosized CNC-induced colloidal bacterial aggregation through depletion mechanisms, and the consequently reduced bacterial adhesion to solid surfaces. The results showed that CNC can flocculate and phase-separate bacteria at very low concentrations—lower than the theoretical estimate. This finding is likely associated with the fact that bacterial cells are not ideal, smooth, and hard spherical particles, but cylindrical particles with soft surfaces and surface appendages (such as EPS). Further study verified that bacteria with more EPS aggregated

to a higher degree in the presence of CNC compared to bacteria with less EPS. After bacteria aggregated, the subsequent initial adhesion to solid surfaces was reduced. Thus, CNC might be an excellent candidate for creating and manipulating bacterial flocs and for preventing bacterial initial adhesion and subsequent biofilm development. The role of solution chemistry, such as pH and IS, was studied on bacterial aggregation and adhesion in the presence of CNC. The results reveal that pH and IS have marked effects on CNC-induced bacterial aggregation and reduced adhesion. In the presence of CNC at pH 5.2–7.2 and IS 10–50 mM, bacterial aggregation and adhesion inhibition were the highest at pH 7.2 and IS 10 mM. Theoretical classic DLVO interaction energy and depletion interaction energy calculation revealed that depletion was the dominant mechanism inducing bacterial aggregation which could consequently result in decreased convective-diffusive transport to the silica surface.

When bacterial EPS was isolated and added to a bacterial suspension in the presence of CNC, the extent of bacterial aggregation was reduced. This is likely the result of steric repulsion due to the presence of EPS. As the predominant monosaccharide and humic substances, glucose and HA were selected as the model monosaccharide and humic substances in EPS to evaluate the role glucose and HA play in CNC-induced bacterial aggregation. The results showed that glucose increased CNC-induced bacterial aggregation while HA reduced CNC-induced bacterial aggregation in the presence of CNC. The possible reason for this difference might be associated with steric interaction and electrostatic interaction due to the presence of glucose and HA. However, in order to understand the exact role of glucose, HA, and EPS on CNC-induced bacterial

aggregation, as well as the mechanisms involved, polymer characterizations—including the structure, charge, and size—of the EPS are needed.

References

- Abraham PM, Barnikol S, Baumann T, Kuehn M, Ivleva NP, Schaumann GE. Sorption of silver nanoparticles to environmental and model surfaces. *Environmental Science & Technology* 2013; 47: 5083-5091.
- Absolom DR, Lamberti FV, Policova Z, Zingg W, van Oss CJ, Neumann AW. Surface thermodynamics of bacterial adhesion. *Applied and Environmental Microbiology* 1983; 46: 90-97.
- Abu-Lail NI, Camesano TA. Role of ionic strength on the relationship of biopolymer conformation, DLVO contributions, and steric interactions to bioadhesion of *Pseudomonas putida* KT2442. *Biomacromolecules* 2003a; 4: 1000-1012.
- Abu-Lail NI, Camesano TA. Role of lipopolysaccharides in the adhesion, retention, and transport of *Escherichia coli* JM109. *Environmental Science & Technology* 2003b; 37: 2173-2183.
- Adoue M, Bacchin P, Lorthois S, Combes D, Schmitz P, Mercier-Bonin M. Experimental methodology for analysing macromolecular interactions in the context of marine bacterial adhesion to stainless steel. *Chemical Engineering Research & Design* 2007; 85: 792-799.
- Akdim B, Hussain S, Pachter R. A density functional theory study of oxygen adsorption at silver surfaces: implications for nanotoxicity. *Computational Science - Iccs* 2008, Pt 2 2008; 5102: 353-359.

- Amal R, Raper JA, Waite TD. Effect of fulvic-acid adsorption on the aggregation kinetics and structure of hematite particles. *Journal of Colloid and Interface Science* 1992; 151: 244-257.
- An YH, Friedman RJ. Concise Review of mechanisms of bacterial adhesion to biomaterial surfaces. *Journal of Biomedical Materials Research* 1998; 43: 338-348.
- An YH, Friedman RJ. *Handbook of bacterial adhesion*. Totowa, NJ: Humana Press, 2000.
- Andreadakis AD. Physical and chemical-properties of activated-sludge floc. *Water Research* 1993; 27: 1707-1714.
- Asakura S, Oosawa F. Interaction between two bodies immersed in a solution of macromolecules. *The journal of physical chemistry* 1954: 1255.
- Asakura S, Oosawa F. Interaction between particles suspended in solutions of macromolecules. *Journal of Polymer Science* 1958; 33: 183-192.
- Badireddy AR, Chellam S, Gassman PL, Engelhard MH, Lea AS, Rosso KM. Role of extracellular polymeric substances in bioflocculation of activated sludge microorganisms under glucose-controlled conditions. *Water Research* 2010; 44: 4505-4516.
- Bayouhdh S, Othmane A, Mora L, Ben Ouada H. Assessing bacterial adhesion using DLVO and XDLVO theories and the jet impingement technique. *Colloids and Surfaces B-Biointerfaces* 2009; 73: 1-9.
- Berg JC. *An introduction to interfaces & colloids The bridge to Nanoscience*. New Jersey: World Scientific, 2010.

- Berger M. Stabilizing antimicrobial nanosilver on a natural porous plant material. 2010. Nanowerk Spotlight, 2007.
- Berkeley RCW. Microbial adhesion to surfaces. Chichester: Ellis Horwood, 1980.
- Bhattacharjee S, Elimelech M. Surface element integration: A novel technique for evaluation of DLVO interaction between a particle and a flat plate. *Journal of Colloid and Interface Science* 1997; 193: 273-285.
- Boluk Y, Lahiji R, Zhao L, McDermott MT. Suspension viscosities and shape parameter of cellulose nanocrystals (CNC). *Colloids and Surfaces a-Physicochemical and Engineering Aspects* 2011; 377: 297-303.
- Boluk Y, Zhao LY, Incani V. Dispersions of nanocrystalline cellulose in aqueous polymer solutions: structure formation of colloidal rods. *Langmuir* 2012; 28: 6114-6123.
- Bond PL, Hugenholtz P, Keller J, Blackall LL. Bacterial community structures of phosphate-removing and non-phosphate-removing activated sludges from sequencing batch reactors. *Applied and Environmental Microbiology* 1995; 61: 1910-1916.
- Bondeson D, Mathew A, Oksman K. Optimization of the isolation of nanocrystals from microcrystalline cellulose by acid hydrolysis. *Cellulose* 2006; 13: 171-180.
- Bos R, van der Mei HC, Busscher HJ. Physico-chemistry of initial microbial adhesive interactions - its mechanisms and methods for study. *Fems Microbiology Reviews* 1999; 23: 179-230.

- Bottero J-Y, Auffan M, Rose J, Mouneyrac C, Botta C, Labille J, et al. Manufactured metal and metal-oxide nanoparticles: properties and perturbing mechanisms of their biological activity in ecosystems. *Comptes Rendus Geoscience* 2011; 343: 168-176.
- Bradford A, Handy RD, Readman JW, Atfield A, Muehling M. Impact of silver nanoparticle contamination on the genetic diversity of natural bacterial assemblages in estuarine sediments. *Environmental Science & Technology* 2009; 43: 4530-4536.
- Bradford SA, Torkzaban S. Colloid transport and retention in unsaturated porous media: a review of interface-, collector-, and pore-scale processes and models. *Vadose Zone Journal* 2008; 7: 667-681.
- Brar SK, Verma M, Tyagi RD, Surampalli RY. Engineered nanoparticles in wastewater and wastewater sludge - evidence and impacts. *Waste Management* 2010; 30: 504-520.
- Busscher HJ, Cowan MM, Vandermei HC. On the relative importance of specific and nonspecific approaches to oral microbial adhesion. *Fems Microbiology Reviews* 1992; 88: 199-209.
- Busscher HJ, Weerkamp AH, van der Mei HC, van Pelt AW, de Jong HP, Arends J. Measurement of the surface free energy of bacterial cell surfaces and its relevance for adhesion. *Applied and Environmental Microbiology* 1984; 48: 980-983.
- Buzzaccaro S, Piazza R, Colombo J, Parola A. Enhancement of depletion forces by electrostatic depletant repulsion. *Journal of Chemical Physics* 2010; 132.

- Cai P, Huang Q, Walker SL. Deposition and survival of *Escherichia coli* O157:H7 on clay minerals in a parallel plate flow system. *Environmental Science & Technology* 2013; 47: 1896-1903.
- Carpentier B, Cerf O. Biofilms and their consequences, with particular reference to hygiene in the food-industry. *Journal of Applied Bacteriology* 1993; 75: 499-511.
- Chen G, Strevett KA. Microbial surface thermodynamics and interactions in aqueous media. *Journal of Colloid and Interface Science* 2003; 261: 283-290.
- Chen GX, Hong YS, Walker SL. Colloidal and bacterial deposition: role of gravity. *Langmuir* 2010; 26: 314-319.
- Chen GX, Walker SL. Role of solution chemistry and ion valence on the adhesion kinetics of groundwater and marine bacteria. *Langmuir* 2007; 23: 7162-7169.
- Cho M, Chung HM, Choi WY, Yoon JY. Different inactivation behaviors of MS-2 phage and *Escherichia coli* in TiO₂ photocatalytic disinfection. *Applied and Environmental Microbiology* 2005; 71: 270-275.
- Choi O, Deng KK, Kim NJ, Ross L, Surampalli RY, Hu ZQ. The inhibitory effects of silver nanoparticles, silver ions, and silver chloride colloids on microbial growth. *Water Research* 2008; 42: 3066-3074.
- Choi O, Hu ZQ. Size dependent and reactive oxygen species related nanosilver toxicity to nitrifying bacteria. *Environmental Science & Technology* 2008; 42: 4583-4588.
- Czaczyk K, Myszka K. Biosynthesis of extracellular polymeric substances (EPS) and its role in microbial biofilm formation. *Polish Journal of Environmental Studies* 2007; 16: 799-806.

- Dale AL, Casman EA, Lowry GV, Lead JR, Viparelli E, Baalousha M. Modeling nanomaterial environmental fate in aquatic systems. *Environmental Science & Technology* 2015; 49: 2587-2593.
- Dan N. The effect of charge regulation on cell adhesion to substrates: salt-induced repulsion. *Colloids and Surfaces B-Biointerfaces* 2003; 27: 41-47.
- De Clercq B, Lant PA, Vanrolleghem PA. Focused beam reflectance technique for *in situ* particle sizing in wastewater treatment settling tanks. *Journal of Chemical Technology and Biotechnology* 2004; 79: 610-618.
- de Gennes PG. Polymers at an interface; a simplified view. *Advances in Colloid and Interface Science* 1987; 27: 189-209.
- Derjaguin B, Landau L. Theory of the stability of strongly charged lyophobic sols and of the adhesion of strongly charged-particles in solutions of electrolytes. *Progress in Surface Science* 1993; 43: 30-59.
- Dimkpa CO, Calder A, Gajjar P, Merugu S, Huang WJ, Britt DW, et al. Interaction of silver nanoparticles with an environmentally beneficial bacterium, *Pseudomonas chlororaphis*. *Journal of Hazardous Materials* 2011; 188: 428-435.
- Dobiás B. Coagulation and flocculation : theory and applications. New York: M. Dekker, 1993.
- Dogic Z, Purdy KR, Grelet E, Adams M, Fraden S. Isotropic-nematic phase transition in suspensions of filamentous virus and the neutral polymer Dextran. *Physical Review E* 2004; 69.

- Dong XM, Revol JF, Gray DG. Effect of microcrystallite preparation conditions on the formation of colloid crystals of cellulose. *Cellulose* 1998; 5: 19-32.
- Dror-Ehre A, Mamane H, Belenkova T, Markovich G, Adin A. Silver nanoparticle-*E. coli* colloidal interaction in water and effect on *E. coli* survival. *Journal of Colloid and Interface Science* 2009; 339: 521-526.
- Ducker WA, Xu Z, Israelachvili JN. Measurements of hydrophobic and DLVO forces in bubble-surface interactions in aqueous solutions. *Langmuir* 1994; 10: 3279-3289.
- Dufrene YF, Boonaert CJP, Rouxhet PG. Adhesion of *Azospirillum brasilense*: role of proteins at the cell-support interface. *Colloids and Surfaces B-Biointerfaces* 1996; 7: 113-128.
- Dunne WM. Bacterial adhesion: seen any good biofilms lately? *Clinical Microbiology Reviews* 2002; 15: 155-+.
- Eboigbodin KE, Newton JRA, Routh AF, Biggs CA. Role of nonadsorbing polymers in bacterial aggregation. *Langmuir* 2005; 21: 12315-12319.
- Edgar CD, Gray DG. Influence of dextran on the phase behavior of suspensions of cellulose nanocrystals. *Macromolecules* 2002; 35: 7400-7406.
- Elechiguerra JL, Burt JL, Morones JR, Camacho-Bragado A, Gao X, Lara HH, et al. Interaction of silver nanoparticles with HIV-1. *J Nanobiotechnology* 2005; 3: 6.
- Elimelech M. Indirect evidence for hydration forces in the deposition of polystyrene latex colloids on glass surfaces. *Journal of the Chemical Society, Faraday Transactions* 1990; 86: 1623-1624.

- Elimelech M, Jia X, Gregory J, Williams R. Particle deposition and aggregation: measurement, modelling and simulation. Oxford, UK.: Butterworth-Heinemann, 1995.
- Elzinga EJ, Huang J-H, Chorover J, Kretzschmar R. ATR-FTIR spectroscopy study of the influence of pH and contact time on the adhesion of *Shewanella putrefaciens* bacterial cells to the surface of hematite. Environmental Science & Technology 2012; 46: 12848-12855.
- Fabrega J, Renshaw JC, Lead JR. Interactions of silver nanoparticles with *Pseudomonas putida* biofilms. Environmental Science & Technology 2009; 43: 9004-9009.
- Fabrega J, Zhang R, Renshaw JC, Liu WT, Lead JR. Impact of silver nanoparticles on natural marine biofilm bacteria. Chemosphere 2011; 85: 961-966.
- Farinato RS, Dubin PL. Colloid-polymer interactions: from fundamentals to practice. New York: John Wiley, 1999.
- Fleer GJ, Scheutjens J. Depletion flocculation and stabilization. Abstracts of Papers of the American Chemical Society 1983; 186: 65-COLL.
- Flemming HC, Wingender J. Relevance of microbial extracellular polymeric substances (EPSs) - Part I: Structural and ecological aspects. Water Science and Technology 2001a; 43: 1-8.
- Flemming HC, Wingender J. Relevance of microbial extracellular polymeric substances (EPSs) - Part II: Technical aspects. Water Science and Technology 2001b; 43: 9-16.
- Flory PJ. Principles of Polymer chemistry. Ithaca: Cornell University Press, 1953.

- Frank BP, Belfort G. Polysaccharides and sticky membrane surfaces: critical ionic effects. *Journal of Membrane Science* 2003; 212: 205-212.
- Fuchs M, Schweizer KS. Structure of colloid-polymer suspensions. *Journal of Physics-Condensed Matter* 2002; 14: R239-R269.
- Gao J, Wang Y, Hovsepyan A, Bonzongo JCJ. Effects of engineered nanomaterials on microbial catalyzed biogeochemical processes in sediments. *J Hazard Mater* 2011;186:940-5.
- Gavrilescu M, Macoveanu M. Process engineering in biological aerobic wastewater treatment. *Acta Biotechnologica* 1999; 19: 111-145.
- Gou N, Onnis-Hayden A, Gu AZ. Mechanistic toxicity assessment of nanomaterials by whole-cell-array stress genes expression analysis. *Environmental Science & Technology* 2010; 44: 5964-5970.
- Grijpspeerdt K, Verstraete W. Image analysis to estimate the settleability and concentration of activated sludge. *Water Research* 1997; 31: 1126-1134.
- Gutman J, Walker SL, Freger V, Herzberg M. Bacterial attachment and viscoelasticity: physicochemical and motility effects analyzed using quartz crystal microbalance with dissipation (QCM-D). *Environmental Science & Technology* 2013; 47: 398-404.
- Habash M, Reid G. Microbial Biofilms: Their development and significance for medical device-related infections. *Journal of Clinical Pharmacology* 1999; 39: 887-898.

- Hahn MW, O'Melia CR. Deposition and reentrainment of brownian particles in porous media under unfavorable chemical conditions: some concepts and applications. *Environmental Science & Technology* 2004; 38: 210-220.
- Hamad WY, Hu TQ. Structure-process-yield interrelations in nanocrystalline cellulose extraction. *Canadian Journal of Chemical Engineering* 2010; 88: 392-402.
- Hayashi H, Tsuneda S, Hirata A, Sasaki H. Soft particle analysis of bacterial cells and its interpretation of cell adhesion behaviors in terms of DLVO theory. *Colloids and Surfaces B-Biointerfaces* 2001; 22: 149-157.
- Hemraz UD, Lu A, Sunasee R, Boluk Y. Structure of poly(N-isopropylacrylamide) brushes and steric stability of their grafted cellulose nanocrystal dispersions. *Journal of Colloid and Interface Science* 2014; 430: 157-165.
- Hermansson M. The DLVO theory in microbial adhesion. *Colloids and Surfaces B-Biointerfaces* 1999; 14: 105-119.
- Hesselink FT. Theory of the stabilization of dispersions by adsorbed macromolecules. I. Statistics of the change of some configurational properties of adsorbed macromolecules on the approach of an impenetrable interface. *The Journal of Physical Chemistry* 1971; 75: 65-71.
- Hogg R, Healy TW, Fuersten.Dw. Mutual coagulation of colloidal dispersions. *Transactions of the Faraday Society* 1966; 62: 1638-&.
- Hogt AH, Dankert J, Feijen J. Adhesion of staphylococcus-epidermidis and staphylococcus-saprophyticus to a hydrophobic biomaterial. *Journal of General Microbiology* 1985; 131: 2485-2491.

- Holbrook RD, Morrow J, Mangel T. Fate of nanoparticles in biological systems — quantum dot behavior in bacterial cells and biofilms. *Microscopy and Microanalysis* 2006;12(Suppl. 02):618-9.
- Hori K, Matsumoto S. Bacterial adhesion: from mechanism to control. *Biochemical Engineering Journal* 2010; 48: 424-434.
- Hou J, Miao L, Wang C, Wang P, Ao Y, Lv B. Effect of CuO nanoparticles on the production and composition of extracellular polymeric substances and physicochemical stability of activated sludge flocs. *Bioresource Technology* 2015; 176: 65-70.
- Hwang ET, Lee JH, Chae YJ, Kim YS, Kim BC, Sang B-I, et al. Analysis of the toxic mode of action of silver nanoparticles using stress-specific bioluminescent bacteria. *Small* 2008; 4: 746-750.
- Hwang G, Kang S, El-Din MG, Liu Y. Impact of an extracellular polymeric substance (EPS) pre-coating on the initial adhesion of *Burkholderia cepacia* and *Pseudomonas aeruginosa*. *Biofouling* 2012; 28: 525-538.
- Hwang G, Liang J, Kang S, Tong M, Liu Y. The role of conditioning film formation in *Pseudomonas aeruginosa* PAO1 adhesion to inert surfaces in aquatic environments. *Biochemical Engineering Journal* 2013; 76: 90-98.
- Israelachvili JN. Intermolecular and surface forces. London, England: Academic Press Ltd., 1992.

- Jackson CR, Roden EE, Churchill PF. Denaturing gradient gel electrophoresis can fail to separate 16S rDNA fragments with multiple base differences. 1. *Molecular Biology Today*, 2000, pp. 49-51.
- Jenkins P, Snowden M. Depletion flocculation in colloidal dispersions. *Advances in Colloid and Interface Science* 1996; 68: 57-96.
- Jeong E, Im W-T, Kim D-H, Kim M-S, Kang S, Shin H-S, et al. Different susceptibilities of bacterial community to silver nanoparticles in wastewater treatment systems. *Journal of Environmental Science and Health Part a-Toxic/Hazardous Substances & Environmental Engineering* 2014; 49: 685-693.
- Jiang L, Wang JF, Liang SZ, Cai J, Xu ZN. Control and optimization of *Clostridium tyrobutyricum* ATCC 25755 adhesion into fibrous matrix in a fibrous bed bioreactor. *Applied Biochemistry and Biotechnology* 2011; 165: 98-108.
- Jin B, Wilen BM, Lant P. A comprehensive insight into floc characteristics and their impact on compressibility and settleability of activated sludge. *Chemical Engineering Journal* 2003; 95: 221-234.
- Johnson ML, Wan J, Huang S, Cheng Z, Petrenko VA, Kim D-J, et al. A wireless biosensor using microfabricated phage-interfaced magnetoelastic particles. *Sensors and Actuators a-Physical* 2008; 144: 38-47.
- Johnson WP, Tong MP. Observed and simulated fluid drag effects on colloid deposition in the presence of an energy barrier in an impinging jet system. *Environmental Science & Technology* 2006; 40: 5015-5021.

- Jorand F, Zartarian F, Thomas F, Block JC, Bottero JY, Villemin G, et al. Chemical and structural (2D) linkage between bacteria within activated-sludge flocs. *Water Research* 1995; 29: 1639-1647.
- Ju-Nam Y, Lead JR. Manufactured nanoparticles: An overview of their chemistry, interactions and potential environmental implications. *Science of the Total Environment* 2008; 400: 396-414.
- Jucker BA, Harms H, Hug SJ, Zehnder AJB. Adsorption of bacterial surface polysaccharides on mineral oxides is mediated by hydrogen bonds. *Colloids and Surfaces B-Biointerfaces* 1997; 9: 331-343.
- Jucker BA, Harms H, Zehnder AJB. Adhesion of the positively charged bacterium *Stenotrophomonas (Xanthomonas) maltophilia* 70401 to glass and teflon. *Journal of Bacteriology* 1996; 178: 5472-5479.
- Jucker BA, Zehnder AJB, Harms H. Quantification of polymer interactions in bacterial adhesion. *Environmental Science & Technology* 1998; 32: 2909-2915.
- Kim HN, Hong Y, Lee I, Bradford SA, Walker SL. Surface characteristics and adhesion behavior of *Escherichia coli* O157:H7: role of extracellular macromolecules. *Biomacromolecules* 2009; 10: 2556-2564.
- Kim HN, Walker SL, Bradford SA. Macromolecule mediated transport and retention of *Escherichia coli* O157:H7 in saturated porous media. *Water Research* 2010; 44: 1082-1093.

- Kim JS, Kuk E, Yu KN, Kim J-H, Park SJ, Lee HJ, et al. Antimicrobial effects of silver nanoparticles (vol 1, pg 95, 2007). *Nanomedicine-Nanotechnology Biology and Medicine* 2014; 10: 1119-1119.
- Kiser MA, Westerhoff P, Benn T, Wang Y, Perez-Rivera J, Hristovski K. Titanium nanomaterial removal and release from wastewater treatment plants. *Environmental Science & Technology* 2009; 43: 6757-6763.
- Klaine SJ, Alvarez PJJ, Batley GE, Fernandes TF, Handy RD, Lyon DY, et al. Nanomaterials in the environment: behavior, fate, bioavailability, and effects. *Environmental Toxicology and Chemistry* 2008; 27: 1825-1851.
- Koenderink GH, Vliegthart GA, Kluijtmans S, van Blaaderen A, Philipse AP, Lekkerkerker HNW. Depletion-induced crystallization in colloidal rod-sphere mixtures. *Langmuir* 1999; 15: 4693-4696.
- Konopka M, Kowalski Z, Wzorek Z. Disinfection of meat industry equipment and production rooms with the use of liquids containing silver nano-particles. *Archives of Environmental Protection* 2009; 35: 107-115.
- Kragelund C, Levantesi C, Borger A, Thelen K, Eikelboom D, Tandoi V, et al. Identity, abundance and ecophysiology of filamentous bacteria belonging to the *Bacteroidetes* present in activated sludge plants. *Microbiology-Sgm* 2008; 154: 886-894.
- Kreft JU, Wimpenny JWT. Effect of EPS on biofilm structure and function as revealed by an individual-based model of biofilm growth. *Water Science and Technology* 2001; 43: 135-141.

- Krogfelt KA. Bacterial Adhesion - Genetics, Biogenesis, and Role in pathogenesis of fimbrial adhesins of *Escherichia Coli*. *Reviews of Infectious Diseases* 1991; 13: 721-735.
- Kumar A, Mortensen NP, Mukherjee PP, Retterer ST, Doktycz MJ. Electric field induced bacterial flocculation of enteroaggregative *Escherichia coli* 042. *Applied Physics Letters* 2011; 98: 253701.
- Kumar CG, Anand SK. Significance of microbial biofilms in food industry: a review. *International Journal of Food Microbiology* 1998; 42: 9-27.
- Kumar RV, Raza G. Photocatalytic disinfection of water with Ag-TiO₂ nanocrystalline composite. *Ionics* 2009; 15: 579-587.
- Larsen MU, Seward M, Tripathi A, Shapley NC. Biocompatible nanoparticles trigger rapid bacteria clustering. *Biotechnology Progress* 2009; 25: 1094-1102.
- Larsen P, Nielsen JL, Otzenj D, Nielsen PH. Amyloid-like adhesins produced by flocculating and filamentous bacteria in activated sludge. *Applied and Environmental Microbiology* 2008; 74: 1517-1526.
- Lekkerkerker HNW, Tuinier R. *Colloids and Depletion*. Springer 2011; 100.
- Lerner RN, Lu QY, Zeng HB, Liu Y. The effects of biofilm on the transport of stabilized zerovalent iron nanoparticles in saturated porous media. *Water Research* 2012; 46: 975-985.
- Li BK, Logan BE. Bacterial adhesion to glass and metal-oxide surfaces. *Colloids and Surfaces B-Biointerfaces* 2004; 36: 81-90.

- Li DH, Ganczarzyk J. Size distribution of activated-sludge flocs. *Research Journal of the Water Pollution Control Federation* 1991; 63: 806-814.
- Li YS, Wang YG, Pennell KD, Abriola LM. Investigation of the transport and deposition of fullerene (C60) nanoparticles in quartz sands under varying flow conditions. *Environmental Science & Technology* 2008; 42: 7174-7180.
- Liang Y, Hilal N, Langston P, Starov V. Interaction forces between colloidal particles in liquid: theory and experiment. *Advances in Colloid and Interface Science* 2007; 134-35: 151-166.
- Limbach LK, Bereiter R, Mueller E, Krebs R, Gaelli R, Stark WJ. Removal of oxide nanoparticles in a model wastewater treatment plant: influence of agglomeration and surfactants on clearing efficiency. *Environmental Science & Technology* 2008; 42: 5828-5833.
- Liu C, Yang JL, Wu G, Zhang S, Li ZX, Guo JB. Estimation of dominant microbial population sizes in the anaerobic granular sludge of a full-scale UASB treating streptomycin wastewater by PCR-DGGE. *World Journal of Microbiology & Biotechnology* 2010; 26: 375-379.
- Liu XM, Sheng GP, Luo HW, Zhang F, Yuan SJ, Xu J, Zeng RJ, Wu JG, Yu HQ. Contribution of extracellular polymeric substances (EPS) to the sludge aggregation. *Environmental Science & Technology* 2010; 44: 4355-4360.
- Liu Y, Li J, Qiu XF, Burda C. Bactericidal activity of nitrogen-doped metal oxide nanocatalysts and the influence of bacterial extracellular polymeric substances

- (EPS). Journal of Photochemistry and Photobiology a-Chemistry 2007a; 190: 94-100.
- Liu Y, Yang CH, Li J. Influence of extracellular polymeric substances on *Pseudomonas aeruginosa* transport and deposition profiles in porous media. Environmental Science & Technology 2007b; 41: 198-205.
- Lok CN, Ho CM, Chen R, He QY, Yu WY, Sun HZ, et al. Proteomic analysis of the mode of antibacterial action of silver nanoparticles. Journal of Proteome Research 2006; 5: 916-924.
- Lombay G, Sundararajan S, Wang KJ, Subramaniam S. A test method for determining adhesion forces and Hamaker constants of cementitious materials using atomic force microscopy. Cement and Concrete Research 2011; 41: 1157-1166.
- Louie SM, Tilton RD, Lowry GV. Effects of Molecular Weight distribution and chemical properties of natural organic matter on gold nanoparticle aggregation. Environmental Science & Technology 2013; 47: 4245-4254.
- Lowry GV, Gregory KB, Apte SC, Lead JR. Transformations of nanomaterials in the environment. Environmental Science & Technology 2012; 46: 6893-6899.
- Lu QY, Wang J, Faghiehnejad A, Zeng HB, Liu Y. Understanding the molecular interactions of lipopolysaccharides during *E. coli* initial adhesion with a surface forces apparatus. Soft Matter 2011; 7: 9366-9379.
- Luongo LA, Zhang XQ. Toxicity of carbon nanotubes to the activated sludge process. Journal of Hazardous Materials 2010; 178: 356-362.

- Lyon DY, Brown DA, Alvarez PJJ. Implications and potential applications of bactericidal fullerene water suspensions: effect of nC(60) concentration, exposure conditions and shelf life. *Water Science and Technology* 2008; 57: 1533-1538.
- Manz W, Wagner M, Amann R, Schleifer KH. *In-situ* characterization of the microbial consortia active in 2 waste-water treatment plants. *Water Research* 1994; 28: 1715-1723.
- Mao Y, Cates ME, Lekkerkerker HNW. Depletion stabilization by semidilute rods. *Physical Review Letters* 1995; 75: 4548-4551.
- Marcus IM, Herzberg M, Walker SL, Freger V. *Pseudomonas aeruginosa* attachment on QCM-D sensors: the role of cell and surface hydrophobicities. *Langmuir* 2012; 28: 6396-6402.
- Marshall KC. Bacterial adhesion in oligotrophic habitats. *Microbiological Sciences* 1985; 2: 321-+.
- Marshall KC, Stout R, Mitchell R. Mechanism of initial events in sorption of marine bacteria to surfaces. *Journal of General Microbiology* 1971; 68: 337-&.
- Mattilasandholm T, Wirtanen G. Biofilm formation in the industry - a review. *Food Reviews International* 1992; 8: 573-603.
- McEldowney S, Fletcher M. Variability of the influence of physicochemical factors affecting bacterial adhesion to polystyrene substrata. *Applied and Environmental Microbiology* 1986; 52: 460-465.
- Metcalf and Eddy. *Wastewater Engineering: Treatment and Reuse (4th Edition)*. McGraw-Hill, New York, 2003.

- Miller M, Bassler B. Quorum sensing in bacteria. *Annual Review of Microbiology* 2001; 165-199.
- Milner ST, Witten TA, Cates ME. Theory of the grafted polymer brush. *Macromolecules* 1988; 21: 2610-2619.
- Mohanty A, Wu Y, Cao B. Impacts of engineered nanomaterials on microbial community structure and function in natural and engineered ecosystems. *Applied Microbiology and Biotechnology* 2014; 98: 8457-8468.
- Moharikar A, Purohit HJ, Kumar R. Microbial population dynamics at effluent treatment plants. *Journal of Environmental Monitoring* 2005; 7: 552-558.
- Morones JR, Elechiguerra JL, Camacho A, Holt K, Kouri JB, Ramirez JT, et al. The bactericidal effect of silver nanoparticles. *Nanotechnology* 2005; 16: 2346-2353.
- Muyzer G, Smalla K. Application of denaturing gradient gel electrophoresis (DGGE) and temperature gradient gel electrophoresis (TGGE) in microbial ecology. *Antonie Van Leeuwenhoek International Journal of General and Molecular Microbiology* 1998; 73: 127-141.
- Ni BJ, Xie WM, Liu SG, Yu HQ, Wang YZ, Wang G, et al. Granulation of activated sludge in a pilot-scale sequencing batch reactor for the treatment of low-strength municipal wastewater. *Water Research* 2009; 43: 751-761.
- Nogueira V, Lopes I, Rocha-Santos T, Santos AL, Rasteiro GM, Antunes F, et al. Impact of organic and inorganic nanomaterials in the soil microbial community structure. *Science of the Total Environment* 2012; 424: 344-350.

- Okunuki S, Kawaharasaki M, Tanaka H, Kanagawa T. Changes in phosphorus removing performance and bacterial community structure in an enhanced biological phosphorus removal reactor. *Water Research* 2004; 38: 2433-2439.
- Olofsson AC, Zita A, Hermansson M. Floc stability and adhesion of green-fluorescent-protein-marked bacteria to flocs in activated sludge. *Microbiology-Sgm* 1998; 144: 519-528.
- Olsson ALJ, van der Mei HC, Busscher HJ, Sharma PK. Novel analysis of bacterium-substratum bond maturation measured using a quartz crystal microbalance. *Langmuir* 2010; 26: 11113-11117.
- Olsson ALJ, van der Mei HC, Busscher HJ, Sharma PK. Acoustic sensing of the bacterium-substratum interface using QCM-D and the influence of extracellular polymeric substances. *Journal of Colloid and Interface Science* 2011; 357: 135-138.
- Ong YL, Razatos A, Georgiou G, Sharma MM. Adhesion forces between *E. coli* bacteria and biomaterial surfaces. *Langmuir* 1999; 15: 2719-2725.
- Otto K, Elwing H, Hermansson M. Effect of ionic strength on initial interactions of *Escherichia coli* with surfaces, studied on-line by a novel quartz crystal microbalance technique. *Journal of Bacteriology* 1999; 181: 5210-5218.
- Palmer J, Flint S, Brooks J. Bacterial cell attachment, the beginning of a biofilm. *Journal of Industrial Microbiology & Biotechnology* 2007; 34: 577-588.

- Poitras C, Tufenkji N. A QCM-D-based biosensor for *E. coli* O157:H7 highlighting the relevance of the dissipation slope as a transduction signal. *Biosensors & Bioelectronics* 2009; 24: 2137-2142.
- Priester JH, Van De Werfhorst LC, Ge Y, Adeleye AS, Tomar S, Tom LM, et al. Effects of TiO₂ and Ag nanoparticles on polyhydroxybutyrate biosynthesis by activated sludge bacteria. *Environmental Science & Technology* 2014; 48: 14712-14720.
- Qu X, Hwang YS, Alvarez PJJ, Bouchard D, Li Q. UV irradiation and humic acid mediate aggregation of aqueous fullerene (nC(60)) nanoparticles. *Environmental Science & Technology* 2010; 44: 7821-7826.
- Quevedo IR, Tufenkji N. Influence of Solution chemistry on the deposition and detachment kinetics of a CdTe quantum dot examined using a quartz crystal microbalance. *Environmental Science & Technology* 2009; 43: 3176-3182.
- Ratte HT. Bioaccumulation and toxicity of silver compounds: a review. *Environmental Toxicology and Chemistry* 1999; 18: 89-108.
- Redman JA, Walker SL, Elimelech M. Bacterial adhesion and transport in porous media: role of the secondary energy minimum. *Environmental Science & Technology* 2004; 38: 1777-1785.
- Rijnaarts HH, Norde W, Bouwer EJ, Lyklema J, Zehnder AJ. Reversibility and mechanism of bacterial adhesion. *Colloids and Surfaces B: Biointerfaces* 1995a: 5-22.

- Rijnaarts HHM, Norde W, Bouwer EJ, Lyklema J, Zehnder AJB. Bacterial adhesion under static and dynamic conditions. *Applied and Environmental Microbiology* 1993; 59: 3255-3265.
- Rijnaarts HHM, Norde W, Lyklema J, Zehnder AJB. The isoelectric point of bacteria as an indicator for the presence of cell-surface polymers that inhibit adhesion. *Colloids and Surfaces B-Biointerfaces* 1995b; 4: 191-197.
- Rijnaarts HHM, Norde W, Lyklema J, Zehnder AJB. DLVO and steric contributions to bacterial deposition in media of different ionic strengths. *Colloids and Surfaces B-Biointerfaces* 1999; 14: 179-195.
- Rodahl M, Hook F, Krozer A, Brzezinski P, Kasemo B. Quartz-crystal microbalance setup for frequency and q-factor measurements in gaseous and liquid environments. *Review of Scientific Instruments* 1995; 66: 3924-3930.
- Salerno MB, Li X, Logan BE. Adhesion characteristics of two *Burkholderia cepacia* strains examined using colloid probe microscopy and gradient force analysis. *Colloids and Surfaces B-Biointerfaces* 2007; 59: 46-51.
- Sebastiao FdA, Pilarski F, Franco Lemos MV. Composition of extracellular polymeric substances (EPS) produced by *Flavobacterium columnare* isolated from tropical fish in Brazil. *Brazilian Journal of Microbiology* 2013; 44: 861-864.
- Sheng ZY, Liu Y. Effects of silver nanoparticles on wastewater biofilms. *Water Research* 2011; 45: 6039-6050.

- Silvestry-Rodriguez N, Bright KR, Slack DC, Uhlmann DR, Gerba CP. Silver as a residual disinfectant to prevent biofilm formation in water distribution systems. *Applied and Environmental Microbiology* 2008; 74: 1639-1641.
- Smith MCW. Microbial adhesion to surfaces - BERKELEY,RCW. *Journal of the American Chemical Society* 1983; 105: 2510-2510.
- Snowden MJ, Clegg SM, Williams PA, Robb ID. Flocculation of silica particles by adsorbing and nonadsorbing polymers. *Journal of the Chemical Society-Faraday Transactions* 1991; 87: 2201-2207.
- Sondi I, Salopek-Sondi B. Silver nanoparticles as antimicrobial agent: a case study on *E. coli* as a model for gram-negative bacteria. *Journal of Colloid and Interface Science* 2004; 275: 177-182.
- Sotiriou GA, Pratsinis SE. Antibacterial Activity of nanosilver ions and particles. *Environmental Science & Technology* 2010; 44: 5649-5654.
- Stamper DM, Walch M, Jacobs RN. Bacterial population changes in a membrane bioreactor for graywater treatment monitored by denaturing gradient gel electrophoretic analysis of 16S rRNA gene fragments. *Applied and Environmental Microbiology* 2003; 69: 852-860.
- Strand SP, Vandvik MS, Varum KM, Ostgaard K. Screening of chitosans and conditions for bacterial flocculation. *Biomacromolecules* 2001; 2: 126-133.
- Strauss J, Liu YT, Camesano TA. Bacterial adhesion to protein-coated surfaces: an AFM and QCM-D study. *Jom* 2009; 61: 71-74.

- Sun X, Danumah C, Liu Y, Boluk Y. Flocculation of bacteria by depletion interactions due to rod-shaped cellulose nanocrystals. *Chemical Engineering Journal* 2012; 198-199: 476–481.
- Sun X, Lu Q, Boluk Y, Liu Y. The impact of cellulose nanocrystals on the aggregation and initial adhesion of *Pseudomonas fluorescens* bacteria. *Soft Matter* 2014; 10: 8923-8931.
- Tiede K, Boxall ABA, Wang XM, Gore D, Tiede D, Baxter M, et al. Application of hydrodynamic chromatography-ICP-MS to investigate the fate of silver nanoparticles in activated sludge. *Journal of Analytical Atomic Spectrometry* 2010; 25: 1149-1154.
- Truesdail SE, Lukasik J, Farrah SR, Shah DO, Dickinson RB. Analysis of bacterial deposition on metal (hydr)oxide-coated sand filter media. *Journal of Colloid and Interface Science* 1998; 203: 369-378.
- Tsuneda S, Aikawa H, Hayashi H, Hirata A. Significance of cell electrokinetic properties determined by soft-particle analysis in bacterial adhesion onto a solid surface. *Journal of Colloid and Interface Science* 2004; 279: 410-417.
- Tufenkji N. Modeling microbial transport in porous media: traditional approaches and recent developments. *Advances in Water Resources* 2007; 30: 1455-1469.
- Tufenkji N, Elimelech M. Breakdown of colloid filtration theory: role of the secondary energy minimum and surface charge heterogeneities. *Langmuir* 2005; 21: 841-852.

- Tuinier R, Rieger J, de Kruif CG. Depletion-induced phase separation in colloid-polymer mixtures. *Advances in Colloid and Interface Science* 2003; 103: 1-31.
- Ubbink J, Schar-Zammaretti P. Colloidal properties and specific interactions of bacterial surfaces. *Current Opinion in Colloid & Interface Science* 2007; 12: 263-270.
- Vadillo-Rodriguez V, Busscher HJ, van der Mei HC, de Vries J, Norde W. Role of lactobacillus cell surface hydrophobicity as probed by AFM in adhesion to surfaces at low and high ionic strength. *Colloids and Surfaces B-Biointerfaces* 2005; 41: 33-41.
- van Loosdrecht MC, Lyklema J, Norde W, Schraa G, Zehnder AJ. The role of bacterial cell wall hydrophobicity in adhesion. *Applied and Environmental Microbiology* 1987; 53: 1893-1897.
- van Loosdrecht MCM, Norde W, Lyklema J, Zehnder AJB. Hydrophobic and electrostatic parameters in bacterial adhesion - Dedicated to Werner Stumm for his 65th birthday. *Aquatic Sciences* 1990; 52: 103-114.
- van Oss CJ, Chaudhury MK, Good RJ. Monopolar surfaces. *Advances in Colloid and Interface Science* 1987; 28: 35-64.
- Van Oss CJ, Good RJ, Chaudhury MK. The role of van der Waals forces and hydrogen bonds in "hydrophobic interactions" between biopolymers and low energy surfaces. *Journal of Colloid and Interface Science* 1986; 111: 378-390.
- Vandevivere P, Kirchman DL. Attachment stimulates exopolysaccharide synthesis by a bacterium. *Applied and Environmental Microbiology* 1993; 59: 3280-3286.

- Vanloosdrecht MCM, Norde W, Lyklema J, Zehnder AJB. Hydrophobic and electrostatic parameters in bacterial adhesion. *Aquatic Sciences* 1990; 52: 103-114.
- Vanoss CJ, Gillman CF. Phagocytosis as a surface phenomenon .1. contact angles and phagocytosis of non-opsonized bacteria. *Journal of the Reticuloendothelial Society* 1972; 12: 283-&.
- Vanoyan N, Walker SL, Gillor O, Herzberg M. Reduced bacterial deposition and attachment by quorum-sensing inhibitor 4-Nitro-pyridine-N-oxide: the role of physicochemical effects. *Langmuir* 2010; 26: 12089-12094.
- Velegol SB, Logan BE. Contributions of bacterial surface polymers, electrostatics, and cell elasticity to the shape of AFM force curves. *Langmuir* 2002; 18: 5256-5262.
- Verwey EJW. Theory of the stability of lyophobic colloids. *Journal of Physical and Colloid Chemistry* 1947; 51: 631-636.
- Vrij A. Polymers at interfaces and interactions in colloidal dispersions. *Pure and Applied Chemistry* 1976; 48: 471-483.
- Wagner M, Loy A, Nogueira R, Purkhold U, Lee N, Daims H. Microbial community composition and function in wastewater treatment plants. *Antonie Van Leeuwenhoek International Journal of General and Molecular Microbiology* 2002; 81: 665-680.
- Walker SL, Redman JA, Elimelech M. Role of cell surface lipopolysaccharides in *Escherichia coli* K12 adhesion and transport. *Langmuir* 2004; 20: 7736-7746.

- Wang H, Sodagari M, Chen YJ, He X, Newby BMZ, Ju LK. Initial bacterial attachment in slow flowing systems: effects of cell and substrate surface properties. *Colloids and Surfaces B-Biointerfaces* 2011; 87: 415-422.
- Wood J, Sharma R. How Long is the long-range hydrophobic attraction? *Langmuir* 1995; 11: 4797-4802.
- Workentine ML, Harrison JJ, Tran V, Stenroos PU, Weljie AM, Zhang P, et al. K-160. metabolic and physiological characterization of phenotypic variants obtained from *Pseudomonas Fluorescens* missing the GacS sensor kinase. 2012, 2008.
- Xu LC, Logan BE. Interaction forces between colloids and protein-coated surfaces measured using an atomic force microscope. *Environmental Science & Technology* 2005; 39: 3592-3600.
- Xu ZH, Liu JJ, Choung JW, Zhou ZA. Electrokinetic study of clay interactions with coal in flotation. *International Journal of Mineral Processing* 2003; 68: 183-196.
- Yang H, Kim H, Tong M. Influence of humic acid on the transport behavior of bacteria in quartz sand. *Colloids and Surfaces B-Biointerfaces* 2012a; 91: 122-129.
- Yang H, Tong M, Kim H. Influence of bentonite particles on representative gram negative and gram positive bacterial deposition in porous media. *Environmental Science & Technology* 2012b; 46: 11627-11634.
- Yang H, Tong M, Kim H. Effect of carbon nanotubes on the transport and retention of bacteria in saturated porous media. *Environmental Science & Technology* 2013; 47: 11537-11544.

- Yang Y, Quensen J, Mathieu J, Wang Q, Wang J, Li M, et al. Pyrosequencing reveals higher impact of silver nanoparticles than Ag^+ on the microbial community structure of activated sludge. *Water Research* 2014; 48: 317-325.
- Yee N, Fein JB, Daughney CJ. Experimental study of the pH, ionic strength, and reversibility behavior of bacteria-mineral adsorption. *Geochimica Et Cosmochimica Acta* 2000; 64: 609-617.
- Yoon KY, Byeon JH, Park JH, Hwang J. Susceptibility constants of *Escherichia coli* and *Bacillus subtilis* to silver and copper nanoparticles. *Science of the Total Environment* 2007; 373: 572-575.
- Zeng H. Polymer adhesion, Friction, Lubrication. New Jersey: John Wiley & Sons, 2013.
- Zheng X, Chen Y, Wu R. Long-term effects of titanium dioxide nanoparticles on nitrogen and phosphorus removal from wastewater and bacterial community shift in activated sludge. *Environmental Science & Technology* 2011; 45: 7284-7290.
- Zheng X, Su YL, Chen YG. Acute and chronic responses of activated sludge viability and performance to silica nanoparticles. *Environmental Science & Technology* 2012; 46: 7182-7188.
- Zhong L, Fu S, Peng X, Zhan H, Sun R. Colloidal stability of negatively charged cellulose nanocrystalline in aqueous systems. *Carbohydrate Polymers* 2012; 90: 644-649.